Proton Conducting Membranes Based on Sulfonated Aromatic Polymers for PEM Fuel Cells: Synthesis and Properties

Emanuela Sgreccia

Dissertation submitted to the faculty of Università di Roma Tor Vergata and Université de Provence in partial fulfilment of the requirements for the degree of

Doctor of Philosophy

in

Scienze Chimiche and Sciences ds Matériaux, Physique, Chimie et Nanosciences

Prof. Bruno Crociani, President

Prof. Rolf Hempelmann, Reviewer

Prof. Gunther G. Scherer, Reviewer

Prof. Mustapha Khadhraoui, Examiner

Prof. Maria Luisa Di Vona, Thesis Supervisor

Prof. Philippe Knauth, Thesis Supervisor

March 04, 2010

Rome, Italy

Proton Conducting Membranes Based on Sulfonated Aromatic Polymers for PEM Fuel Cells: Synthesis and Properties

Emanuela Sgreccia

Dissertation submitted to the faculty of Università di Roma Tor Vergata and Université de Provence in partial fulfilment of the requirements for the degree of

Doctor of Philosophy

in

Scienze Chimiche and Sciences ds Matériaux, Physique, Chimie et Nanosciences

_____	_____
Prof. Bruno Crociani	Prof. Rolf Hempelmann
_____	_____
Prof. Gunther G. Scherer	Prof. Mustapha Khadhraoui
_____	_____
Prof. Maria Luisa Di Vona	Prof. Philippe Knauth

March 04, 2010
Rome, Italy

Table of Contents

Chapter 1: Introduction

1.1. Types of Fuel Cells

Fuel cells are usually classified by the electrolyte employed in the cell. DMFC (Direct Methanol Fuel Cell) are an exception of this classification, because the fuel (methanol) gives the name of the fuel cell. Even if the electrolyte determines the operating temperature, often the classification of fuel cells is made by this parameter. There are, thus, the low and high temperature fuel cells. Alkaline Fuel Cells (AFCs), Proton Exchange Membrane Fuel Cells (PEMFCs, also called Polymer Electrolyte Fuel Cells, PEFCs, or Solid Polymer Electrolyte Fuel Cells, SPEFCs), DMFCs and Phosphoric Acid Fuel Cells (PAFCs) are low temperature fuel cells, while Molten Carbonate Fuel Cells (MCFCs) and Solid Oxide Fuel Cells (SOFCs) are high temperature fuel cells [1-3].

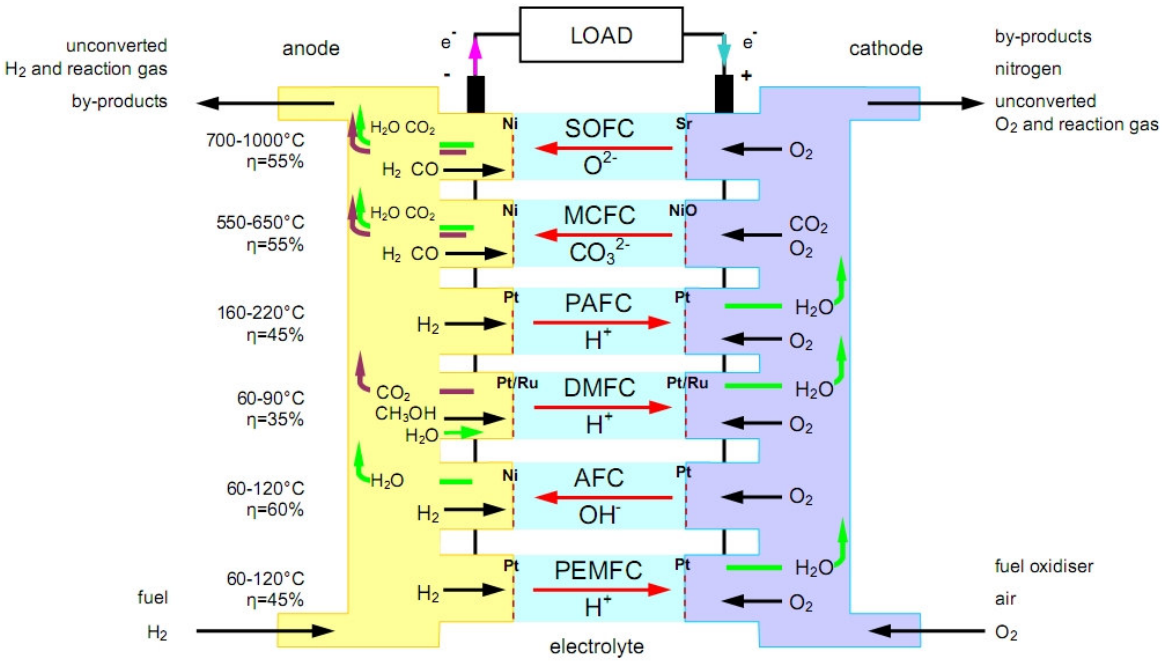

Figure 1.1 Fuel Cells Diagram

An overview of the basic characteristics of several types of fuel cells is given in the following tables [1, 4-6].

AFC: Alkaline Fuel Cells

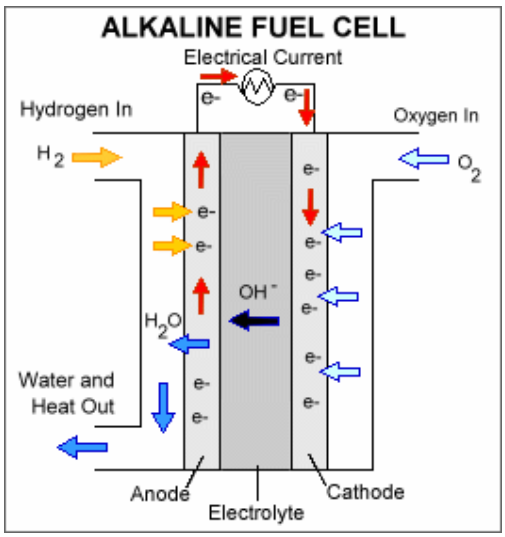

Figure 1.2 Alkaline Fuel Cell Diagram (image source: http://www.eere.energy.gov/hydrogenandfuelcells/fuelcells/fc_types.html)

Electrolyte	Aqueous Solution of Potassium Hydroxide Soaked in a Matrix
Temperature [°C]	65-220
System Output [W]	10 k - 100 k
Electrical Efficiency	60%
Combined Heat and Power (CHP) Efficiency	> 80% (low grade waste heat)
Anode Reaction	$H_2 + 2OH^- \rightarrow H_2O + 2e^-$
Cathode Reaction	$\frac{1}{2}O_2 + H_2O + 2e^- \rightarrow 2OH^-$
Overall Reaction	$H_2 + \frac{1}{2}O_2 \rightarrow H_2O$
Carrier	OH^-
Usable Fuels	Pure Hydrogen
Advantages	• It can work at low temperature • Fast start • High efficiency • Lower cost due to the small quantity of catalyst used • No corrosion problems • Simple operation • Low weight and volume

Disadvantages	• Extremely intolerant to CO_2 (up to 350 ppm) and shows intolerance to CO. This limits both the type of oxidant and fuel. Oxidant must be pure oxygen or air free of CO_2; the fuel must be pure hydrogen • Handling problems due to liquid electrolyte • Requires an evacuation of the water treatment complex • Relatively short lifetime
Applications	• Military • Space

PEMFC: Polymer Electrolyte Membrane Fuel Cells

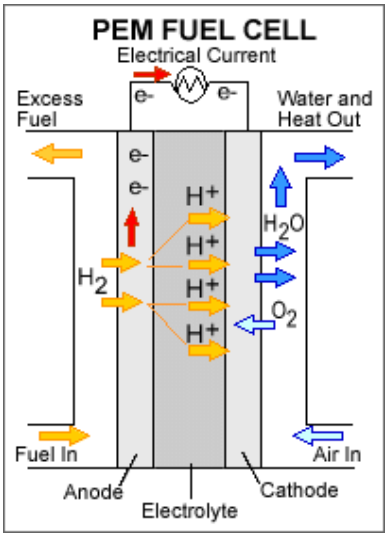

Figure 1.3 Polymer Electrolyte Fuel Cell Diagram (image source: http://www.eere.energy.gov/hydrogenandfuelcells/fuelcells/fc_types.html)

Electrolyte	Polymer Membrane
Temperature [°C]	30 - 100
System Output [W]	1k - 200k
Electrical Efficiency	53% – 58% (transportation) 25% - 35% (stationary)
Combined Heat and Power (CHP) Efficiency	70% - 90% (low grade waste heat)
Anode Reaction	$H_2 \rightarrow 2H^+ + 2e^-$
Cathode Reaction	$\frac{1}{2}O_2 + 2H^+ + 2e^- \rightarrow H_2O$
Overall Reaction	$H_2 + \frac{1}{2}O_2 \rightarrow H_2O$

Carrier $(H_2O)_n H^+$

Usable Fuels

- H_2
- Natural Gas
- Methanol

Advantages

- Solid electrolyte and the relatively low temperature of operations make the handling, assembly or tightness less complex then other types of fuel cells
- Increased security; the use of non corrosive electrolyte avoids the handling of acid or any other corrosive
- Tolerant to CO_2, so it can use the atmospheric air
- Employs a solid and non-volatile electrolyte
- Thank to the employment of solid and non-volatile electrolyte, problems linked to the handling of liquids and resupply are eliminated
- High current, voltage and power density
- Work at low pressure (1 or 2 bars) adds security
- Good tolerance to the difference of pressure of the reactants
- Compact and robust
- Simple mechanical design
- Uses stable building materials

Disadvantages

- High sensitivity to impurities of hydrogen; in order to use conventional fuels, a number of reforming units were developed. PEM fuel cells that use directly methanol as fuel without reforming are called direct methanol fuel cell (DMFC)
- Do not tolerate more than 50 ppm of CO and have a low tolerance to sulphur particles
- Need humidification units of reactive gases.
- Uses expensive catalyst (platinum) and polymer membrane

Applications

- Backup Power
- Small Stationary
- Portable Power
- Small Distributed Generation
- Transportation
- Specialty Vehicles

DMFC: Direct Methanol Fuel Cells

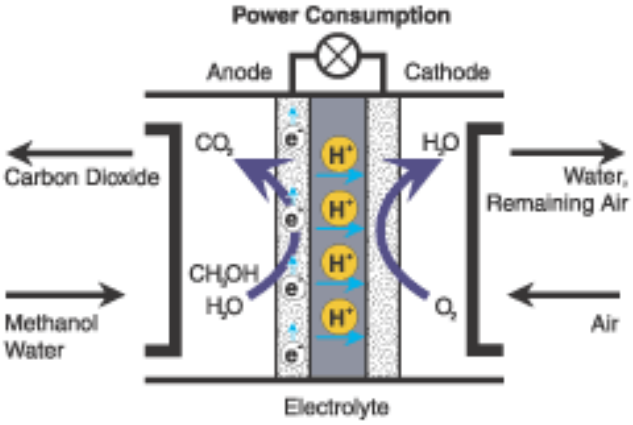

Figure 1.4 Direct Methanol Fuel Cell Diagram (image source: http://www.sfc.com/)

Electrolyte	Polymer Membrane
Temperature [°C]	Around 130
System Output [W]	~ 0,1 ~ 10
Anode Reaction	$CH_3OH + H_2O \rightarrow CO_2 + 6H^+ + 6e^-$
Cathode Reaction	$\frac{3}{2} O_2 + 6H^+ + 6e^- \rightarrow 3H_2O$
Overall Reaction	$CH_3OH + \frac{3}{2} O_2 \rightarrow CO_2 + 2H_2O$
Carrier	H^+
Usable Fuels	Methanol
Advantages	• Use a liquid fuel. The size of the deposits is less and can take advantage of existing infrastructure • Do not need any reforming process • Electrolyte is a proton exchange membrane (similar to PEM fuel cell type). This kind of electrolyte increases the security because eliminates the handling of acid or any other corrosive. Moreover their solid nature eliminates the handling of liquids and the problems of resupply
Disadvantages	• Low efficiency with respect to hydrogen cells • Needs large amount of catalyst (noble metal) for the electro-oxidation of methanol at the anode
Applications	• 3C (Computers/Cameras/Cell-phones) products • Consumer Electronics

PAFC: Phosphoric Acid Fuel Cells

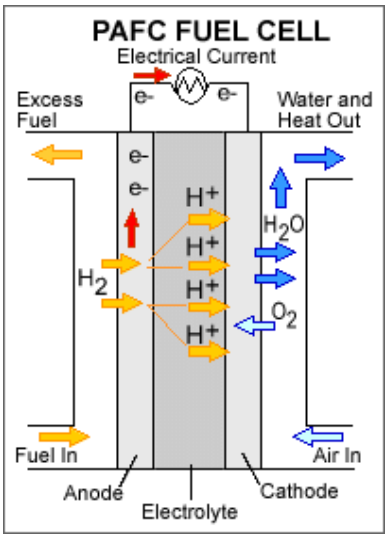

Figure 1.5 Phosphoric Acid Fuel Cell Diagram (image source: http://www.eere.energy.gov/hydrogenandfuelcells/fuelcells/fc_types.html)

Electrolyte	Liquid phosphoric acid soaked in a matrix
Temperature [°C]	150 - 200
System Output [W]	~ 200 k
Electrical Efficiency	> 40%
Combined Heat and Power (CHP) Efficiency	> 85%
Anode Reaction	$H_2 \rightarrow 2H^+ + 2e^-$
Cathode Reaction	$\frac{1}{2}O_2 + 2H^+ + 2e^- \rightarrow H_2O$
Overall Reaction	$H_2 + \frac{1}{2}O_2 \rightarrow H_2O$
Carrier	H^+
Usable Fuels	• Natural Gas • Methanol • Naphtha
Advantages	• Uses air directly from the atmosphere, because it tolerates up to 30% CO_2 • Higher overall efficiency with CHP (Combined Heat and Power) • Uses an electrolyte with stable characteristics, low volatility even at temperatures above 200°C
Disadvantages	• Maximum tolerance of 2% CO

- Handling and safety problems due to the use of liquid and corrosive electrolyte
- Dilution of acid electrolyte due to allowed entry of water
- Cannot autoreform fuel
- Elevated operating temperature (do not start before reaching a certain temperature)

Applications

- Distributed Generation

MCFC: Molten Carbonate Fuel Cells

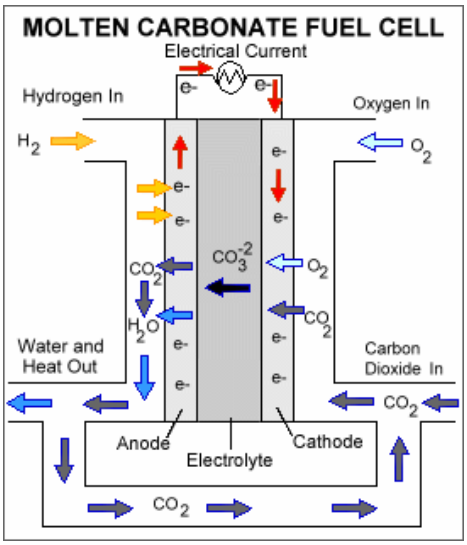

Figure 1.6 Molten Carbonate Fuel Cell Diagram (image source: http://www.eere.energy.gov/hydrogenandfuelcells/fuelcells/fc_types.html)

Electrolyte	Liquid Solution of lithium, sodium and/or potassium carbonates, soaked in a matrix
Temperature [°C]	600 - 650
System Output [W]	~ 500 k
Electrical Efficiency	45% - 47%
Combined Heat and Power (CHP) Efficiency	> 80%
Anode Reaction	$H_2 + CO_3^{2-} \rightarrow H_2O + CO_2 + 2e^-$
Cathode Reaction	$\frac{1}{2} O_2 + CO_2 + 2e^- \rightarrow CO_3^{2-}$
Overall Reaction	$H_2 + \frac{1}{2} O_2 \rightarrow H_2O$
Carrier	CO_3^{2-}

Usable Fuels

- Natural Gas
- Hydrogen
- Carbon Oxides

Advantages

- Allow spontaneous internal reforming
- Fuel flexibility
- Suitable for CHP (Combined Heat and Power)
- High-speed reactions
- High efficiency
- No need for noble metal catalyst (cost reduction)

Disadvantages

- For further development, it needs to be designed using materials resistant to corrosion and dimensionally stable. The catalyst of nickel oxide cathode can be dissolved in the electrolyte, causing a malfunction. Dimensional instability can cause distortion, changing the active area of the electrodes.
- High intolerance to sulphur (the anode does not tolerate more than 1.5 ppm of sulphur particles in the fuel)
- Handling problems due to the corrosive liquid electrolyte
- Requires preheating before starting work

Applications

- Electric Utility
- Large Distributed Generation

SOFC: Solid Oxide Fuel Cells

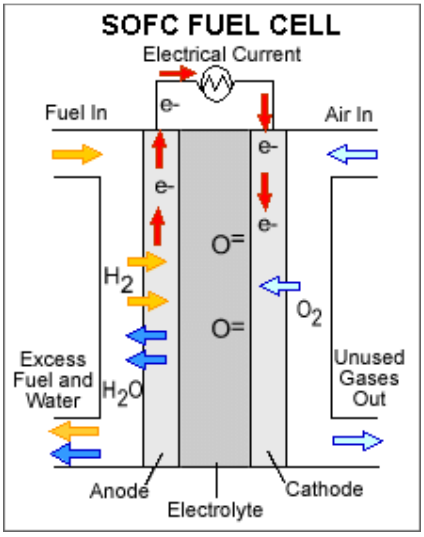

Figure 1.7 Solid Oxide Fuel Cell Diagram (image source: http://www.eere.energy.gov/hydrogenandfuelcells/fuelcells/fc_types.html)

Electrolyte	Yttria Stabilized Zirconia
Temperature [°C]	600 - 1000
System Output [W]	< 1 k – 3 M
Electrical Efficiency	35% - 43%
Combined Heat and Power (CHP) Efficiency	< 90%
Anode Reaction	$H_2 + O^{2-} \rightarrow H_2O + 2e^-$
Cathode Reaction	$\frac{1}{2} O_2 + 2e^- \rightarrow O^{2-}$
Overall Reaction	$H_2 + \frac{1}{2} O_2 \rightarrow H_2O$
Carrier	O^{2-}
Usable Fuels	• Natural Gas • Coal • Methanol • Petroleum
Advantages	• Allows spontaneous internal reforming fuel. Because oxide ions migrate through the electrolyte, fuel cell can be used to oxidize any combustible gas. • Generates a lot of heat; suitable for CHP (Combined Heat and Power) • Chemical reactions are very fast • High efficiency • Higher current densities then molten carbonate fuel cells • No liquid handling problems: the electrolyte is solid • No need of noble metal catalysts (can use a variety of catalysts)
Disadvantages	• For market penetration, one needs to develop materials that have sufficient conductivity, remain solid at temperatures of operation, are dimensionally stable and have high mechanical resistance • Moderate intolerance to sulphur (50 ppm)
Applications	• Auxiliary Power • Electric Utility • Large Distributed Generation

1.2. History of Fuel Cells

Fuel cells are *electrochemical devices that continuously convert chemical energy into electric energy (and some heat) for as long as fuel and oxidant are supplied.* They bear similarities both to batteries and to engines. Fuel cells generate electrical energy by converting chemical energy via redox reactions at anode and cathode [7]. Unlike batteries, fuel cells do not need recharging; compared to combustion engines they operate quietly, because there are no mobile parts, and more efficiently [8].

Systems based on Fuel Cells can help reducing pollution, in fact when hydrogen is used as the fuel, the only final exhaust product is water. They can be also useful for reducing the petrol dependence and for reducing CO_2 insertion in the atmosphere.

For the future power generation, the combination of renewable energy sources, such as wind, water and sun, to produce hydrogen in co-operation with fuel cells represents an attractive option [9].

Although in the last 20 years the development of fuel cells accelerated to replace internal combustion engines and to power stationary and portable applications, their history covers almost two centuries, as shown in **Figure 1.8** [6, 10].

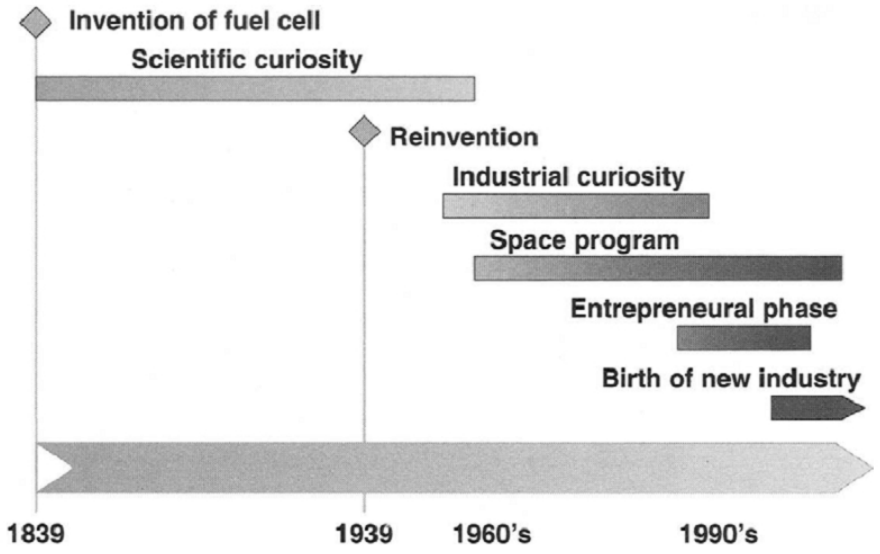

Figure 1.8 Timeline of Fuel Cells development history

The conversion of chemical energy into electrical energy in a primitive fuel cell was successfully demonstrated the first time 170 years ago by Sir W. R. Grove. In reality the principle was discovered by accident during an electrolysis experiment. The apparatus was

composed by two platinum electrodes having one end immersed in a solution of sulphuric acid and the other ends separately sealed in containers containing water and oxygen and water and hydrogen. When Sir Grove disconnected the battery and connected the two electrodes together, he observed a current flowing in the opposite direction (**Figure 1.9**) [11]. During the flow of the current, Grove observed that hydrogen and oxygen were consumed and the level of water raised in both tubes [11, 12]. His next step was to understand that connecting in series several pairs of electrodes, it was possible to produce a higher voltage drop. This first fuel cell (**Figure 1.10**), consisted of 50 monocells, was described by Grove in 1842 and was called "gas battery" [11, 13].

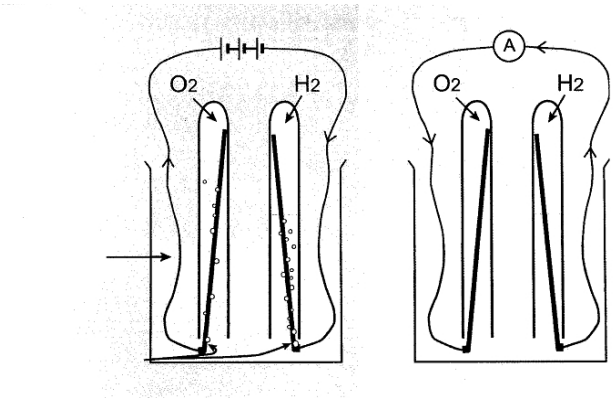

Figure 1.9 Principle of an electrolyser (left) and a fuel cell (right)[11]

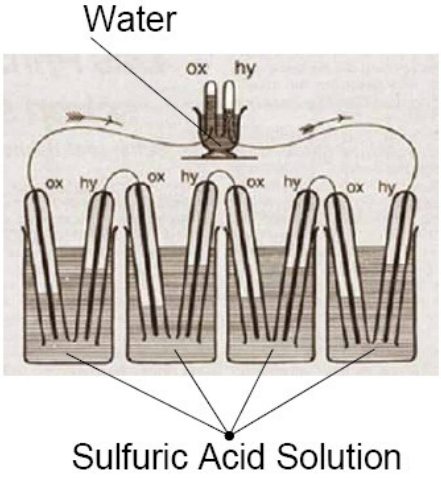

Figure 1.10 Grove's gas battery

The most important observation that Grove made about his cell, was the necessity for a significant interface between the gas, the electrolyte and the electrode metal:

"*As the chemical or catalytic action ... could only be supposed to take place, with ordinary platina foil, at the line or water-mark where the liquid, gas and platina met, the chief difficulty was to obtain anything like* ***a notable surface of action****. I determined to try the platina platinized .... It is obvious that, by allowing the platina to touch the liquid the latter* ***would spread over its surface by capillary action and expose an extended superficies to the gaseous atmosphere***."[13]

The words in bold characters, taken together, are the leitmotif of the development of today's fuel cell electrodes [14].

The poor capability to produce power from hydrogen and oxygen made Grove's series fuel cell a scientific curiosity. The scarce current produced by these devices was strictly connected to the small effective active area of each electrode. However, he did realize the need for the highest area of contact between the electrolyte, the gaseous reagent and the electrocatalytic conductor. The optimization of reaction surface is still today the basis of research and development on fuel cell electrodes. Because of this realization, Grove can be truly considered the inventor of the fuel cell [14].

Mond and Langer were the first to refine Grove's cell, following the concept that increasing the interface increases the performance [6, 14]. Grove's electrodes had a two-dimensional meniscus in which current was collected parallel to their plane. The electrodes of Mond and Langer were porous, three-dimensional and rotated by 90, this structure had all the features of the modern fuel cell. Their cells operated with hydrogen and oxygen at 0.73 V and a current density of 3.5 mA/cm^2 [14]. With the consolidation of coal as fuel, they realized that it could be used as source of hydrogen for the fuel cells, contrary to Grove that asserted that only pure hydrogen could be used as fuel [14]. Mond and Langer believed that hydrogen could become a common fuel, such as coal, reflecting the visionary hope of Oswald that the 20^{th} century would be the beginning of the "Age of Electrochemical Combustion", where the steam heat engine would be replaced by fuel cells, devices that are much more efficient and pollution-free [6, 14]. Oswald's expectation was disappointed because the electrochemical reaction rates of fossil fuels were too slow and because various types of internal combustion engines using cleaner liquid (or gaseous) fuels were produced [14]. The competition between the new engines and electric storage batteries led to the vanishing of the latter from transportation applications and, consequently, to the lack of interest in electrochemical power and fuel cells development [14].

E. Baur and W. W. Jacques were the first researchers to start again the research in the field of fuel cells. In 1921, Baur build the first molten carbonate fuel cell with gas-operated anodes [14], while Jacques was the first one to build high power systems: a 1.5-kW fuel cell with a stack of 100 tubular units and a fuel cell of 30 kW power. During the 1930s, Baur experimented solid oxide electrolytes at high temperature [6].

In early 1933, T. F. Bacon developed the first fuel cell based on hydrogen and oxygen for practical use. In that time he began to work on alkaline fuel cells. Bacon wished to use ordinary materials (i.e. no noble metals), a non-corrosive environment for maximum lifetime, and highest efficiency, i.e. the highest possible electrode reactions rates, measured in current density, at the highest practical cell voltage [14]. In 1939 he built a cell with nickel electrodes working at high pressure (200 atm) (to prevent the flooding of electrolyte to the electrode's pores) [6]. Although he liked to use steel, he employed nickel given its stability, like its oxide, in alkaline solution at both hydrogen and oxygen electrodes (although it is not stable in acid) [14]. The removal of water and heat from the high power system was obtained by circulating hot potassium hydroxide. Bacon chose as fuel hydrogen, like in Grove's cell, because he wanted to maintain an unmodified composition of the electrolyte (for this reason he avoided the use of carbonaceous fuels or air containing carbon dioxide). For a long lifetime, the working temperature of Bacon's cell was limited to 200°C, which meant that at 45 atm pressure it was possible to obtain performances of about 1 A/cm^2 at 0.8 V, or 0.4 A at 0.85 V, which would be remarkable even today [14].

Bacon continued to work on his cell up the early 1960s, as long as funding was available [14]. After this, the concept was transferred to Pratt & Whitney Company, in Connecticut, where it was modified for space applications that meant to reduce the pressure by a factor ten and at the same time to increase the temperature up to 260°C and to increase the electrolyte concentration (to 75% KOH) to prevent boiling. These modifications, together with the replacement of the circulating electrolyte (to remove heat and water) with a close-loop hydrogen cycle, did not increase cell performances, but the system was still capable of 0.15 A/cm^2 at 0.85 V [14]. Bacon's cell, modified by Pratt & Whitney, was the on-board power system for the Apollo lunar missions [14] (**Figure 1.11**). Without fuel cell technology, the lunar landings would have been impossible, because at that time alternative technologies with sufficient power and energy densities did not exist [14, 15].

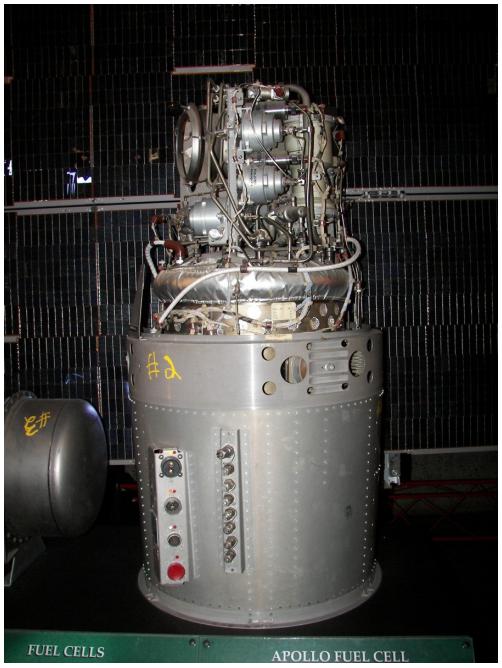

Figure 1.11 Apollo Fuel Cell Simulator

In 1950, a polymeric material called Teflon (polytetrafluoroethylene or PTFE) began to be available [6, 14]. It was used in fuel cells having platinum electrodes and acid electrolyte, or carbon electrodes and alkaline electrolyte. The employment of this material helped the development of fuel cells with aqueous electrolyte to its current status [6].

In the early 1960s, the scientists focused their attention on fuel cells having acid electrolyte and platinum catalyst. Two kinds of technologies were developed. The first one, which was simple and reliable, employed polymeric electrolytes, the latter was developed to use directly fuels derived from coal, which was not possible in alkaline fuel cells. This type of fuel cell was able to work at high temperatures (150-200°C) [6]. At the same time G. H. J. Broers and J. A. A. Ketelaarstart started to work with molten salt electrolytes, abandoning the line of oxides. The operating temperatures of these fuel cells reached 650°C.

In 1961, G. V. Elmore and H. A. Tanner obtained a fuel cell having a mixture of 35% of phosphoric acid and 65% of silicon dust stuck to the Teflon as electrolyte. They observed that the electrochemical reduction did not occur during the fuel cell operation and it could work directly with air instead of oxygen. They stated that their fuel cell could work for 6 months at 90 mA/cm^2 and 0.25 V without any apparent deterioration [6].

Finally, in 1962, J. Weissbart and R. Kuka raised the operating temperature of fuel cells up to 1000°C. They adapted the doped zirconia conducting ceramic oxide of Nernst lamp as solid electrolyte [6].

The development of fuel cells after 1970 have been characterized by the suppression of diffusion limitations in the electrodes to obtain a greater area of action, reduction of the cost of the catalysts, an increased performance and a longer lifetime [6].

Nowadays many manufacturers are working on fuel cells for several applications. Fuel cells are employed in the transportation sector (buses, cars, motorcycles, and forklifts), in vending machines, etc. Moreover, they are employed to replaces batteries in mobile phones, laptops and portable electric devices. Fuel cell systems are also used to generate electrical power at facilities of hospitals, police stations, etc. Water treatment plants and waste dumps are beginning to use fuel cells to convert methane gas produced for electricity generation [6].

1.3. Polymer Electrolyte Membrane Fuel Cells

Proton exchange membrane fuel cells (PEMFCs) have been recognized as the most promising energy converting devices, because of the low or zero emissions and the high efficiency [16].

PEM fuel cells have been the first type of fuel cells to find an application: they were the power source for NASA's Gemini space flights in the 1960s [17]. Although this technology was dormant for about 20 years, a new impulse to their development for transportation applications was given in 1990s by the California Environmental Legislations and the USA Partnership for a New Generation of Vehicles program (PNGV). The reason of the great interest on these devices was due to their fast startup, the immediate response to changes in the demand and their tolerance to shock and vibrations due to plastic materials and an immobilized electrolyte [16]. The renewed interest on PEMFCs technology, in turn, gave birth to the R&D programs for the portable power and power generation applications [17].

1.3.1. Fuel Cell Performances

The key performance of a fuel cell is the polarization curve, which displays the voltage output as a function of the electrical current density drawn (see **Figure 1.12**).

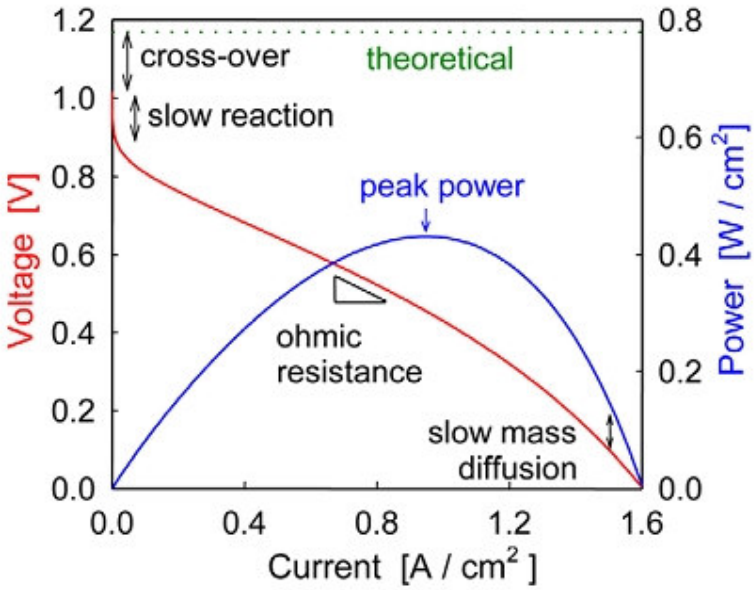

Figure 1.12 Schematic fuel cell polarization (voltage vs. current density) and power density curves [18]

In the case of an ideal fuel cell, the maximum electrical work (W_e) which can be obtained at constant temperature and pressure is related to the change of Gibbs free energy (ΔG) of the electrochemical reaction by the following equation:

(1.1) $$W_e = \Delta G = -nFU$$

where n is the number of electrons involved in the reaction, F is the Faraday constant (defined as the charge carried by one mole of electrons; its value is 96485 $C \cdot mol^{-1}$) and U is the equilibrium potential, described by the Nernst equation:

(1.2) $$U = U^0 + \frac{RT}{nF} \ln\left(\frac{\prod(\text{reactant activity})}{\prod(\text{product activity})}\right)$$

where U^0 is the equilibrium potential at standard conditions obtained from the difference between the potentials of cathode and anode. In a PEMFC which has as fuel pure hydrogen the standard potential is about 1.23 V:

Anode Reaction: $H_2 \rightarrow 2H^+ + 2e^-$ $U^0_{anode} = 0.00\ V$

Cathode Reaction: $O_2 + 4H^+ + 4e^- \rightarrow 2H_2O$ $U^0_{cathode} = 1.23\ V$

Instead for a PEM fuel cell fed by methanol (DMFC) the standard potential is of about 1.18 V:

Anode Reaction: $CH_3OH + H_2O \rightarrow CO_2 + 6H^+ + 6e^-$ $U^0_{anode} = 0.05\ V$

Cathode Reaction: $\frac{3}{2} O_2 + 6H^+ + 6e^- \rightarrow 3H_2O$ $U^0_{cathode} = 1.23\ V$

The equilibrium potential, U_{eq}, can be evaluated, in principle, knowing the reaction thermodynamics. One first determines the change in Gibbs free energy, ΔG, for the reaction under the given conditions and then calculates U_{eq} by the equation:

$$U_{eq} = -\frac{\Delta G}{nF} \tag{1.3}$$

with n the number of electrons and F the Faraday constant. In the case of the reaction $\frac{1}{2} O_2 + H_2 \rightarrow H_2O$, ΔG is given by:

$$\Delta G = \Delta G^0(T) + RT \ln \frac{P_{H_2} P_{O_2}^{1/2}}{P_{H_2O}} \tag{1.4}$$

where $\Delta G^0(T)$ is the standard Gibbs free energy of the reaction, when all species involved are in their standard states (1 bar, pure gases); this term is tabulated or can be calculated from the standard formation energies and entropies of the species involved (in the case of the reaction $\frac{1}{2} O_2 + H_2 \rightarrow H_2O$ its value is -242 kJ/mol + (45.8 J/mol K) * T for all components in the vapour phase) [18]. This term alone is used to define the standard potential of a particular reaction:

$$U^0 = -\frac{\Delta G^0}{nF} \tag{1.5}$$

In a fuel cell to know the standard potential means to know the partial pressure of all the species involved in the reaction. With hydrocarbon-based fuel, the partial pressures of the gases produced are neither measured nor controlled and cell potential is usually compared to the standard potential [18].

Under open circuit conditions (no current is drawn) the measured voltage should be the same as the equilibrium voltage.

When the fuel cell is delivering current, the measured voltage U can be written as:

$$U = U_{eq} - \eta_{act} - \eta_{iR} - \eta_{diff} \quad (1.6)$$

where U_{eq} is the equilibrium potential (Nernstian voltage), η_{act} is the activation overpotential due to the slow electrode reactions, η_{iR} is the overpotential due to the ohmic resistances in the cell and η_{diff} is the overpotential due to the mass diffusion limitations [18].

The voltage measured is reduced by losses due to [18, 19]:

- Activation overpotential (η_{act}) due to the slow reactions at both the cathode and the anode. It is dominant at low current density giving to the polarization curve the logarithmic characteristic. This loss is directly related to the barriers that must be overcome by the reacting species prior the current flow.
- Overpotential due to the mass diffusion (η_{diff}). Its value is specific to the geometry under consideration, but it is generally established by the rate of reactants flowing to the electrolyte through the electrodes and the rate of products flowing away.
- Ohmic overpotential (calculated by: $\eta_{iR} = iR$, where R is the area specific resistance) includes terms from the electrolyte, electrodes, current collectors and lead wires in the system. This loss varies directly with the current density and the cell resistance. Because the latter term remains constant, the Ohmic loss increases with the current density.

The impact of these losses on cell voltage is shown in **Figure 1.12**. The power density is given by the product of the voltage and the current density, and as shown in the figure, it reaches a maximum at intermediate voltages (or current density).

Concerning the polarization curve, high power densities result when gas diffusion and electron transport through the electrolytes are absent, electrocatalysis at the electrodes is rapid, the conductivity of each of the components, in particular, the electrolyte, is high, and mass

diffusion through the porous electrodes is facile. Thus, the ideal fuel cell electrolyte is not only highly ionically conducting, but also impermeable to gases, electronically resistive and chemically stable under a wide range of conditions. Moreover, the electrolyte must exhibit sufficient mechanical and chemical integrity so as not to develop cracks or pores either during manufacture or in the course of long-term operation [18].

The efficiency of a fuel conversion device is defined as the amount of useful energy produced relative to the change in enthalpy, ΔH, between the product and feed streams.

$$\eta = \frac{Useful\ Energy}{\Delta H} \tag{1.7}$$

Most of the chemical energy stored in the reactant can be converted by fuel cells into electricity:

$$\text{Chemical Energy} \rightarrow \text{Electrical Energy}$$

The ideal efficiency of the fuel cell that operates reversibly can be calculated from the Gibbs free energy change (ΔG) and the enthalpy change (ΔH) of the electrochemical reaction:

$$\eta = \frac{\Delta G}{\Delta H} \tag{1.8}$$

Eq. **(1.8)** describes the ratio between the maximum electric work that can be obtained from a fuel cell and the overall energy that can be transformed into heat. Ideally the free energy of the reaction can be completely converted into electrical energy. Thus the energy of an ideal fuel cell operating reversibly on pure hydrogen and oxygen in standard conditions (1 atm and 25°C) would be 0.83.

In the case of an actual fuel cell, the efficiency is expressed in terms of the ratio of the operating cell voltage to ideal voltage. An actual fuel cell has a lower efficiency because of losses associated with cell polarization and ohmic losses, the efficiency of a hydrogen/oxygen fuel cell can be written in terms of the actual cell voltage by:

$$\eta_{actual} = \frac{0.83 \cdot V_{actual}}{U_{ideal}} \tag{1.9}$$

1.3.2. Basic Cell Structure and Components

The basic structure and the main components of a PEM fuel cell are shown in **Figure 1.13**. The single cell contains [16, 20]:

- Porous gas diffusion electrodes (anode and cathode);
- Proton conducting electrolyte;
- Anodic and cathodic catalyst layers;
- Current collectors with the reactant flow fields.

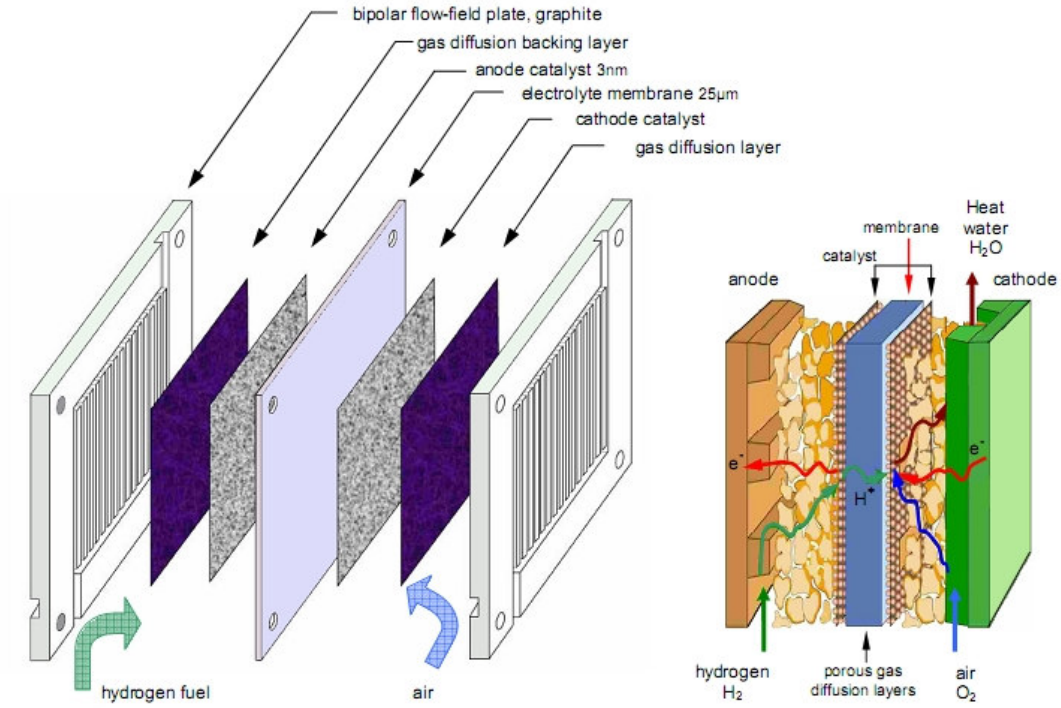

Figure 1.13 The parts of a fuel cell/membrane/electrode assembly with backing layers. Enlarged cross-section of a membrane/electrode assembly showing structural details

The proton conducting membrane (electrolyte) is the heart of the fuel cell. On both sides of the membrane there is a porous electrode. The electrodes must be porous because the reactant gases are fed from the back and reach the interface between the electrodes and the membrane, where the electrochemical reactions take place in the so-called catalyst layers, or more precisely on the catalyst surface. Technically, the catalyst layer may be a part of the porous electrode or part of the membrane, depending on the manufacturing process [21]. The assembly of the membrane sandwiched between the two electrodes is commonly called Membrane Electrode Assembly (MEA). The MEA is then sandwiched between the collector/separator plates that conduct electrical current (collector) and separate the gases in the adjacent cells (separator) in

multicell configuration. At the same time, in multicell configuration they physically and electrically connect the cathode of one cell to the anode of the adjacent cell, and that is why they are also called the bipolar plates. They provide the pathways for flow of reactant gases (so called flow fields), and they also provide the cell structural rigidity [21].

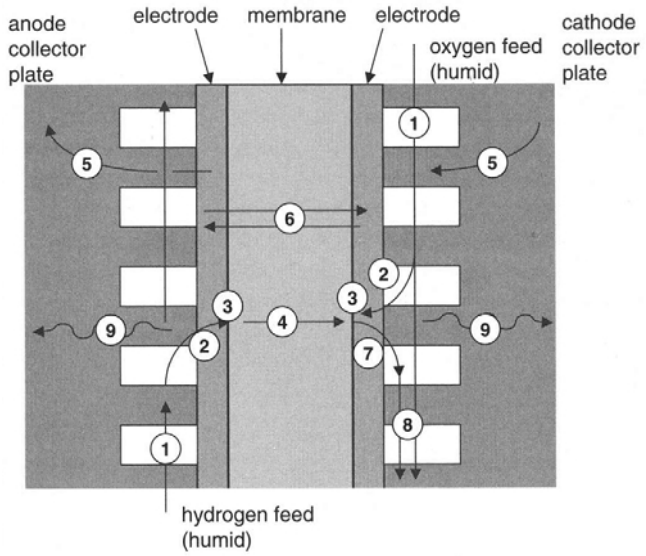

Figure 1.14 Main fuel cell components and processes

During the fuel cell operation, the following processes take place [21]:

1. Gas flows through the channels; some convective flows may be induced in the porous layers.
2. Gas diffusion through porous media.
3. Electrochemical reactions, including all the intermediary steps.
4. Proton transport through proton conducting membrane.
5. Electron conduction through electrically conductive cell components.
6. Water transport through polymer membrane including both electrochemical drag and back diffusion.
7. Water transport (both vapour and liquid) through porous catalyst layer and gas diffusion layers.
8. Two-phase flow of unused gas carrying water droplets.
9. Heat transfer, including both conduction through solid components of the cell and convection to reactant gases and cooling medium.

Electrodes

The electrodes consist of a conducting catalyst support material (often a porous form of carbon), which is impregnated with platinum or platinum alloy catalyst [20]. On this layer the electrochemical reactions take place. More precisely, the electrochemical reactions take place on the catalyst surface [21], where all the species that participate in the reactions (gases, electrons and protons) have access. While electrochemical reactions take place,

- The electrons travel through the electrically conductive solids, including the catalyst itself. The electrons migration is guaranteed only if the catalyst particles are electrically connected to the substrate.
- The protons travel through the electrolyte. The migration of protons is guaranteed only if the catalyst is in intimate contact with the electrolyte.
- The reactant gases travel only through voids; the requirement of the porosity of electrodes guarantees that gases travel to the reactions sites.

At the same time the water produced from reactions must be effectively removed (otherwise the electrode would be flooded and this would prevent the oxygen access at the cathode) [20, 22].

Polymer Electrolyte Membrane

A polymer electrolyte membrane must exhibit in the fuel cell environment the following properties [23-26]:

- High proton conductivity to support high currents with minimal resistive losses and zero electronic conductivity;
- Present an adequate barrier to mixing of fuel and reactant gases;
- Chemical and electrochemical stability;
- Adequate mechanical strength and stability;
- Production costs compatible with intended application.

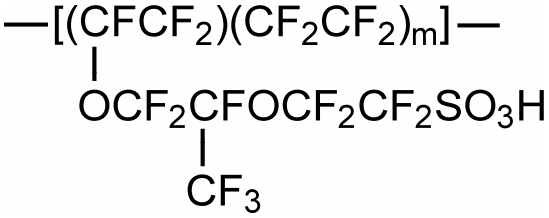

Figure 1.15 Nafion® structure

Nafion® made by DuPont Inc. (structure shown in **Figure 1.15**) is the best known membrane material used in PEMFCs. In commercial Nafion®, m varies from about 5 to 11. This generates an equivalent weight (EW) ranging from about 1000 to 1500 g of dry Nafion per mole of sulfonic acid groups, corresponding to an ion exchange capacity ranging from 1.0 to 0.67 meq/g.

The membranes based on Nafion® meet a lot of requirements listed above. They posses high acidity and in a fuel cell environment they offer high proton conductivity, chemical stability and longevity [1, 27]. Nafion® consists of a polytetrafluoroethylene-based (PTFE) structure which is chemically inert in reducing and oxidising environments [1]. PTFE structure provides furthermore mechanical and thermal stability. The perfluorinate side chains terminating with hydrophilic sulfonic acid groups provide the channels for proton conduction (see **Figure 1.16**) [23, 28, 29].

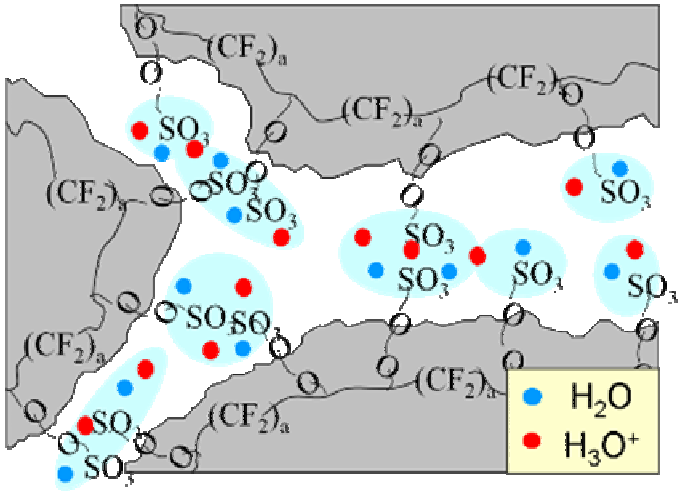

Figure 1.16 The Nafion structure: the grey zone are the hydrophobic regions consisting of PTFE backbone and the white zone is the hydrophilic region with sulphonate ions and dissociated H^+[1] (image source:www.tagen.tohoku.ac.jp/labo/kawamura/each_member/horiuchi/kenkyu/sample.htm)

In addition to Nafion, different polymers are under development. Examples of such polymers (**Figure 1.17**) are radiation-grafted membranes 1) PVDF (Poly-VinyliDene-Fluoride), 2) heterocyclic polymers such as PBI (Poly-Benz-Imidazole) and 3) sulfonated aromatic hydrocarbons. Some of these materials, especially PBI and sulfonated aromatic polymers, exhibit high chemical and thermal stability associated to a high value of conductivity.

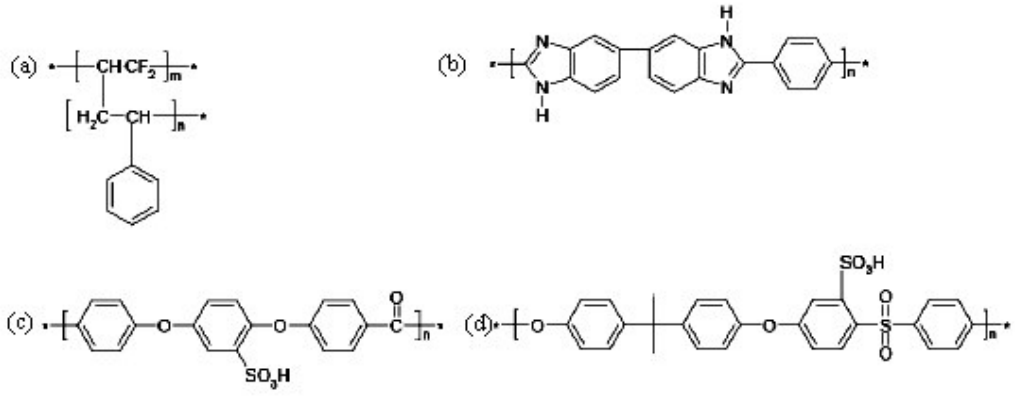

Figure 1.17 Molecular Structure of (a) PVDF-g-PSSA, (b). PBI, (c), S-PEEK, (d) S-PSU

1.3.3 Water Management

Water Management is of vital importance to ensure stable operation, high efficiency and to maintain the power density of PEM fuel cells in the long run [30]. On one hand it is important keep the membrane humidified for high proton conductivity [30]. The lack of water in the membranes and gas diffusion electrodes decreases their proton conductivity and significantly increases the cell resistance [31]. On the other hand the accumulation of too much water also impacts performance and lifetime of the fuel cell. An excess of water in the cathode causes "flooding", which restricts oxygen transport through the porous gas diffusion electrode (and slows down the oxidation reaction) [24, 30-33].

Figure 1.18 shows the different modes of water transport through PEMFCs. Contributing factors to water transport are the water drag through the cell, back diffusion to the cathode and the diffusion of water in the fuel stream through the anode [34]. Water transport is not a function of the operating conditions but also the characteristics of the membrane and the electrode [34].

The electro-osmotic drag term is a measure of hydration and is defined as the number of water molecules transported per proton [24, 31]. The production of water at the cathode results in a gradient of water content across the membrane that may result in back diffusion of water from cathode to anode. If a differential pressure exists, hydraulic pressure may also force water from cathode to anode. In the absence of the latter, the net water flux across the membrane is a combination of diffusion and electro-osmotic drag, which has a profound impact on fuel cell performance [31].

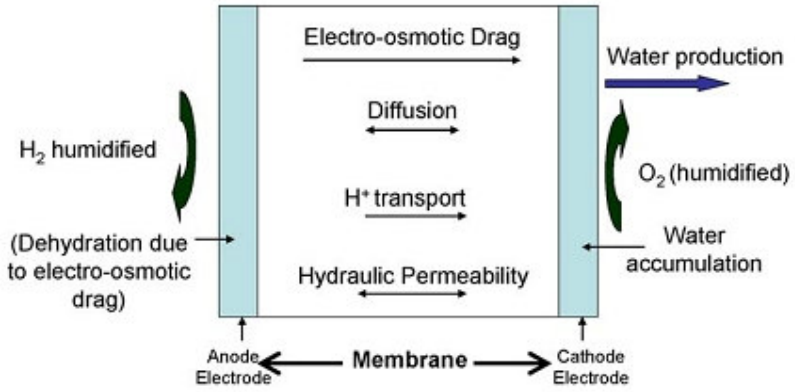

Figure 1.18 Scheme of water transport modes in a PEMFC

One way to improve fuel cell performance and avoid water drag or water cross over is to reduce the membrane thickness. The reduced membrane thickness allows lower membrane resistance, lower cost and rapid hydration. However, there is a limit to the extent to which membrane thickness can be reduced because of difficulties with durability and fuel by-pass. An ideal way to balance this would be to spatially control the acidic regions or increase the charge density in the chemical microstructure of the proton exchange membrane to obtain highly conductive materials [24].

1.4. Proton Exchange Membranes Based on Sulfonated Aromatic Polymers

In spite of their many good qualities, Nafion-based membranes have several deficiencies. They are expensive, allow methanol crossover in Direct Methanol Fuel Cells, with adverse effect on performance, cannot function well at low humidity (below ~80% RH), or high temperatures (above 80°C) and require external humidification and therefore management of water [23, 27]. However, it is desirable to operate at temperatures above 80°C in the range of 120-140°C to reduce the anode (containing Pt as a catalyst) poisoning due to the adsorbed CO, present as fuel impurity, and to improve the fuel oxidation kinetics leading to an enhancement of fuel cell efficiency. Furthermore, due to the low operating temperature, liquid water is continuously produced at the cathode compartment that can cause its flooding [35-37]. The strong dependence of proton conductivity on hydration is another limitation of perfluorinated ionomers [33].

Whereas water sorption improves on one hand the proton conductivity, it leads on the other hand to morphological instability and at elevated water content to membrane swelling. Membrane swelling at high temperature is a serious drawback for use in a membrane electrode assembly, leading to risks of rupture and degradation of electrical contacts as well as to

mechanical stress of the ionomer due to drastic cycles of hydration-dehydration of the membranes.

Thus it is essential to develop new polymer electrolytes that have good proton conductivity up to 120-130°C, good mechanical and thermal stability, good water retention at high temperature, good chemical stability in the strong oxidation environment present in the fuel cell, low fuel permeability. These materials should preferably retain a high conductivity at low levels of humidification.

Aromatic hydrocarbon based membranes are a promising alternative to Nafion because of their low cost, processability, wide latitude to tune chemistry, and mechanical, thermal and oxidative stability [38]. Among them, sulfonated aromatic polymers (SAPs) exhibits high conductivity and are therefore of interest for PEMFCs. Most important examples are Poly-Ether-Ether-Ketone (PEEK), Poly-Ether-Ether-Ketone-WC (PEEK-WC), Poly-Ether-Sulfone (PES) and Poly-Phenyl-SUlfone (PPSU) polymer families, shown in **Figure 1.19**. Due to the aromatic rings, these hydrocarbon polymers as backbones allow the introduction of sulfonic acid moieties to render the desired level of conductivity for fuel cell application and also possess good chemical resistance and mechanical properties. From a chemical point of view, the good oxidation resistance of aromatic hydrocarbons is due to the fact that the C-H bonds of the benzene ring have typical bond strength of around 435 kJ mol^{-1}, compared with aliphatic C-H bond strengths, around 350 kJ mol^{-1} [39]. Proton conduction in SAP is water assisted; consequently the hydration content is a crucial factor for better electrochemical performance.

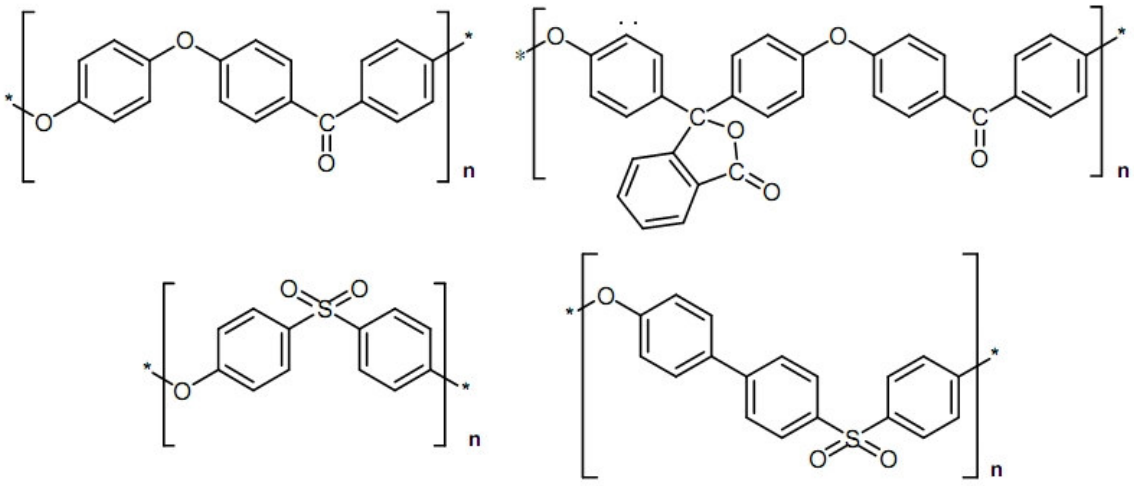

Figure 1.19 Some important SAPs: Poly-Ether-Ether-Ketone, Poly-Ether-Ether-Ketone-WC, Poly-Ether-Sulfone and Poly-Phenyl-Sulfone, respectively.

Water uptake increases with degree of sulfonation (DS = number of -SO_3H groups per repeated unit) thereby improving the conductivity of the hydrated membrane. However, highly polar water molecules act as a plasticizer, undermining the electrostatic interactions between SAP molecular chains and favouring membrane swelling. Highly sulfonated aromatic polymers swell rather strongly in water and become even soluble if the sulfonation degree is high enough [40, 41]. Besides of the large swelling of SAP membranes, several degradation phenomena can reduce their lifetime. The main four types of degradation are [42, 43]:

- Chemical degradation. The hydrogen and oxygen crossover to opposite sides of the membrane leads to a thickening of the fuels. H_2 and O_2 react with a very exothermal combustion to give H_2O_2 molecules. The peroxide decomposes, giving •OH or •OOH radicals that attack the polymer structure initiating the chemical decomposition.
- Thermal degradation. Usual SAP membranes stop working at high temperatures due to the low glass transition temperatures of the polymers. Furthermore membrane protonic conductivity decreases significantly when the fuel cell is operated at high temperature and under low humidity.
- Mechanical degradations. During fuel cell operation, dimensional changes, due to the swelling/contraction of the membrane in different humidification conditions and the exothermic combustion of the reductant, cause perforations, fractures and pinholes. These defects further increase gas crossover and therefore a critical sequence of increasing gas crossover and pinhole formation is quickly established.
- Conductivity degradation. It was recently found that the decay of proton conductivity can be associated with the occurrence of an anisotropic membrane swelling in the direction parallel to the electrodes. In fact permanent deformations can be created when water is taken up (swelling) and the decay is essentially due to a transition of the original polymer conformation to a new conformation of lower conductivity [24].

In order to reduce the excessive swelling of highly sulfonated SAP-based membranes and enhance their lifetime reducing degradation processes, three principal strategies have been followed:

- Development of cross-linked ionomers with controlled swelling properties and/or reduced crossover of oxygen;
- Development of new materials more stable with regard to the physico-chemical processes in the cell;

- Development of additives which can improve the stability of existing materials. The stabilizing agent must not only present sufficient activity versus the degradation vectors formed in the cell, but also be perfectly compatible with the polymer matrix. In fact, phase segregation would lead to loss of efficiency of the stabilizing agent and a loss of performance of the fuel cell.

1.4.1. Hybrid Polymers Approach

Before to tackle the concept of hybrid polymers, it is useful to remind some definitions. A useful criterion for hybrid materials classification is based on their chemical nature [44, 45] (**Figure 1.20**):

- **Class I**: organic and inorganic components are dispersed and held together only by weak forces, such as Van der Waals interactions. In this context, Van der Waals interactions are considered to include permanent dipole interactions (Keesom forces, including also hydrogen bonds), interactions between permanent and induced dipoles (Debye forces) and interactions between induced dipoles (London forces).
- **Class II**: organic and inorganic moieties are linked through strong bonds, such as covalent bonds [46].

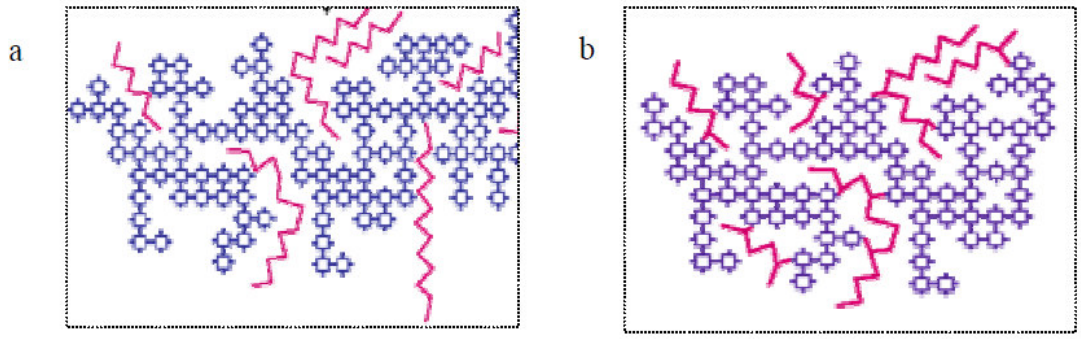

Figure 1.20 (a) Class 1 and (b) Class II hybrids

Class I hybrid materials and composites differ from each other in respect to the dimension of dispersion. However this difference is minimal when we consider 'nanocomposites'. A nanocomposite is a material with nanometric domains of two coexisting phases without mutual solubility. In the following we will use the two terms, Class I and composite as interchangeable [39].

Recently, in our laboratories, a method for the formation of a Class II organic-inorganic hybrid polymer, where the organic and inorganic moieties were linked through covalent bonds, was reported [47-49].

The strategy followed in this thesis was to find an optimal compromise between enhancement of proton conductivity by sulfonation and improvement of thermal and morphological stability by silylation. We have prepared nanocomposite materials with a majority partner, sulfonated PEEK with high degree of sulfonation, and a minority partner, PPSU in unsubstituted or silylated form. The majority partner should assure good proton conductivity of the composite membrane and the minority partner, the anchor phase, should improve the mechanical properties and stabilize the morphology of the composite polymer.

A parallel strategy is to disperse an inorganic component in an organic polymer, obtaining a composite belonging to Class I hybrids. The organic matrix used was sulfonated poly(ether ether ketone) (S-PEEK) while the inorganic components added to the organic matrix were organically functionalized TiO_2 nano-powders.

Nanostructured TiO_2, with a typical dimension less than 100 nm, is used in many applications. In particular its chemical stability, even under strongly acidic or basic conditions, and its capability to modify the hydrophilic/hydrophobic balance in the hybrid systems make the material suitable to be used as filler in polymeric electrolyte membranes [50]. In fact the presence of the inorganic filler is expected to accentuate the phase separation between the hydrophobic and hydrophilic domains, which is a factor controlling the water channeling and proton conductivity in PEMFCs [51].

1.4.2. Cross-Link Approach

1.4.2.1. Cross-Linking Formed by Thermal Treatments

The formation of cross-links is a well established technique to improve the performances of polymers [52, 53].

The covalent approach was investigated especially by Kerres et al. They studied both covalent and ionically crosslinked sulfonated polysulfone that exhibit an increased dimensional stability compared to uncrosslinked membranes. In particular they investigated two types of covalent crosslinking [53, 54]. In the first type, the polysulfone contains both sulfonate and sulfinate groups. The sulfonate functions ensure the conductivity, while the sulfinate leads to a cross-linked ionomer. In the second type, the membrane contains a mixture of polysulfone-

sulfinate and polysulfone-sulfonate polymers resulting in a semiinterpenetrated network. For both cross-linking systems, it has to be emphasized that swelling and water solubility can be improved compared to uncrosslinked membranes.

The main drawbacks of this technique are the presence of cross-linker molecules that are in general sensible to the severe conditions in a fuel cell and the elaborate or expensive procedures that make the entire process little competitive from an industrial point of view.

A direct cross-linking reaction performed in situ during the casting procedure can be instead an interesting and promising methodology to obtain stable membranes. (**Figure 1.21**).

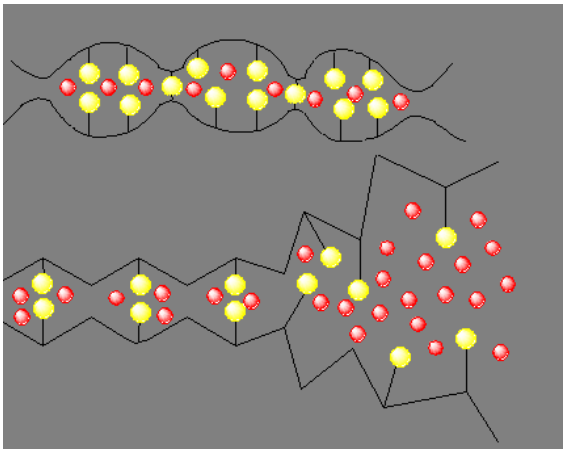

Figure 1.21 Schematic representation of non cross-linked (below) and cross-linked polymer (above) (Red dots represent water molecules, yellow dots represent sulfonic acid groups)

The aim of the present strategy is to explore whether it is possible to enhance the performance of sulfonated aromatic polymers in a simple and economical way by appropriate thermal "curing" treatments. We will also examine if the formation of covalent bonds among macromolecular chains can stabilize the polymer microstructure and can make them suitable for further investigations.

1.4.2.2. Cross-Linking by Cold Plasmas

Non-isothermal glow discharge treatment of polymer surfaces can give rise to desirable properties. The active plasma medium consists of atomic and molecular species, as well as ions, electrons, and a broad electromagnetic spectrum. Plasma is a highly reactive and complex

medium, which can offer a low cost, environmentally friendly means for altering the physicochemical characteristics of a polymer surface at ambient temperature. Inert gas plasmas interact with organic substrates via a direct energy transfer component arising from ions and metastable species down to ≈1 nm and a radiative transfer component consisting of vacuum ultraviolet (VUV) photoirradiation, which can penetrate up to ≈10 μm below a polymer surface. In terms of surface modification, the most important criteria of a glow discharge are the nature, the arrival rates, and the angular and energy distributions of the species impinging upon the surface. [55].

1.5. Outline of Our Work

In this thesis, we will study hybrid composite membranes, where only Van der Waals bonds are present, based on S-PEEK with a hybrid polymer or an inorganic oxide as second phase. We will also investigate the effect of a thermal treatment of SAP membranes and the formation of covalent cross-links between macromolecular chains.

The studied physical and chemical properties include generally structure and microstructure by X-Ray Diffraction, Atomic Force Microscopy, NMR and FTIR spectroscopies, thermal stability investigated by thermogravimetric analysis, water uptake by immersion in liquid water and water vapour sorption isotherms, mechanical properties, studied by stress-strain tests and dynamic mechanical analysis, and proton conductivity, studied by impedance spectroscopy and dielectric analysis. Some fuel cell tests of cross-linked SAP membranes are reported at the end.

1.6. References

[1] L. Carrette, K. A. Friedrich and U. Stimming, *Chemphyschem* **2000**, *1*, 162-193.

[2] K. Joon, *Journal of Power Sources* **1997**, *71*, 12-18.

[3] B. W. Williams, *Principles and Elements of Power Electronics: Devices, Drivers, Applications, and Passive Components*, Barry W. Williams, **2006**, p. 835-942.

[4] *Comparison of Fuel Cells Technology*, *Vol.* (Ed. D. o. E. H. P. (www.hydrogen.energy.gov)), DOE Hydrogen Program, **2008**.

[5] K. V. Kordesch and G. R. Simader, *Chemical Reviews* **1995**, *95*, 191-207.

[6] J. M. Andujar and F. Segura, *Renewable and Sustainable Energy Reviews* **2009**, *13*, 2309-2322.

[7] M. Winter and R. J. Brodd, *Chemical Reviews* **2004**, *104*, 4245-4269.

[8] G. Hoogers, *Fuel Cell Technology Handbook*, CRC Press, **2003**, p. 1-20.

[9] S. Cleghorn, W. Kolde and W. Liu, *Handbook of Fuel Cells-Fundamentals, Technology and Application*, J. Wiley and Sons, Ltd, Chichester, **2003**, p.

[10] F. Barbir, *PEM Fuel Cells: Theory and Practice*, Elsevier Inc., **2005**, p. 1-16.

[11] B. Cook, *Enginnering Science and Educational Journal* **2002**, *11*, 205-216.

[12] W. R. Grove, *Philosophical Magazine Series 3, 14 (86)*, **1839**, p. 127.

[13] W. R. Grove, *Philosophical Magagazine Series 3, 21 (140)*, **1842**, p. 417.

[14] A. J. Appleby, *Journal of Power Sources* **1990**, *29*, 3-11.

[15] K. Ledjeff, *Brennstoffzellen: Entwicklung - Technologie - Anwendung*, C.F.Müller, Heidelberg, **1995**, p.

[16] Y. Y. Shao, G. P. Yin, Z. B. Wang and Y. Z. Gao, *Journal of Power Sources* **2007**, *167*, 235-242.

[17] P. Costamagna and S. Srinivasan, *Journal of Power Sources* **2001**, *102*, 242-252.

[18] S. M. Haile, *Acta Materialia* **2003**, *51*, 5981-6000.

[19] *Fuel Cells Handbook (7th edition)*, U.S. Departement of Energy National Energy Technology Laboratory, **2004**, p. 2.1-2.34.

[20] A. F. Ismail, R. Naim and N. A. Zubir, *Fuel Cell Technology Review*, Springer Science + Business Media, LLC, **2009**, p. 27-49.

[21] F. Barbir, *PEM Fuel Cells: Theory and Practice*, Elsevier Inc., **2005**, p. 73-113.

[22] *Fuel Cells Handbook (7th edition)*, U.S. Department of Energy National Energy Technology Laboratory, **2004**, p. 1.1 - 1.34.

[23] V. Neburchilov, J. Martin, H. J. Wang and J. J. Zhang, *Journal of Power Sources* **2007**, *169*, 221-238.

[24] B. Smitha, S. Sridhar and A. A. Khan, *Journal of Membrane Science* **2005**, *259*, 10-26.

[25] G. G. Scherer, *Fuel Cells I and II (Advances in Polymer Science)* Springer, **2008**, p.

[26] T. Kobayashi, M. Rikukawa, K. Sanui and N. Ogata, *Solid State Ionics* **1998**, *106*, 219-225.

[27] R. Devanathan, *Energy & Environmental Science* **2008**, *1*, 101-119.

[28] J. A. Kerres, *Journal of Membrane Science* **2001**, *185*, 3-27.

[29] K. D. Kreuer, *Journal of Membrane Science* **2001**, *185*, 29-39.

[30] W. Schmittinger and A. Vahidi, *Journal of Power Sources* **2008**, *180*, 1-14.

[31] J. L. Zhang, Z. Xie, J. J. Zhang, Y. H. Tanga, C. J. Song, T. Navessin, Z. Q. Shi, D. T. Song, H. J. Wang, D. P. Wilkinson, Z. S. Liu and S. Holdcroft, *Journal of Power Sources* **2006**, *160*, 872-891.

[32] M. L. Di Vona, E. Sgreccia, S. Licoccia, M. Khadhraoui, R. Denoyel and P. Knauth, *Chemistry of Materials* **2008**, *20*, 4327-4334.

[33] M. Casciola, G. Alberti, M. Sganappa and R. Narducci, *Journal of Power Sources* **2006**, *162*, 141-145.

[34] *Fuel Cells Handbook (7th edition)*, U.S. Department of Energy National Energy Technology Laboratory, **2004**, p. 3.1 - 3-25.

[35] N. Gourdoupi, A. K. Andreopoulou, V. Deimede and J. K. Kallitsis, *Chemistry of Materials* **2003**, *15*, 5044-5050.

[36] Q. F. Li, R. H. He, J. O. Jensen and N. J. Bjerrum, *Chemistry of Materials* **2003**, *15*, 4896-4915.

[37] G. Alberti, M. Casciola, L. Massinelli and B. Bauer, *Journal of Membrane Science* **2001**, *185*, 73-81.

[38] G. Maier and J. Meier-Haack, *Sulfonated Aromatic Polymers for Fuel Cell Membranes in Fuel Cells II* G. G. Scherer (Ed) Springer, **2008**, p.

[39] Y. D. Premchand, M. L. Di Vona and P. Knauth, *Proton-Conducting Nanocomposites and Hybrid Polymers*, Springer, **2008**, p. 71 - 117.

[40] P. X. Xing, G. P. Robertson, M. D. Guiver, S. D. Mikhailenko, K. P. Wang and S. Kaliaguine, *Journal of Membrane Science* **2004**, *229*, 95-106.

[41] V. S. Silva, S. Weisshaar, R. Reissner, B. Ruffmann, S. Vetter, A. Mendes, L. M. Madeira and S. Nunes, *Journal of Power Sources* **2005**, *145*, 485-494.

[42] A. Collier, H. J. Wang, X. Z. Yuan, J. J. Zhang and D. P. Wilkinson, *International Journal of Hydrogen Energy* **2006**, *31*, 1838-1854.

[43] C. Perrot, L. Gonon, M. Bardet, C. Marestin, A. Pierre-Bayle and G. Gebel, *Polymer* **2009**, *50*, 1671-1681.

[44] C. Sanchez, G. Soler-Illia, F. Ribot and D. Grosso, *Comptes Rendus Chimie* **2003**, *6*, 1131-1151.

[45] P. H. Mutin, G. Guerrero and A. Vioux, *Comptes Rendus Chimie* **2003**, *6*, 1153-1164.

[46] C. Sanchez and F. Ribot, *New Journal of Chemistry* **1994**, *18*, 1007-1047.

[47] M. L. Di Vona, D. Marani, C. D'Ottavi, M. Trombetta, E. Traversa, I. Beurroies, P. Knauth and S. Licoccia, *Chemistry of Materials* **2006**, *18*, 69-75.

[48] D. Marani, M. L. Di Vona, E. Traversa, S. Licoccia, I. Beurroies, P. L. Llewellyn and P. Knauth, *Journal of Physical Chemistry B* **2006**, *110*, 15817-15823.

[49] M. L. Di Vona, D. Marani, A. D'Epifanio, S. Licoccia, I. Beurroies, R. Denoyel and P. Knauth, *Journal of Membrane Science* **2007**, *304*, 76-81.

[50] M. Watanabe, H. Uchida, Y. Seki, M. Emori and P. Stonehart, *Journal of the Electrochemical Society* **1996**, *143*, 3847-3852.

[51] Y. Yang and S. Holdcroft, *Fuel Cells* **2005**, *5*, 171-186.

[52] J. Kerres, W. Cui, R. Disson and W. Neubrand, *Journal of Membrane Science* **1998**, *139*, 211-225.

[53] J. A. Kerres, *Fuel Cells* **2005**, *5*, 230-247.

[54] J. Kerres, W. Zhang and W. Cui, *Journal of Polymer Science Part a-Polymer Chemistry* **1998**, *36*, 1441-1448.

[55] D. Ramdutt, C. Charles, J. Hudspeth, B. Ladewig, T. Gengenbach, R. Boswell, A. Dicks and P. Brault, *Journal of Power Sources* **2007**, *165*, 41-48.

Chapter 2: Experimental - Materials and Measurements

2.1. Materials

Poly-Ether-Ether-Ketone (PEEK) was obtained from Victrex (450P, MW = 38300 g/mol and 132 repeat unit per mol) and Poly-Phenyl-SUlfone (PPSU) from Solvay (5100P, MW = 46173 g/mol and 115 repeat units per mol). Poly-Ether-Sulfone (PES) was obtained from Victrex (300 P, MW = 67080 g/mol, 32 meq). Functionalized titanium dioxide (TiO_2) was provided by Tronox Pigments GmbH (Germany) (Titanoxide-Hydrate, Anatase, 350 m^2/g). All polymers and TiO_2 were in the form of powder and were used as received.

Anhydrous THF (Tetrahydrofuran) was prepared according to literature procedures [1]. All other chemicals (Aldrich) were reagent grade and were used as received.

2.1.1. Synthesis of S-PEEK: Sulfonation of PEEK

Sulfonated PEEK (S-PEEK) was prepared by reaction of PEEK with concentrated sulfuric acid (H_2SO_4) at 50°C or at RT for times between 5 hours and 11 days (for reaction conditions see **Table 2.1**), depending on the wanted degree of sulfonation. The solution was poured in excess of ice-cold water, under continuous stirring, obtaining a white precipitate. After standing overnight, the precipitate was filtered and washed several times to neutral pH. The sulfonated polymer (S-PEEK) was dried in an oven for 17 hours at the temperature of 80°C - 85°C [2]. The degree of sulfonation (DS), defined as the number of sulfonic groups per monomeric unit, was evaluated by ^1H NMR [3, 4] and by titration with according results.

DS	Temperature [°C]	Time [h]
0.60	25	100
0.70	25	170
0.75	25	265
0.90	50	120

Table 2.1 Degree of sulfonation, temperature and time of sulfonation of PEEK

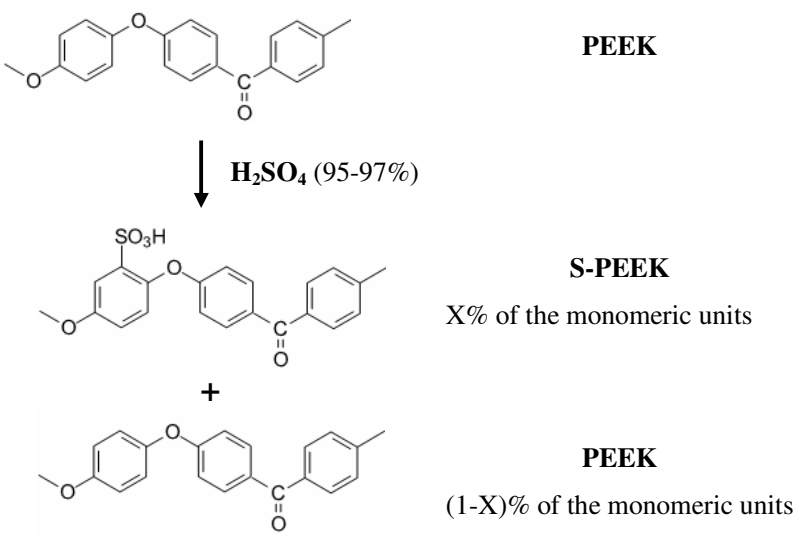

Figure 2.1 Scheme of sulfonation of PEEK

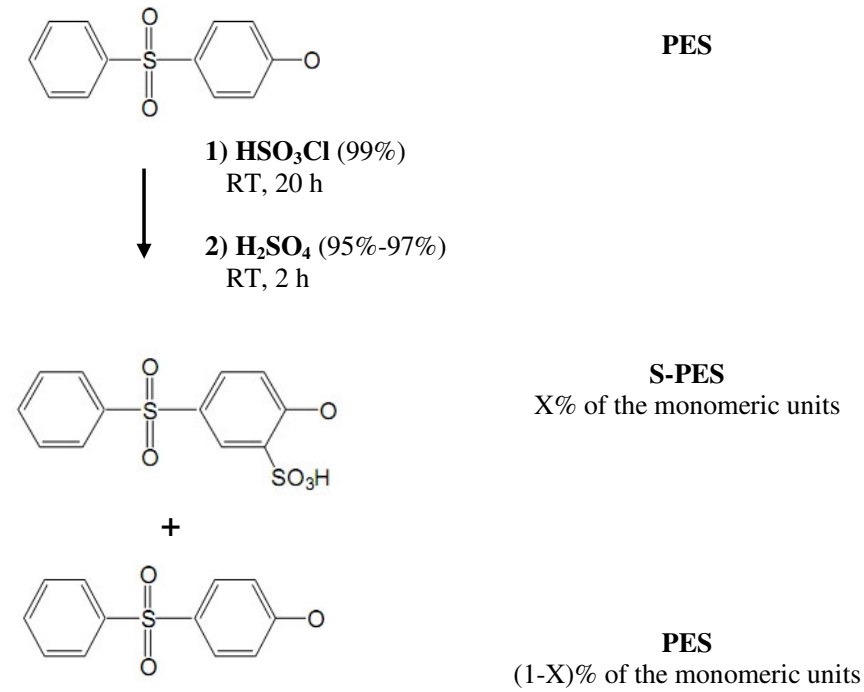

Figure 2.2 Sulfonation of PES using chlorosulfonic acid and sulfuric acid

2.1.2. Synthesis of S-PES: Sulfonation of PES

Sulfonated Polyethersulfone (S-PES) was obtained by adding the polymer in chlorosulfonic acid (HSO_3Cl, 99%) and stirring the solution at RT for 20 hours. The solution was then poured in concentrated sulfuric acid (H_2SO_4) and stirred at RT. After 2 hours the solution obtained was poured into a large excess of ice-cold water under continuous stirring obtaining a white precipitate. After standing overnight, the precipitate was washed with ice-cold water until pH value of 5-6 and dried at 80°C for 20 hours under vacuum [5]. The degree of sulfonation, evaluated both by titration and NMR, was 0.83.

The sulfonation of PES was also tried using sulfuric acid. The procedure followed was to dissolve the polymer in concentrated H_2SO_4 and to keep the solution stirring at RT or at 50°C for times between 4 hours and 24 hours. The solution was poured in excess of ice-cold water, under continuous stirring, obtaining a white precipitate. After standing overnight, the precipitate was filtered and washed several times to neutral pH. The sulfonated polymer (S-PES) was dried in an oven for 17 hours at the temperature of 80°C - 85°C.

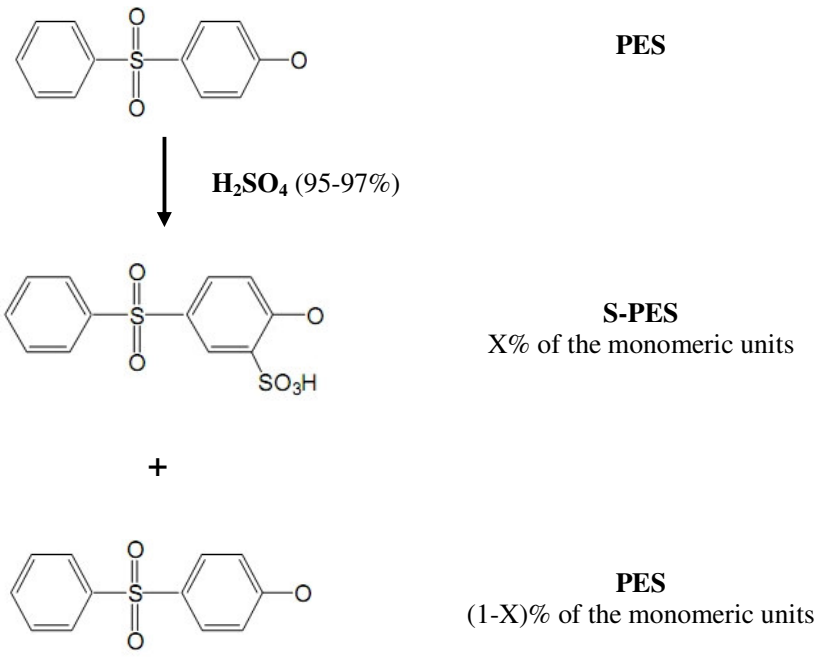

Figure 2.3 Sulfonation of PES using sulfuric acid

The degree of sulfonation of the resulting polymers was evaluated both by titration and NMR; the results are summarized in **Table 2.2**.

DS	Temperature [°C]	Time [h]
0.080	25	5
0.085	25	8
0.117	25	24
0.163	50	24

Table 2.2 Degree of sulfonation, temperature and time of sulfonation of PES

2.1.3. Synthesis of S-PPSU: Sulfonation of PPSU

S-PPSU was obtained by adding the polymer in concentrated sulfuric acid (H_2SO_4) and keeping the solution stirring at 50°C for 5 days. The solution was then cooled to room temperature and poured in ice cold water, under continuous stirring, obtaining a white precipitate. After standing overnight the precipitate was filtered and washed several times to neutral pH. Sulfonated PPSU was first dried in an oven for one night at the temperature of 80°C - 85°C and then dried under vacuum for 4 hours at room temperature [2, 6]. The degree of sulfonation was evaluated by ^{1}H NMR [3] and by titration and it was 2.00.

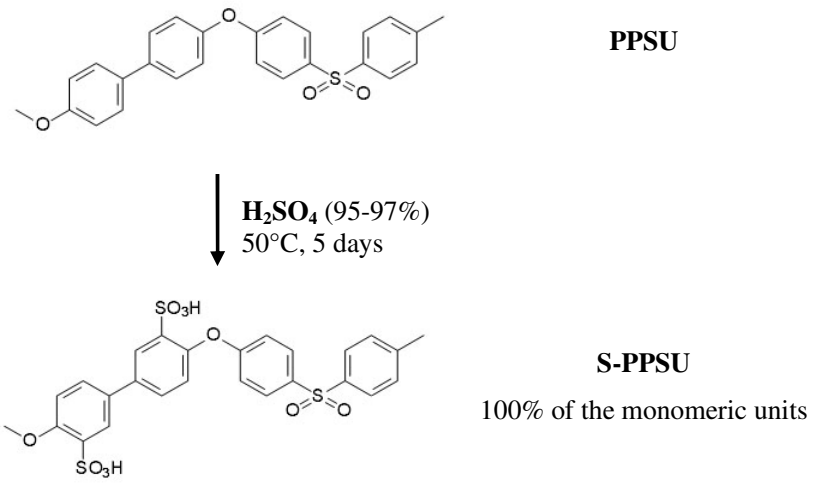

Figure 2.4 Sulfonation of PPSU

2.1.4. Synthesis of Si-PPSU: Silylation of PPSU

PPSU was added in nitrogen atmosphere to anhydrous tetrahydrofuran (THF). The solution was stirred at room temperature for 1 hour and then cooled to -60°C. After 1 hour, an excess of *n*-Butyllithium (BuLi) and N,N,N',N'-tetramethylethylenediamine (TMEDA) were added and the solution was stirred for 4.5 hours at -60°C. After that, phenyltrichlorosilane ($PhSiCl_3$, 97%)

was added and the resulting solution was stirred for 30 minutes again at -60°C. At this point the solution was slowly warmed to room temperature and kept at reflux for 2 hours. After standing overnight, the precipitate was washed in ice cold water to neutral pH and until no chlorides were detected. Silylated PPSU was first dried in an oven for one night at the temperature of 80°C - 85°C and then dried under vacuum for 4 hours at room temperature [2, 6]. The product obtained was analyzed by elemental analysis which showed a degree of silylation of 0.05.

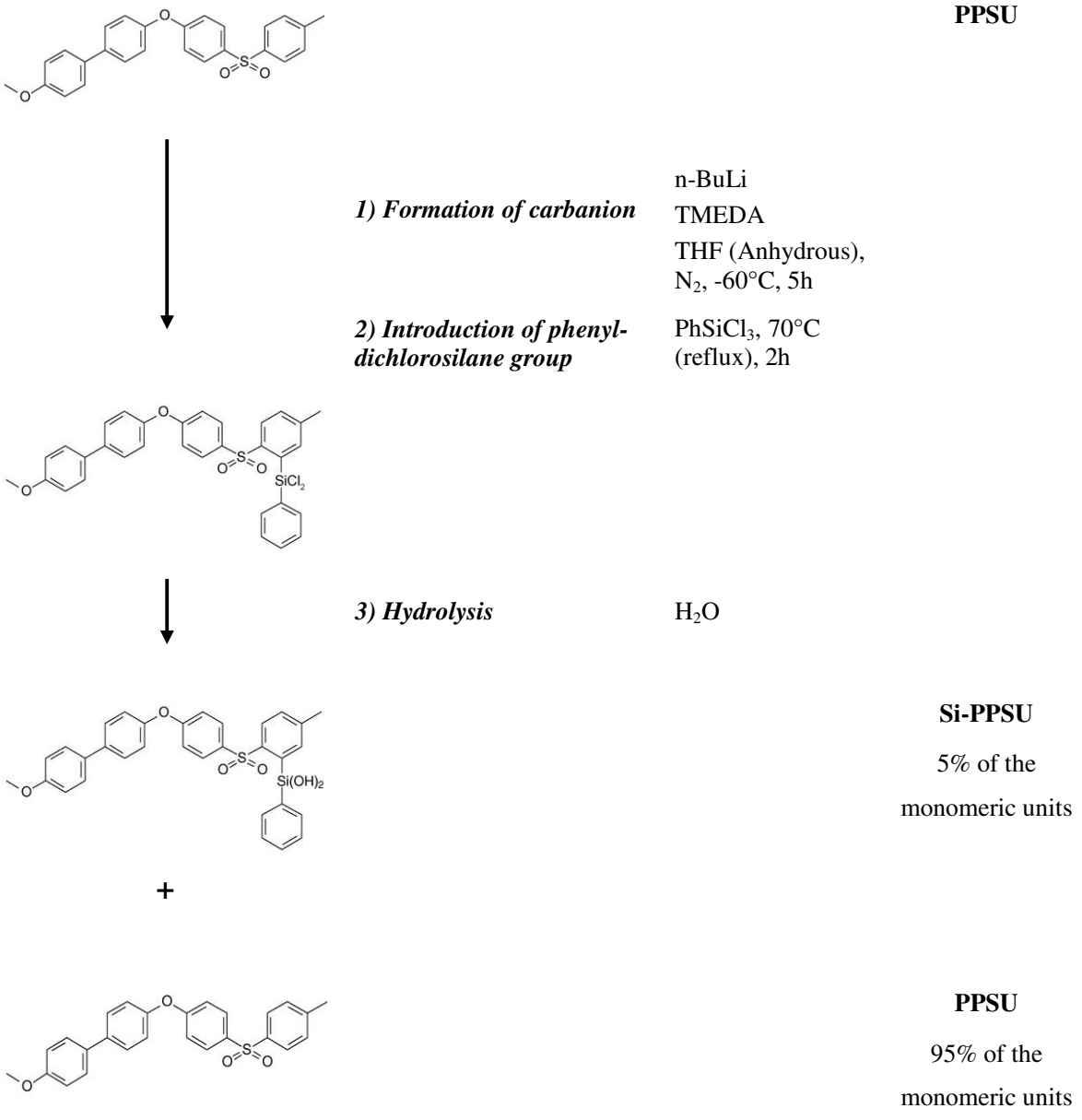

Figure 2.5 Silylation of PPSU

2.1.5. Synthesis of SiS-PPSU: Sulfonation of SiPPSU

Si-PPSU was added to concentrated sulfuric acid (H_2SO_4) and the solution was kept stirring at 50°C for 5 hours. The solution was cooled to room temperature and it was poured in ice-cold water, under continuous stirring, obtaining a precipitate, which was washed in ice-cold water to neutral pH, after standing overnight. The polymer obtained was then dried at 80°C for 5 hours under vacuum [6, 7]. The product was analyzed by several techniques (NMR, IR, etc.) and the elemental analysis showed a degree of sulfonation of 2.0 and a degree of silylation of 0.05.

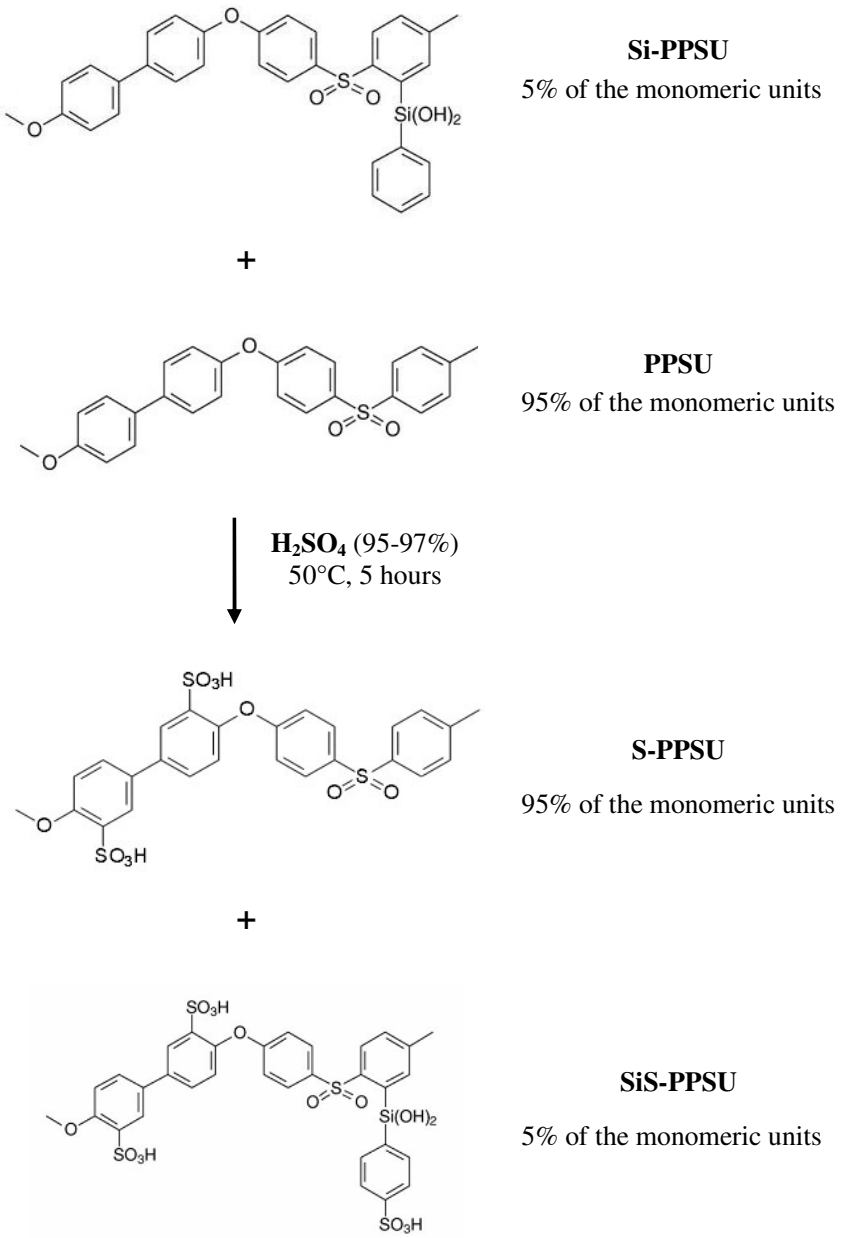

Figure 2.6 Sulfonation of Si-PPSU

2.1.6. Casting of Membranes

All membranes were obtained by solution casting technique using as solvent Dimethylsulfoxide (DMSO; Boiling Point: 189°C) or N,N-Dimethylacetamide (DMAc; Boiling Point: 165°C).

S-PEEK membranes were obtained dissolving around 250 mg of sample in 20 mL of solvent and stirring the solution for 4 hours. The solutions were evaporated to 5 mL, cast onto a Petri dish and heated to dryness for 12 hours at 80°C. After cooling at room temperature the membranes were peeled off and dried under vacuum 24 hours at 80°C for complete solvent removal.

The composite membranes were achieved adding to the solution, made up of 250 mg of S-PEEK and 20 mL of solvent, the appropriate quantity of the second partner (7 weight % of substituted PPSI and 5 weight % of functionalized titanium dioxide), which was one of the following compounds:

- S-PPSU (sulfonated PPSU)
- Si-PPSU (silylated PPSU)
- SiS-PPSU (silylated and sulfonated PPSU)
- hphi-TiO_2 (hydrophilic TiO_2)
- hpho-TiO_2 (hydrophobicTiO_2)

As all the above compounds, except S-PPSU, are insoluble in DMSO or DMAc, the membranes were prepared by obtaining the best possible dispersion of the second partner in the solution by stirring the mixtures for several days and by sonication. The solutions were evaporated to 5 mL, then cast onto a Teflon plate and heated to dryness. After cooling at room temperature, the membranes were peeled off and dried in an oven for 12 hours at 80°C and then further dried under vacuum at 80°C for 24 hours to remove completely the solvent.

The membranes achieved using DMSO as solvent were made heating the Petri dish for 16 hours at 120°C. The reason of the modified oven temperature is the higher solvent boiling point.

2.2. Membrane Characterization

The characterization of membranes was performed using several techniques. All the procedures are described below.

2.2.1. Structure and Microstructure

2.2.1.1. Nuclear Magnetic Resonance Spectroscopy

The degree of sulfonation of the polymers synthesized was evaluated by ^{1}H-NMR [3, 4] spectra, recorded with a Bruker 300 spectrometer operating at 300 MHz, using d_6-DMSO or DMAc as solvent. In the latter case, the spectra were recorded using D_2O as external lock.

2.2.1.2. Infrared Spectroscopy

FTIR spectra of membranes were collected in transmission mode in the range of 4000 cm^{-1} ÷ 400 cm^{-1} (32 scans, 2 cm^{-1} resolution) with a Bruker Equinox 55. The membrane thickness was ca. 60 μm in all cases. A background spectrum was run and sample spectra were normalized against the background spectrum.

2.2.1.3. X-Ray Diffraction

X-Ray Diffraction (XDR) patterns were recorded at room temperature using a Siemens D5000 diffractometer with CuKα radiation (λ = 0.1540 nm), steps of 0.04° and 1 step time.

2.2.1.4. Atomic Force Microscopy

The AFM images were obtained using an Autoprobe CP (Park Scientific Instuments) with scans of 80, 20 and 5 μm using a standard silicon cantilever. All AFM measurements were carried out in air at 25°C in non-contact mode.

2.2.1.5. Scanning Electron Microscopy

Scanning Electron Microscopy (SEM) images were obtained in a Philips XL-30 SEM working in ambient mode under water vapour pressure of 1 mbar.

2.2.1.6. Contact Angle

Contact Angle measurements were performed using a "KRUSS" EasyDrop contact-angle measuring system. Each test was performed depositing a known quantity of liquid (1 mL) on the sample using an automatic syringe. The baseline was measured automatically and the angle was determined between the baseline of the drop and the tangent of the drop.

The measurement of contact angle gives information about the wettability of a surface. The shape (spherical) of a drop of a liquid in contact with a solid shows the interaction between solid and liquid. The contact angle of a drop with a surface gives information about the minimum free energy of the system. When the solvent used is water, the measure of contact angle allow to know about the nature of the sample: hydrophobic (wide angle of contact) or hydrophilic (small contact angle) [8].

Knowing the contact angle of different solvents (polar and non polar) allows calculating the surface energy of a sample (solid) using the Owens and Wendt method [9]. In order to evaluate the surface energy, water (ultra pure CHROMANORM for HPLC, VWR), formamide (99% GC, Sigma), diiodomethane (99% GC, Aldrich) and ethylene glycol (99+%, Acros) were used as solvents.

2.2.2. Thermogravimetric Analysis

High Resolution Thermogravimetric Analysis (TGA Q500, TA Instruments) was performed under air flux following the variation percentage of the weight in the temperature range between 25°C and 600°C with a maximum heating rate of 5 K/min in platinum sample holders.

2.2.3. Water Uptake

The water uptake of membranes was measured by two complementary experiments: i) By full immersion in deionized water. Excess water was removed with absorbing paper and then the mass change of the samples was measured. The experiment was repeated at water temperatures between 25°C and 145°C, using above 100°C hermetically closed Teflon vessels. After the immersion and before weighting the samples were immersed in deionized water at room temperature for 24 hours [10]. ii) By equilibration with water vapour at 25°C or 50°C under 0% - 95% RH using TA5000 Thermogravimetric Analyzer. RH was modified in 10% or 5% steps and the water uptake recorded at each step during 2 hours. Prior to all experiments, the membranes were first dried in situ for 3 hours at 80°C under 0% RH.

In both experiments the water uptake was evaluated using two parameters. The first one, called simply Water Uptake (W.U.), measures the weight gain of the absorbed water and is calculated by [4, 11]:

$$W.U. = \frac{W_{wet} - W_{dry}}{W_{dry}} \times 100 \quad (2.1)$$

where W_{dry} and W_{wet} are the weight of the dry and the wet sample, respectively. The latter, called Water Uptake Coefficient (λ), measures the number of water molecules absorbed per sulfonic group. It is calculated by [12]:

$$\lambda = \frac{W_{wet} - W_{dry}}{W_{dry} \times IEC \times MW(H_2O)} \times 1000 \quad (2.2)$$

where $MW(H_2O)$ is the molar mass of water and *IEC* (expressed in meq/g) is the Ion Exchange Capacity of the polymer, which can be calculated using the degree of sulfonation and the mean molecular mass of the repeat units (equivalent weight).

2.2.4. Mechanical Properties

2.2.4.1. Stress-Strain Tests

The mechanical properties of membranes were investigated using an ADAMEL Lhomargy DY30 test machine on membrane samples of 100 μm thickness, 5 mm width and 25 mm length. All measurements were performed at ambient temperature and humidity and were made at a constant crosshead speed of 1 mm/min and using adhesive tape sample holders to optimize the mechanical tests.

The parameters obtained from stress-strain curves were the Elastic Modulus, the Ultimate (or Tensile) Strength and the percentage of elongation at the Tensile Strength and at the fracture of the samples.

The Elastic Modulus (or Young's Modulus) defines the properties of a material as it undergoes stress, deforms and then returns to its original shape after the stress is removed. It is a measure of the stiffness of a given material and is calculated as the ratio of stress (σ; is the force per unit cross-section area) and strain (ε; is the change in length divided by the original length) [13]:

$$E = \frac{\sigma}{\varepsilon} \quad (2.3)$$

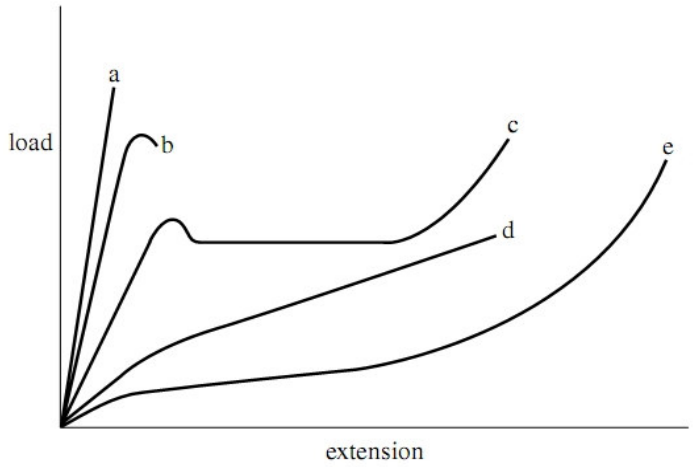

Figure 2.7 Possible forms of the load-extension curve for a polymer: (a) low extensibility followed by brittle fraction; (b) localized yielding (c) followed by fracture; (c) necking and cold drawing; (d) homogeneous deformation with indistinct yield; (e) rubber-like behaviour[14]

Its value is experimentally determined from the slope of the short initial part of the Stress-Strain curve, where the deformation is nonpermanent; it means that the sample returns to its original shape when the applied load is released (**Figure 2.8**).

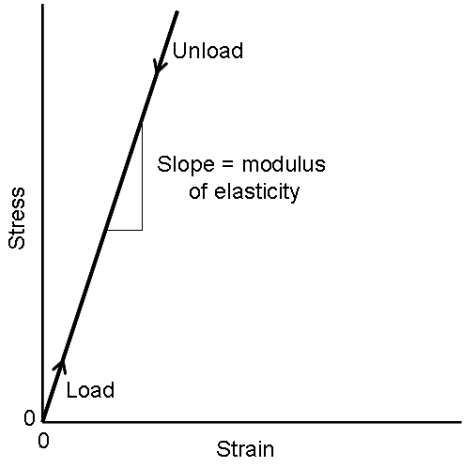

Figure 2.8 Schematic stress-strain curve showing Linear elastic deformation for loading and Unloading cycles

Sometimes the behaviour of the material is more complex and the Young's Modulus is evaluated in a different manner [15].

Another parameter studied is the Ultimate (or Tensile) Strength: it corresponds to the maximum stress which can be sustained by a structure in tension mode [15]. Its value can be obtained directly from the Stress-Strain curve.

The other two mechanical parameters studied are the Deformation at the Ultimate Strength and the Deformation at the Rupture. All parameters were directly evaluated from the stress-strain curve.

2.2.4.2. Dynamic Mechanical Analysis

Dynamic Mechanical Analysis (DMA) was performed on a DMA 2980 dynamic analyzer (TA Instruments) in tension mode. DMA was performed in air applying a 1 Hz sinusoidal stress with a static component of 1 N and a maximum dynamic component producing a strain deformation of 10 μm (for S-PEEK membranes) or the 125% of the initial length (for blends).

The Dynamic Mechanical Analysis consists to apply an oscillating force (stress) to a sample and analyzing the materials response to that force (strain). If the material analyzed is purely elastic the phase difference between the stress and strain sine waves is 0° (i.e., they are in phase). If the material is purely viscous, the phase difference is 90°. However, most real-world materials including polymers are viscoelastic and exhibit a phase difference between those extremes (**Figure 2.9**). This phase difference, together with the amplitudes of the stress and strain waves, is used to determine a variety of fundamental material parameters such as the Complex Modulus, which is defined by the following equation [16, 17]:

(2.4) $$E^* = \frac{stress}{strain}$$

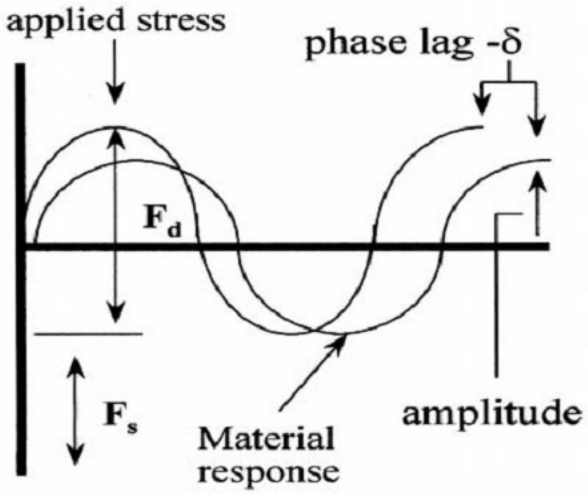

Figure 2.9 The DMA technique supplies a sinusoidal stress to the sample, which generates a sinusoidal strain. The different phase between stress and strain depends on the viscoelasticity of the sample.

The complex modulus measured in DMA, is different from the Young's Modulus obtained from the classic stress-strain curve. Young's Modulus is the slope of a stress-strain curve in the initial linear region. In DMA, the complex modulus and the other parameters related to it, such as the Storage Modulus (E') and the Loss Modulus (E''), are calculated from the material response to the sine wave. These parameters allow a better characterization of the material, because it is possible to evaluate the ability of the material to return or store energy (E') or to dissipate or lose energy (E'') (**Figure 2.10**) [17].

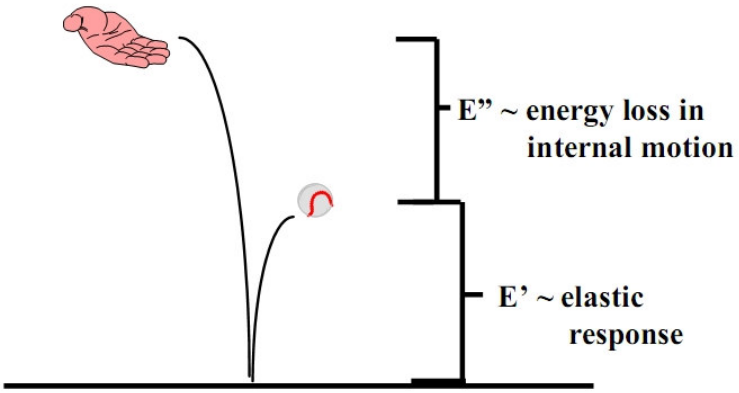

Figure 2.10 The Storage Modulus (E') is the ability of the material to return or store energy, while the Loss Modulus is the ability to lose energy[18]

The Storage Modulus (E') and the Loss Modulus (E'') are related to the Complex Modulus (E*) by the following equations [19]:

(2.5) $E^* = E' + iE''$

(2.6) $E' = E^* \cos\delta$

(2.7) $E'' = E^* \sin\delta$

The ratio between the loss and storage modulus is a measure of the amount of deformation energy that is dissipated as heat during each cycle and gives the quantity knows as the Mechanical Damping Factor (δ) [19]:

(2.8) $\tan\delta = \frac{E''}{E'}$

The storage modulus (E'), loss modulus (E'') and damping (δ) spectra were evaluated obtained at a heating rate of 3 K/min between 50°C and 250°C.

2.2.5. Electrical Properties

2.2.5.1. Dielectric Analysis

Dielectric Analysis (DEA) was performed with a DEA 2970 dielectric analyzer (TA Instruments) mounting ceramic parallel plate electrodes (**Figure 2.11**). The experiments were carried out on 25 mm x 25 mm membrane samples under argon atmosphere at a gas flow rate of 500 ml/min and with heating rate of 2 K/min. The results were recorded in the range of frequency between 10 Hz and 100 kHz.

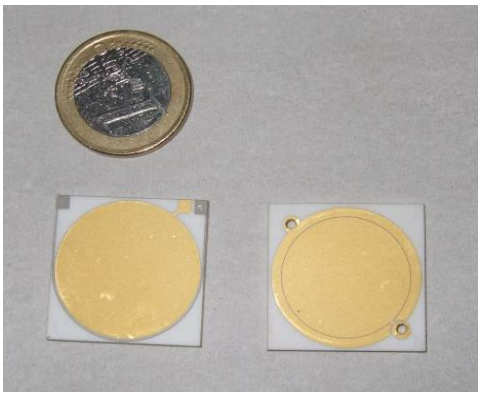

Figure 2.11 Electrodes used to perform DEA measurements

The Dielectric Analysis (DEA) can be defined as the electric analogous of DMA. In dielectric measures the material is exposed to an alternative electric field generated by applying a sinusoidal voltage. This process polarizes the sample causing an oscillation of molecules (as far as possible) at the applied frequency but with a phase shift angle (θ). The magnitude of the phase shift angle is determined measuring the resulting current. The capacitance (C in farad) and resistance (in ohm) are then calculated from the relationship between the applied voltage ($V_{applied}$), the resulting current ($I_{measured}$) and the phase shift angle (θ):

$$C = \frac{I_{measured}}{V_{applied}} \times \frac{\sin\theta}{2\pi f} \quad (2.9)$$

(2.10) $$\frac{1}{R} = \frac{I_{measured}}{V_{applied}} \times \cos\theta$$

The capacitance and the conductance are related to the dielectric permittivity (*ε'*) and the dielectric loss factor (*ε''*), respectively.

(2.11) $$\varepsilon' = \frac{Cd}{\varepsilon_0 A}$$

(2.12) $$\varepsilon'' = \frac{1}{R} \times \frac{d}{\omega \varepsilon_0 A}$$

here *d* is the distance of the plates, *A* the electrode plate area, ω ($2\pi f$) the angular frequency of the applied sinusoidal voltage and ε_0 the absolute permittivity of free space ($\varepsilon_0 = 8.85 \times 10^{-12}\ F/m$).

The two equations used to calculate *ε'* and *ε''* (Eq. (2.11) and Eq. (2.12)) quantify these relationships:

ε' = permittivity due to induced dipoles + permittivity due to alignment of dipoles
ε'' = dipole loss factor + ionic conductance

The dielectric permittivity, *ε'*, represents the amount of dipole alignment (both induced and permanent). It has a low value for polymers when the measure is preformed at low temperature, that is below the glass transition, because molecules are immobilised at their positions and the dipoles cannot move to align themselves with the electric field. The dielectric loss factor, *ε''*, measures the amount of energy needed to align the dipoles and move ions. The term "*dipole loss factor*" is predominant below the glass transition temperature, while the "*ionic conductance*" is predominant above that temperature and can be evaluated by the following equation:

(2.13) $$\sigma = \varepsilon'' \omega \varepsilon_0$$

Both ε' and ε'' are function of the measured frequency. The ratio $\varepsilon'/\varepsilon''$ is called Dissipation or Loss Tangent, and is another parameter commonly used to express the dielectric response of the sample [20-22]:

(2.14) $\tan\theta = \frac{\varepsilon''}{\varepsilon'}$

2.2.5.2. Conductivity Measurements

Through-plane conductivity measurements were carried out on membranes, 8 mm in diameter and 90 μm thick, sandwiched between gas diffusion electrodes (ELAT containing 1 mg/cm^2 Pt loading), which were pressed on the membrane faces by means of porous stainless steel discs. The pressure clamping the membrane between the electrodes (60 kg/cm^2) was applied before starting the measurements and not controlled during the experiment. The membrane conductivity was determined as a function of temperature and relative humidity by impedance spectroscopy with a Solartron Sl 1260 Impedance/Gain Phase Analyser connected to a Solartron 1480 Multistat potentiostat – galvanostat in the frequency range 10 Hz to 1MHz at a signal amplitude ≤ 100mV. All reported conductivity values had reached a constant value for at least 2 h. Relative humidity was controlled as described in Ref. [16].

The conductivity σ of the samples in the transverse direction was calculated from the impedance data, using the relation σ = d/RS, where d and S are the thickness and area of the sample, determined before and after the measurements. The resistance R was derived from the high frequency intercept with the real axis on a complex plane impedance plot. The spectra were analyzed using the Zview® software.

2.3. References

[1] B. S. Furniss, A. J. Hannaford, P. W. G. Smith and A. R. Tatchell, *Texbook of Practical Organic Chemistry*, **1989**, p. 406.

[2] M. L. Di Vona, L. Luchetti, G. P. Spera, E. Sgreccia and P. Knauth, *Comptes Rendus Chimie* **2008**, *11*, 1074-1081.

[3] P. X. Xing, G. P. Robertson, M. D. Guiver, S. D. Mikhailenko, K. P. Wang and S. Kaliaguine, *Journal of Membrane Science* **2004**, *229*, 95-106.

[4] S. M. J. Zaidi, S. D. Mikhailenko, G. P. Robertson, M. D. Guiver and S. Kaliaguine, *Journal of Membrane Science* **2000**, *173*, 17-34.

[5] J. B. Rose in *Sulphonated Polyaryletherketones*, *Vol. US 4,268,650* Imperial Chemical Industies Limited, London, Emagland, United States, **1981**.

[6] M. L. Di Vona, E. Sgreccia, S. Licoccia, M. Khadhraoui, R. Denoyel and P. Knauth, *Chemistry of Materials* **2008**, *20*, 4327-4334.

[7] D. Marani, M. L. Di Vona, E. Traversa, S. Licoccia, I. Beurroies, P. L. Llewellyn and P. Knauth, *Journal of Physical Chemistry B* **2006**, *110*, 15817-15823.

[8] V. Roche, F. Vacandio, D. Bertin, D. GigrneS and M. Eyraud, *Comptes Rendus Chimie* **2008**, *11*, 1055-1062.

[9] D. K. Owens and R. C. Wendt, *Journal of Applied Polymer Science* **1969**, *13*, 1741-1747.

[10] G. Alberti, R. Narducci and M. Sganappa, *3rd International Conference on Polymer Batteries and Fuel Cells* (Rome, ITALY) **2007**, pp. 575-583.

[11] S. M. J. Zaidi, *Arabian Journal for Science and Engineering* **2003**, *28*, 183-194.

[12] M. L. Di Vona, S. Licoccia and P. Knauth, *Solid State Ionics* **2008**, *179*, 1161-1165.

[13] M. Meyers and K. Chawla, *Mechanical Behavior of Materials*, Cambridge University Press, **2009**, p. 71-155.

[14] D. I. Bower, *An Introduction to Polymer Physics*, Cambridge University Press, Cambridge, **2002**, p. 162-186.

[15] W. D. Callister Jr., *Fundamentals of Material Science and Engineering*, Wiley and Sons Ltd, **2004**, p. 177-225.

[16] J. Foreman, *American Laboratory* **1997**, *29*, 21-24.

[17] K. P. Menard, *Dynamic Mechanical Analysis: A Practical Introduction*, CRC Press LLC, **1999**, p. 1-16.

[18] L. Li, *Dynamic Mechanical Analysis (DMA), Basics and Beyond*, Perkin Elmer Inc., **2000**, p. 16.

[19] Z. Zhang, P. Klein and K. Friedrich, *Composites Science and Technology* **2002**, *62*, 1001-1009.

[20] N. C. Guma, K. Kale and K. R. Morris, *Journal of Pharmaceutical Sciences* **1997**, *86*, 329-334.

[21] K. Mohomed, T. G. Gerasimov, F. Moussy and J. P. Harmon, *Polymer* **2005**, *46*, 3847-3855.

[22] L. Nunez, S. Gomez-Barreiro, C. A. Gracia-Fernandez and M. R. Nunez, *Polymer* **2004**, *45*, 1167-1175.

Chapter 3: Composite Sulfonated Aromatic Polymers

In this chapter two approaches are followed for the development of composite systems, in which two partners are bonded by Van der Waals interactions, in order to improve the properties of sulfonated aromatic polymer electrolytes: the preparation of hybrid composite materials, where the minority partner is playing the role of an "anchor" phase, and the use of an inorganic filler, surface-modified titanium dioxide.

3.1. Composites of Sulfonated PEEK and Substituted PPSU

In this work, the majority partner is an ionomer (S-PEEK) which guarantees sufficient proton conductivity and a minority partner (substituted PPSU) is added to stabilize the morphology of the material and provide high performance mechanical properties. The blending technique has the advantage of combining the positive features of each component while being very simple [1].

Several reasons were considered in choosing PPSU as second component: its structural affinity with S-PEEK that can avoid the inhomogeneity observed when blends between different polymers are prepared [2], its solubility in organic solvents that allows to easily carry out functionalization reactions in homogeneous conditions, and the possibility to introduce sulfonic acid groups.

In this section the results obtained for blends having sulfonated PEEK with a high degree of sulfonation (DS = 0.9) as majority partner (93 weight %). and unsubstituted, sulfonated and/or silylated PPSU as minority partner (7 weight %) are reported. This concentration was chosen after previous work indicated particularly interesting properties. Above this concentration, the dispersion of second phase becomes very difficult [3]. All the composite membranes were obtained following the procedure described in section 2.1.6 and using N,N-Dimethylacetamide as solvent.

In **Figure 3.1** are reported the investigated systems.

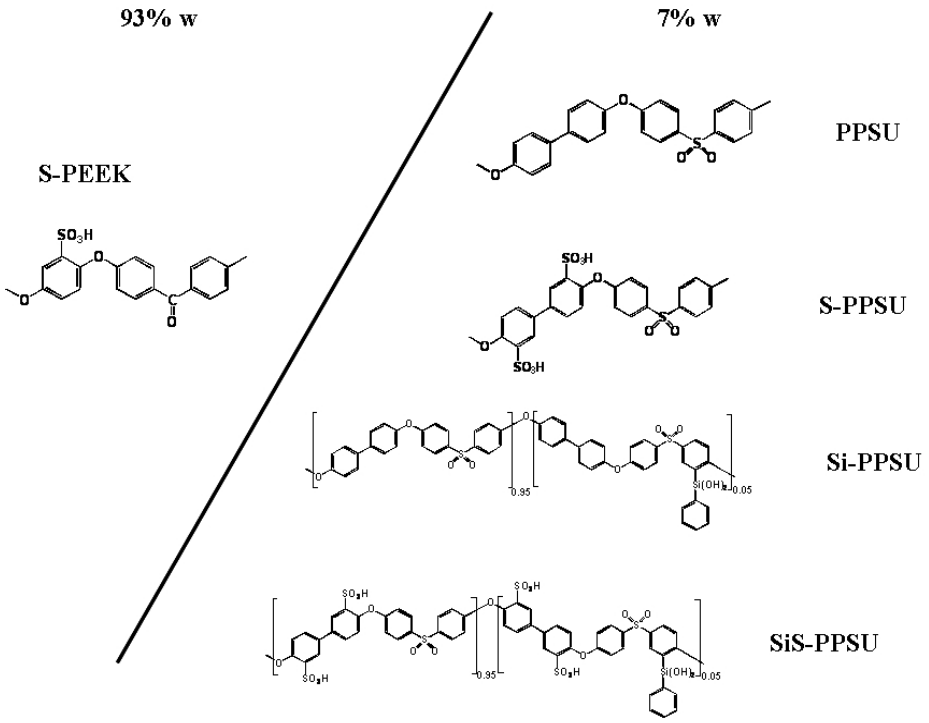

Figure 3.1 Chemical formula of investigated composites

3.1.1. Structure

A common characteristic of all membranes is their completely amorphous structure. **Figure 3.2** shows a typical XRD pattern obtained for S-PEEK/SiS-PPSU. Here a broad peak is observed around the reflections of crystalline S-PEEK, confirming the absence of crystalline domains in the membrane [4].

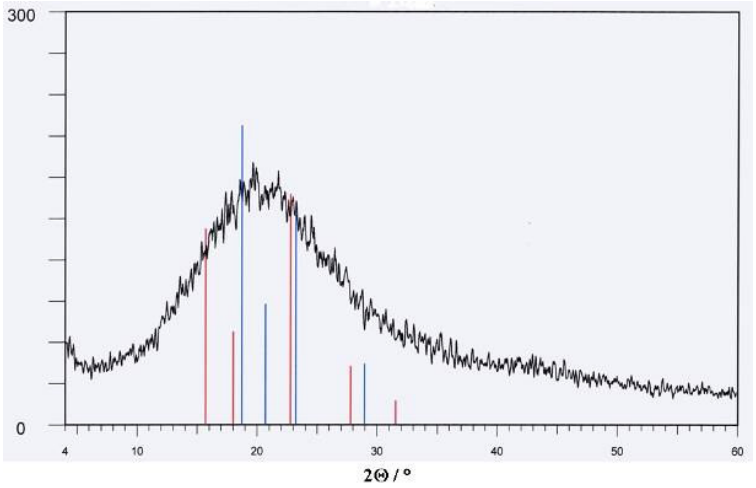

Figure 3.2 X-Ray diffractogram of S-PEEK/SiS-PPSU composite. The indicated reflections correspond to crystalline PEEK polymer (JCPDS data files 00-052-2277 and 00-052-2278)

Figure 3.3 and **Figure 3.4** show ^{1}H-NMR and ^{13}C-NMR spectra of S-PEEK, SiS-PPSU and S-PEEK/SiS-PPSU systems. In the ^{1}H spectrum all the resonances of the composite are shifted toward lower field with respect to the resonances present in the spectra of both components.

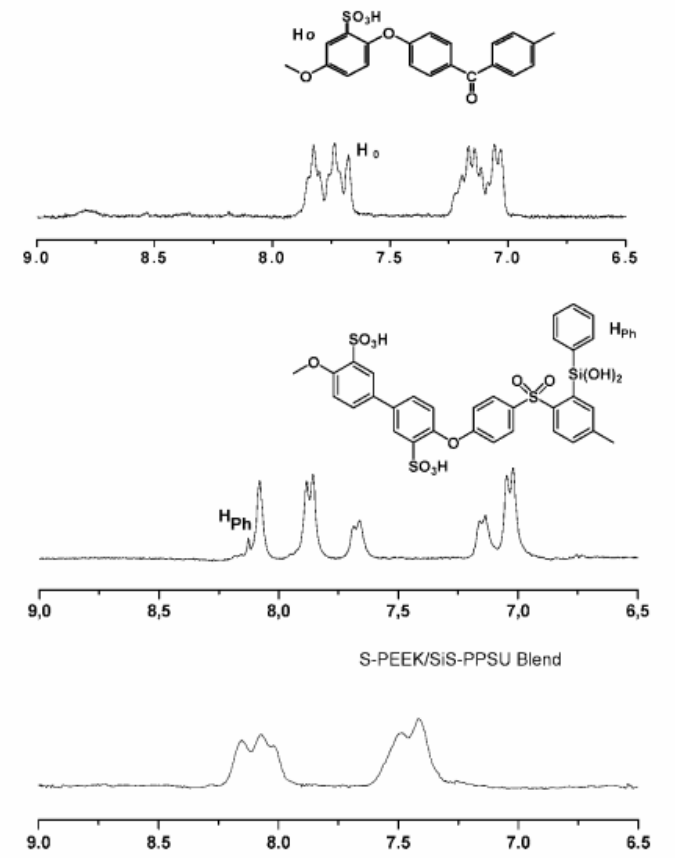

Figure 3.3 ^{1}H NMR spectra in DMAc. From top to bottom: S-PEEK, SiS-PPSU and S-PEEK/SiS-PPSU composite

In the ^{13}C spectrum, instead, the peaks are shifted towards higher field. The two different shifts observed both in ^{1}H and ^{13}C are indicative of the interactions between the two components of the blend and can be explained by dipole-dipole interactions between the two polymers [5]. The ^{13}C spectra can be used to observe which carbons of S-PEEK are more influenced by the interactions of the second phase. **Figure 3.4** shows that the most influenced peak is the one related to the ketone groups (carbon labelled with 11): it is splitted in two peaks. The effect cannot be attributed to the interactions with sulfonic acid groups, because they have a high concentration also in pure S-PEEK. It might instead be related to the interactions with phenyl-silanol groups of SiS-PPSU [5].

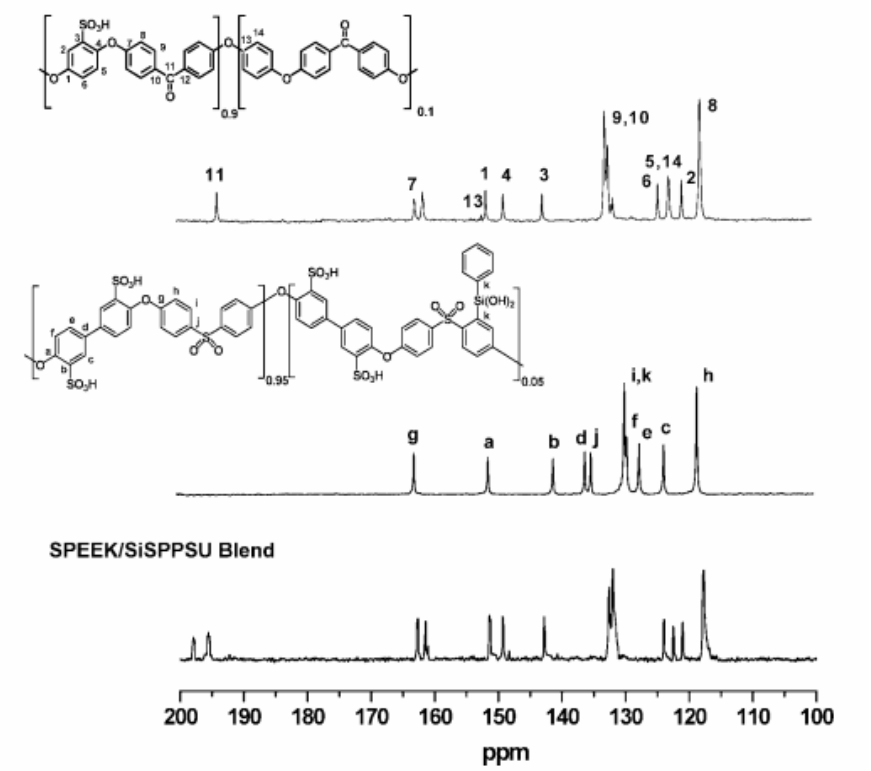

Figure 3.4 ^{13}C NMR spectra in DMAc. From top to bottom:S-PEEK, SiS-PPSU and S-PEEK/SiS-PPSU composite

3.1.2. Thermal Properties

Figure 3.5 shows typical high resolution thermogravimetric curves of S-PEEK/SiS-PPSU and S-PEEK/Si-PPSU blends. The initial weight loss revealed at the beginning of the measurement can be attributed to the evaporation of the water remained in the membranes, which were in equilibrium with the ambient. For both samples two main weight losses were observed. The first weight loss revealed for the sample S-PEEK/SiS-PPSU comprises two sublosses: the first, of about 6%, at 150°C - 160°C can be attributed to the residual solvent removal. The second between 220°C and 300°C, of approximately 20%, corresponds to the decomposition of sulfonic groups. The complete decomposition of polymers main chain is revealed between 450°C and 470°C [6-9]. Concerning the sample S-PEEK/Si-PPSU, the first weight loss of approximately 20%, associated to the degradation of sulfonic groups, is observed between 200°C and 350°C. The second loss of mass, which corresponds to the complete decomposition of polymer main chain, is revealed between 400°C and 450°C.

The subloss observed between 150°C and 160°C for S-PEEK/SiS-PPSU, and which is conjectured due to the solvent removal, is absent in the curve obtained for S-PEEK/Si-PPSU

membrane. This result is confirmed by the water uptake measurements, discussed below. The absence of sulfonic groups in Si-PPSU probably reduces the interactions with DMAc, so that the solvent is better removed during membrane preparation.

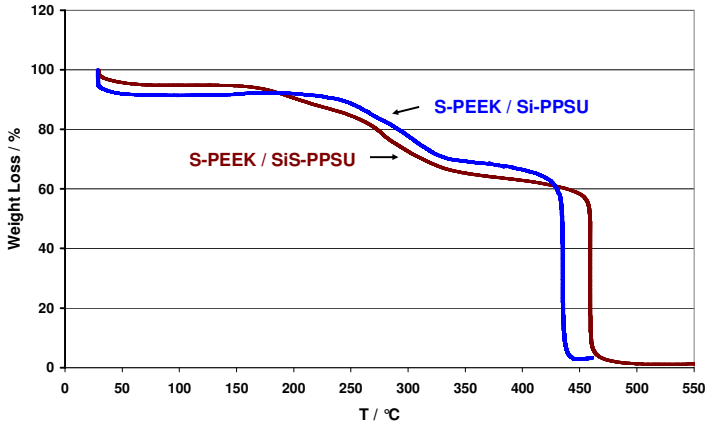

Figure 3.5 HR-TGA of S-PEEK/Si-PPSU and S-PEEK/SiS-PPSU blends

3.1.3. Mechanical Properties

Figure 3.6 shows typical Stress-Strain curves, obtained for the four different blends (S-PEEK/PPSU, S-PEEK/S-PPSU, S-PEEK/Si-PPSU and S-PEEK/SiS-PPSU). The corresponding mechanical parameters (Young's Modulus, ultimate strength and elongation at rupture) evaluated in these tests are resumed in **Table 3.1**. All the values were obtained calculating the mean values of at least three experiments.

Both Young's Modulus and ultimate strength are strongly influenced by the second phase of the composites. These parameters decrease in blends with S-PPSU. The presence of sulfonic groups in the second phase softens the membranes. If phenyl-silanol groups are added, the elastic modulus and membrane strength are considerably enhanced (S-PEEK/SiS-PPSU). The absence of sulfonic groups in the second phase allows further enhancement of mechanical properties (S-PEEK/Si-PPSU). Mechanical properties between S-PEEK/SiS-PPSU and S-PEEK/Si-PPSU blends were obtained for S-PEEK/PPSU membrane. While the Young's modulus is very close to the value obtained for SiS-PPSU composite, the ultimate strength is close to the one obtained for Si-PPSU blend.

The presence of phenyl-silanol groups in the second phase makes the material less ductile, while the sulfonic groups make it more ductile. This feature can be observed by the elongation at

rupture. This parameter is higher when the second phase is S-PPSU or PPSU and lower in SiS-PPSU and Si-PPSU blends.

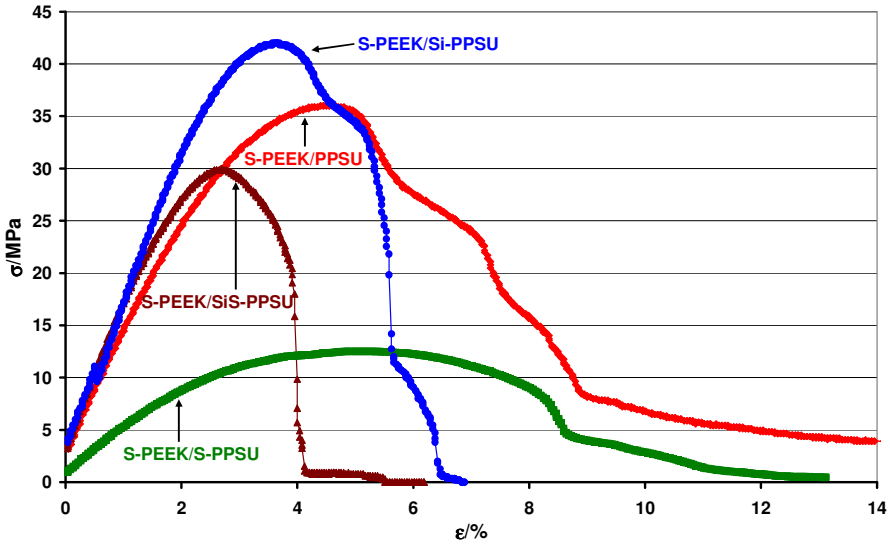

Figure 3.6 Comparison of Stress-Strain curves of S-PEEK/(Si,S)-PPSU blends

Blend	*IEC [meqv/g]*	*λ*	*E [MPa]*	*σ [MPa]*	*ε [%]*
S-PEEK/PPSU	2.48	---	1100±200	35±2	4.4±0.3
S-PEEK/S-PPSU	2.67	soluble	400±100	10±3	8.5±1.0
S-PEEK/SiS-PPSU	2.67	15	1200±300	26±4	2.9±0.5
S-PEEK/Si-PPSU	2.48	9	1500±100	41±2	3.6±0.4

Table 3.1 Ion Exchange Capacity (IEC), Water Uptake Coefficient (λ) obtained at the stability in full immersion in water at RT, Young's Modulus (E), Ultimate Strength (σ) and Elongation at Rupture (ε).

3.1.4. Water Uptake

The second phase strongly influences also the capability of the membranes to absorb water. In **Table 3.1** water uptake obtained in full immersion in water at RT at the stability is summarized. The composites which have silanol moieties in the second phase reach a stable value of λ that is 9 for Si-PPSU blend and 15 for SiS-PPSU blend. The presence of sulfonic groups increases λ, but leads to the dissolution of membrane in the case of S-PPSU.

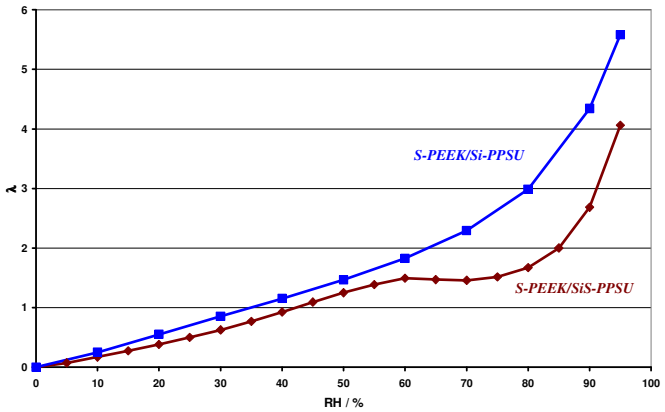

Figure 3.7. Water Uptake Coefficient obtained during the water sorption isotherm at 25°C

Figure 3.7 shows the water uptake coefficients obtained at different RH during water vapour sorption experiments at 25°C. The blends have apparently almost the same behaviour when the relative humidity is under the 60%. However, an artefact appears due to loss of residual DMAc solvent during the experiments, as evidenced by a net mass loss after a full cycle of RH. This result is consistent with the absence of solvent loss in TGA experiments, as discussed above. Only the composite with Si-PPSU did not show this artefact.

Water sorption isotherms enable to evaluate the chemical Diffusion Coefficient of water (*D*). The equation used to calculate its value is the following:

$$\frac{M(t)}{M_\infty} = \frac{4}{L}\sqrt{\frac{D \cdot t}{\pi}} \qquad (3.1)$$

where *L* is the thickness of the sample, *M(t)* is the water uptake at time *t* and M_∞ is the Water Uptake at infinite time. Eq. (3.1) is a special solution of Fick's second law:

$$\frac{\partial C}{\partial t} = D\left(\frac{\partial^2 C}{\partial x^2}\right) \qquad (3.2)$$

(here *x* is the position in the film and *C* is the concentration of the sorbed molecules) when the sorption curves are linear in $t^{1/2}$, that is in their initial part ($0 \le m_t \le 0{,}4m_\infty$) [10-12].

Figure 3.8 shows the diffusion coefficients obtained for the four blends at different relative humidity.

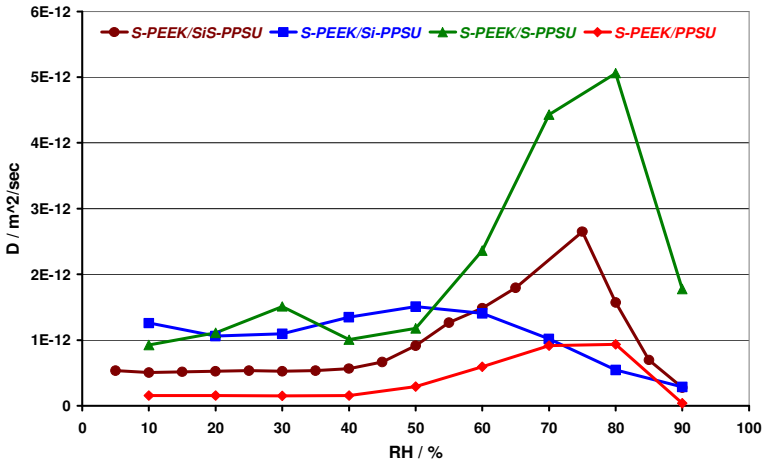

Figure 3.8. Water Diffusion Coefficient of S-PEEK(0,9) and unsubstituted and substituted PPSU (T=25°C)

The blends with sulfonic groups in the second phase (S-PEEK/S-PPSU and S-PEEK/SiS-PPSU) show higher apparent diffusion coefficients at high relative humidity. This artefact is due to the swelling that these membranes show at high relative humidity: the proportionality of D with L^2 (see Eq. (3.1)) gives an apparently higher diffusion coefficient. S-PEEK/PPSU shows a behaviour similar to S-PEEK/S-PPSU and S-PEEK/SiS-PPSU membranes. The less noticeable increasing of diffusion coefficient at high RH is probably due to the absence of sulfonic groups in the second phase that make the sample less hydrophilic than the other two membranes. The RH dependence of chemical diffusion coefficient of S-PEEK/Si-PPSU membrane is consistent with literature predictions: it increases with RH up to a maximum at 50% of RH and decreases at high RH [5]. This variation is related to the thermodynamic factor (variation of activity coefficient of water). The self-diffusion coefficients $\tilde{D}$ can be calculated from the chemical diffusion coefficients D according to the equation:

$$D = \tilde{D}\left(\frac{d\ln a(H_2O)}{d\ln x(H_2O)}\right) \qquad (3.3)$$

The thermodynamic water activity $a(H_2O)$ is equal, for an ideal system, to the relative humidity, whereas the water molar fraction $x(H_2O)$ is directly related to the water uptake coefficients λ at different RH values. The initial small enhancement of self-diffusion coefficients with increasing molar fraction of water is related to the increasing number of percolating pathways containing water molecules.

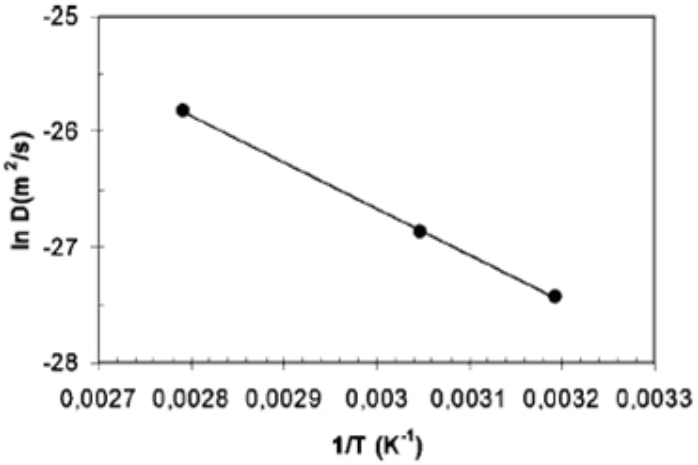

Figure 3.9. Temperature dependence of water chemical diffusion coefficient in S-PEEK/Si-PPSU polymer membrane

The temperature dependence of chemical diffusion coefficient at 75% RH is shown as Arrhenius plot in **Figure 3.9**. An activation energy of around 30 kJ/mol can be calculated, which is consistent with previous data obtained from conductivity measurements in related membranes and indicates that a Grotthuss-type diffusion mechanism is operating in this range of relative humidity.

3.1.5 Discussion

This study confirms the correlation between mechanical strength, water uptake coefficient, and swelling of proton conducting polymer membranes.

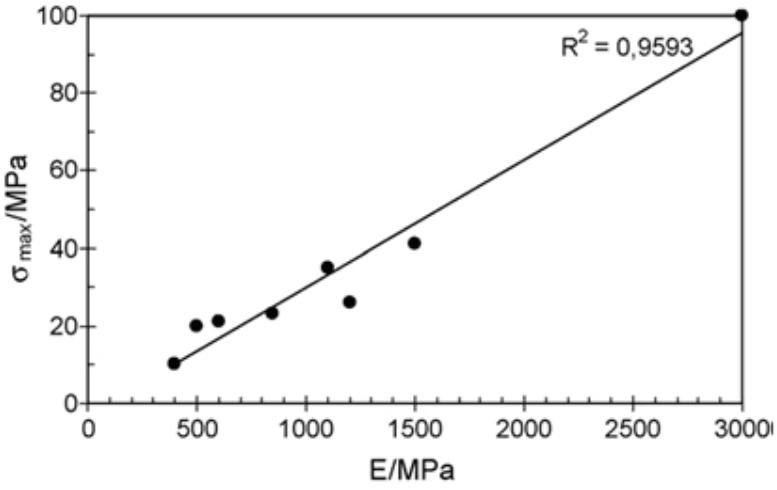

Figure 3.10 Correlation between maximum strength σ and elastic modulus E of investigated polymer membranes

Membrane	*E [MPa]*	*σ [MPa]*	*ε [%]*	*λ*
PEEK	3000	100	2.5	0 [(a)]
S-PEEK	600±200	25±1	4.9±0.9	17
S-PEEK/7% S-PPSU	400±100	10±3	8.5±1.0	17
S-PEEK/7% PPSU	1100±200	35±2	4.4±0.3	15
S-PEEK/7% Si-PPSU	1500±100	41±2	3.6±0.4	6
S-PEEK/5% SiS-PPSU	500	20	2.6	13[3, 10]
S-PEEK/7% SiS-PPSU	1200±300	26±4	2.9±0.5	8
S-PEEK/10% SiS-PPSU	850	23	3.5	6[3, 10]

Table 3.2 Apparent elastic modulus *E*, maximum strength *σ*, elongation at rupture ε, and water uptake coefficient λ after 1 h full immersion for various membranes
[(a)]Victrex Data Sheet

Figure 3.10 is a plot of maximum strength versus elastic modulus, showing a fairly linear relation. The data refer to **Table 3.2**.

The relation between water uptake coefficient after 1 h of full immersion and the elastic modulus of different membranes in the S-PEEK family is plotted in **Figure 3.11.**

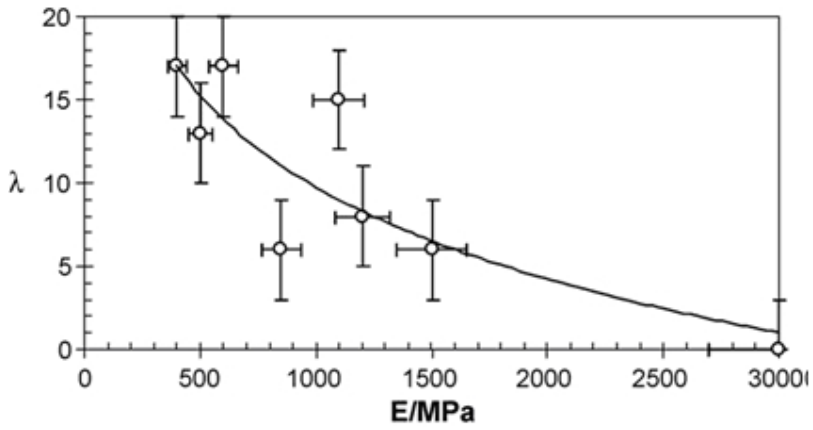

Figure 3.11 Water uptake coefficient λ after 1 h full immersion as function of elastic modulus E of studied polymer membranes (see Table 3.2).

The stress–strain curves show a very strong influence of the secondary PPSU phase. Elastic modulus and maximum strength data are consistent: whereas sulfonation of PPSU softens the polymer, silylation of PPSU enhances the membrane strength considerably. It might be surprising that addition of such a small amount of silanol groups changes the mechanical

properties of the membranes so strongly. Only 7 w% secondary phase is added, which contains furthermore only a small concentration of phenyl-silanol groups (only 5% of macromolecular units are silylated); in fact, the molar concentration of silicon is only about 0,3 mol%. However, it is well known that small additions of a second element can very strongly modify the mechanical properties of solids, the best known case being steel, where addition of about 1 mol% carbon hardens considerably the relatively soft iron matrix. Tentatively, one may attribute the hardening of the polymer matrix to the presence of the large phenyl-silanol side chains (**Figure 3.12**) that will counteract the motion of majority S-PEEK polymer chains, when a shear force is applied to the material.

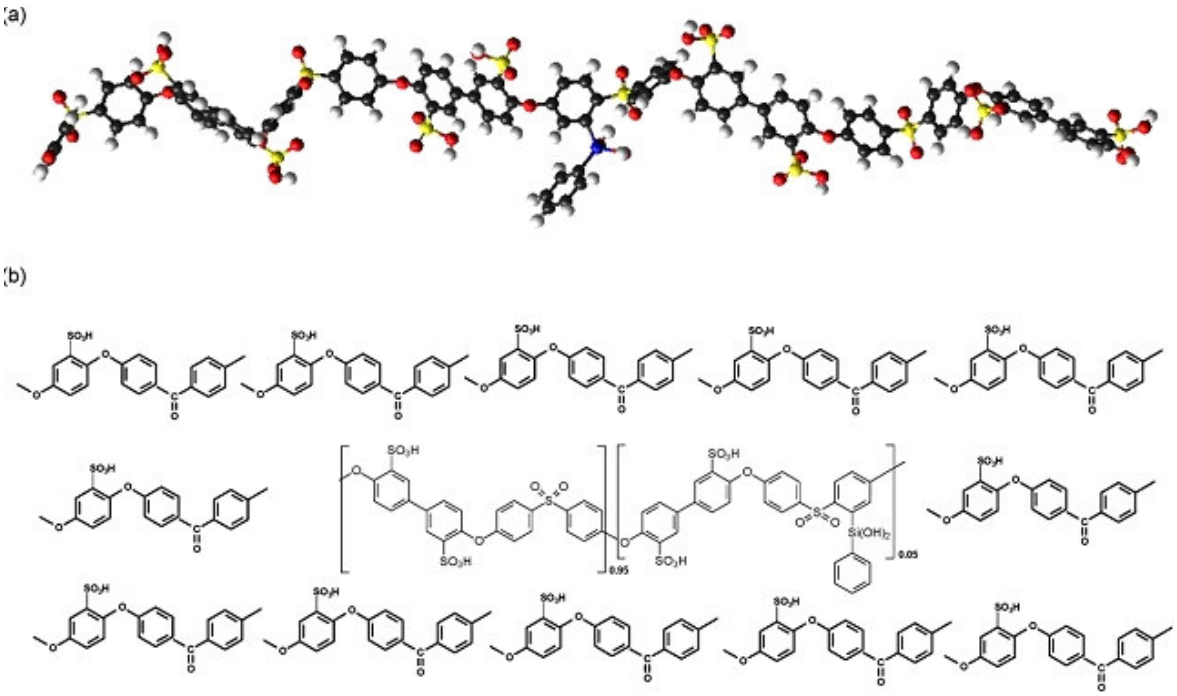

Figure 3.12 . **Schematic model of SPEEK/SiS-PPSU composite.**

Furthermore, hydrogen bond interactions will be strong between the silanol groups and sulfonate groups of the S-PEEK matrix. This might explain the considerable hardening by addition of silanol groups. Considering the water uptake properties of different membranes in the S-PEEK family, our data show unambiguously that the lower the elastic modulus, the higher the water uptake.

Considering that too high water uptake leads to swelling of the membrane, the importance of elastic properties for membrane swelling under fuel cell operation conditions is underlined. On the other hand, given the relation between water uptake and proton conductivity of hydrated

acidic polymer membranes, one must find a compromise between low membrane swelling and high proton conductivity, which should correspond to an optimum value of elastic modulus.

The experiments show that composites with silylated PPSU have a high strength and tend much less to membrane swelling at RH above 50%. The mechanical reinforcement is related to the bulky phenyl-silanol groups in the silylated macromolecule. When membrane swelling is suppressed by addition of Si-PPSU, water uptake coefficients calculated after equilibration with water vapor at different RH are consistent with values calculated after immersion in liquid water. Water diffusion coefficients are in good agreement with previously reported values for other members of the S-PEEK family. Furthermore, they are a sensitive indicator of membrane swelling phenomena, given the dependence of chemical diffusion coefficients on the square of membrane thickness [13].

Given that the best properties were observed with composites of Si-PPSU, the following experiments were therefore made on this composite.

3.2. Composites with Si-PPSU

In this section the results obtained for blends having sulfonated PEEK, with a degree of sulfonation $0.6 \leq DS \leq 0.9$ as majority partner (93 weight %) and silylated PPSU as minority partner (7 weight %) are reported.

All the composites were obtained using Dimethylsulfoxide as solvent. After the casting procedure the membrane were treated at 120 for 168 h and 140 °C for 64h.

3.2.1. Thermal Properties

Figure 3.13 shows typical high resolution thermogravimetric curves of a blend and comparison with SPEEK (DS = 0.9). The initial mass loss (about 10%) corresponds to removal of water molecules from the polymer membrane. For the blend, one can estimate that about 2.5 water molecules are eliminated per sulfonic group (expressed as water uptake coefficient λ) using the molar masses of water and polymer blend. One can then recognize the loss of sulfonic acid groups between 225°C and 325 °C followed by the oxidative degradation of the polymer main chain around 430°C [6-9]. In comparison with pure S-PEEK, one notices an increase of the decomposition temperature of sulfonate groups, whereas the temperature of degradation is slightly lower, but completely sufficient for use in intermediate temperature fuel cells.

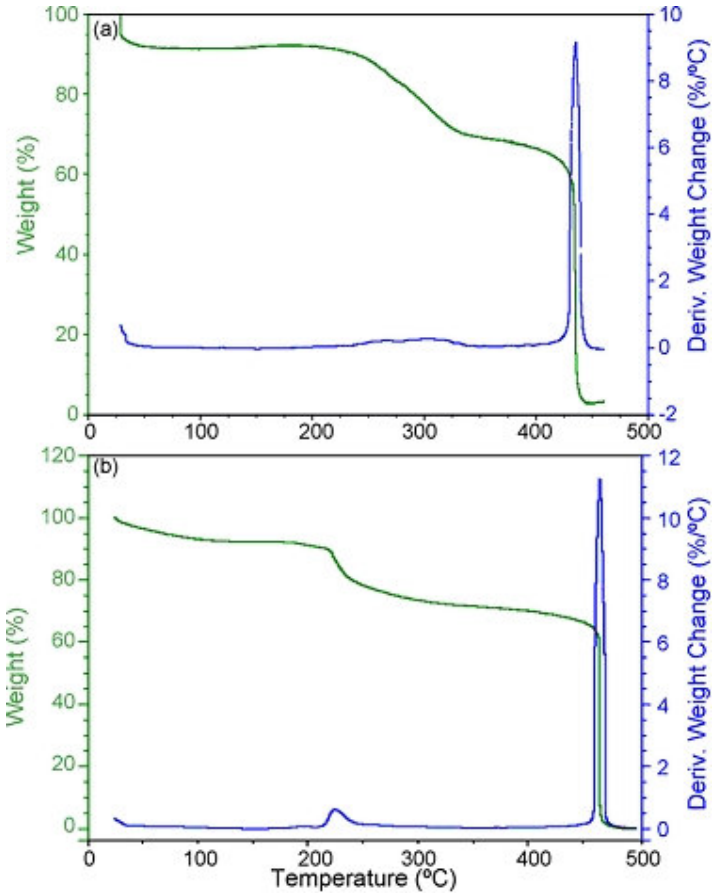

Figure 3.13 High resolution thermogravimetric curve of (a) S-PEEK (0,9)/Si-PPSU blend and (b) SPEEK (0,9).

3.2.2. Mechanical Properties

3.2.2.1 Stress-Strain Tests

Thermal treatments influence not only the capability of membranes to absorb water, but also their mechanical properties. **Figure 3.14** shows typical stress strain curves obtained for S-PEEK(0.9)/Si-PPSU blend cured at different temperatures. The corresponding mechanical properties are resumed in **Table 3.3**. The values of Young's Modulus (E) and Ultimate Strength (σ) obtained for the untreated sample are very low. The comparison with the values obtained for blends synthesized using DMAc as solvent shows that the membranes made using DMSO as solvent have inferior mechanical properties. It is well known in literature that the solvent used during the preparation of membranes influences their behaviour and interacts with sulfonic groups of sulfonated PEEK [7, 14, 15]. Robertson et al. [7] have shown that DMAc interacts with S-PEEK forming hydrogen bonds between amine groups and protons of the sulfonic

groups. The reduction of the number of free protons due to S-PEEK/solvent interactions reduces the proton conductivity of membranes and probably influences their mechanical behaviour. Ye et al. [14] have also shown that membranes made using DMSO as solvent have a higher water content than those made using other solvents. The higher water content implies the mobility of the polymer backbones and weaker interactions between polymer chains. All mechanical tests were performed in ambient conditions (RH about 50%) and the higher water content in DMSO-made blends can further degrade mechanical properties by plastification.

Mechanical properties of composites change after thermal treatments. The sample cured at 120°C for 168 hours (1 week) shows a Young's Modulus and Ultimate Strength very close to the untreated one, but also an increased ductility with a higher value of the elongation at the rupture (ε). An increase of the temperature of thermal treatment improves the strength of membranes but reduces its ductility. The sample thermally treated at 140°C for 64 hours shows a very high value of both Young's Modulus and Ultimate strength and a reduced elongation at rupture.

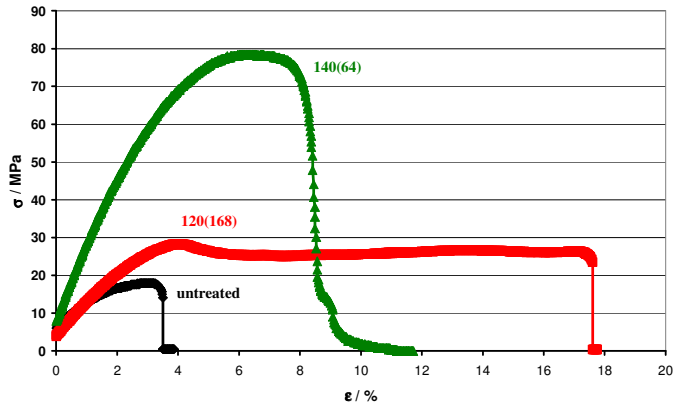

Figure 3.14 Comparison of Stress-Strain curves of S-PEEK(0.9)/Si-PPSU blends thermally treated

Thermal Treatment Temperature (time)	***E [MPa]***	***σ [MPa]***	***ε [%]***
untreated	705±20	15±2	3±1
120(168)	890±170	26±5	13±5
140(64)	2060±170	71±7	9±1

Table 3.3 Young's Modulus (E), Ultimate Strength (σ) and Elongation at the Rupture (ε) of SPEEK(0.9)/Si-PPSU composite made in DMSO and cured at different temperatures for different time.

On the base of these results the following experiments were made on samples treated at 140 °C for 64h.

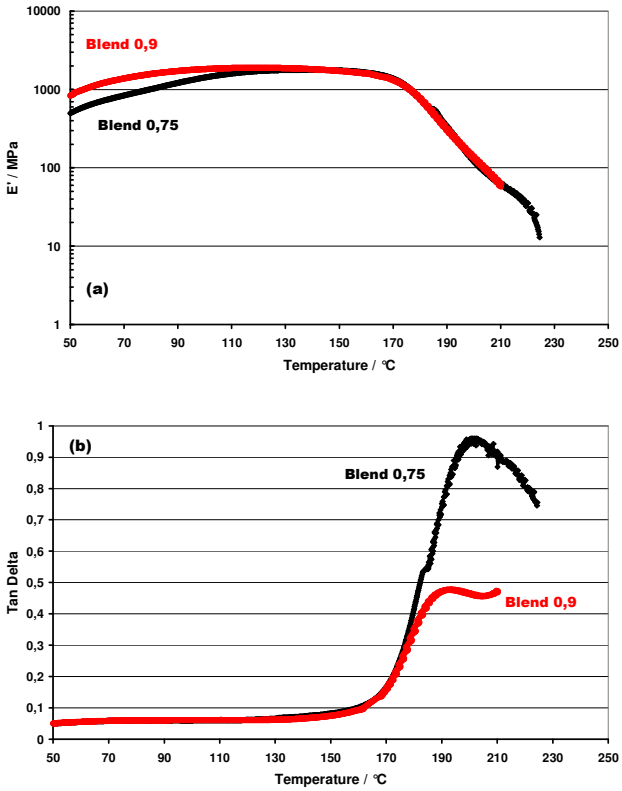

Figure 3.15 Dynamic Mechanical Analysis curves of S-PEEK/Si-PPSU with different degree of sulfonation, DS = 0.75 (black symbols) or DS = 0.9 (red symbols). All samples are cured at 140°C for 64 hours. (a) Storage Modulus and (b) Tan Delta

3.2.2.2 Dynamic Mechanical Analysis

Figure 3.15 shows typical DMA curves in dry condition presenting the storage modulus and tan δ vs. temperature of S-PEEK (0.75) and S-PEEK (0.9) blends thermally treated at 140°C for 64 hours. **Figure 3.15 (a)** shows that the storage modulus varies strongly with the temperature. The experiment was not performed with a constant force, but with variable force. The important decrease of the storage modulus above 170°C is related to the glass transition temperature (T_g), defined as the temperature at which the material transforms from the glassy state to the rubbery state. Speaking of amorphous materials, there is no specific transition temperature but a range of temperatures (of the order of 20°C) where many properties of the material change [16, 17]. The glass transition temperature can be evaluated by curves obtained by DMA; as reported in Ref. [18] it is possible to use five different methods. In **Table 3.4** are

summarized the glass transition temperatures obtained for blends and calculated from the onset of tan δ peak. The glass transition temperature is strongly influenced by thermal treatments. As confirmed in literature [15], in both samples, treated and untreated ones, a lower glass transition temperature for S-PEEK (0.75) blends is observed. As can be seen in **Table 3.4** the glass transition temperature of untreated samples is about 45°C below that of PEEK (T_g = 150°C - 156°C). Thermally treated samples have a T_g above that of PEEK by about 50°C.

Thermal Treatment temperature (time)	T_g (°C)	
	S-PEEK(0.75)	S-PEEK(0.9)
Untreated	105	117
140(64)	193	201

Table 3.4 Glass transition Temperature (T_g) of thermally treated and untreated S-PEEK (0.9)/Si-PPSU and S-PEEK (0.75)/Si-PPSU blends.

3.2.3. Water Uptake

Figure 3.16 shows water vapour adsorption/desorption isotherms of S-PEEK (0.9) and blend at 25 °C. The water uptake coefficient of blend around RH = 60%, which is about ambient humidity, is consistent with the value calculated above from the initial water loss in TGA. The water vapour uptake of pure S-PEEK is higher than for the blend, in agreement with the hydrophobicity of Si-PPSU secondary phase.

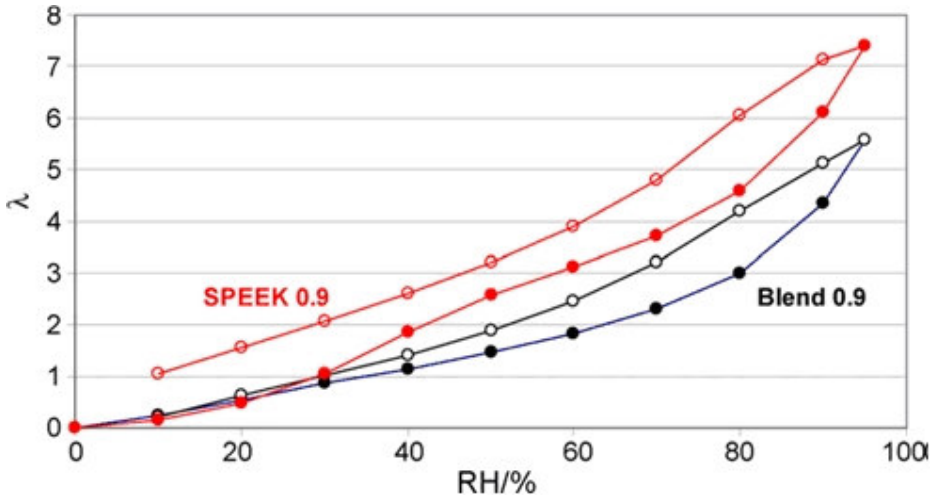

Figure 3.16 Water adsorption/desorption isotherm for SPEEK (0.9) and SPEEK (0.9)/SiPPSU blend at 25 °C.

Water uptake coefficients measured by immersion in liquid water between 25°C and 140°C are reported in **Figure 3.17**.

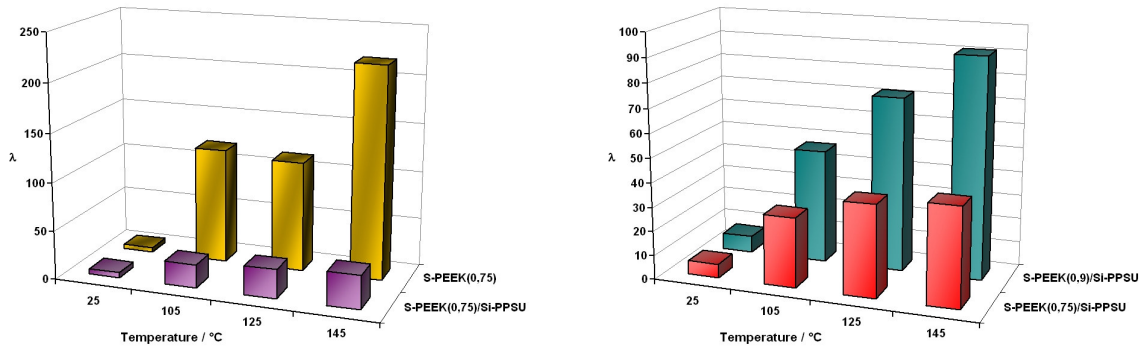

Figure 3.17 Water Uptake coefficients measured after 1 hour of full immersion in water at different temperatures (left side) and at the stability (right side)

No dissolution is observed, even at 140°C, in contrast with pure S-PEEK. Using water uptake coefficients λ at different temperatures, one can estimate the activation energy E_a from an Arrhenius plot using the equation:

$$\ln \lambda = \ln \lambda^0 - \frac{E_a}{RT} \quad (3.4)$$

Linear correlations are indeed observed (**Figure 3.18**), confirming the applicability of Arrhenius equation; the calculated activation energies, around 20 kJ mol^{-1}, are in good agreement with activation energy values for water diffusion in S-PEEK (17–20 kJ mol^{-1} [19]). Given that the membrane composition changes during water uptake, the temperature dependence is assumed to be related to chemical diffusion of water, including thus a term related to activity coefficients of water. The activation energy includes the partial molar enthalpy of water in the polymer matrix. The slightly lower activation energy value for the sample with smaller DS might be related to a smaller partial molar enthalpy of water in the less sulfonated polymer; this would correspond to a lower amount of hydrogen bonding between sulfonic acid groups and water.

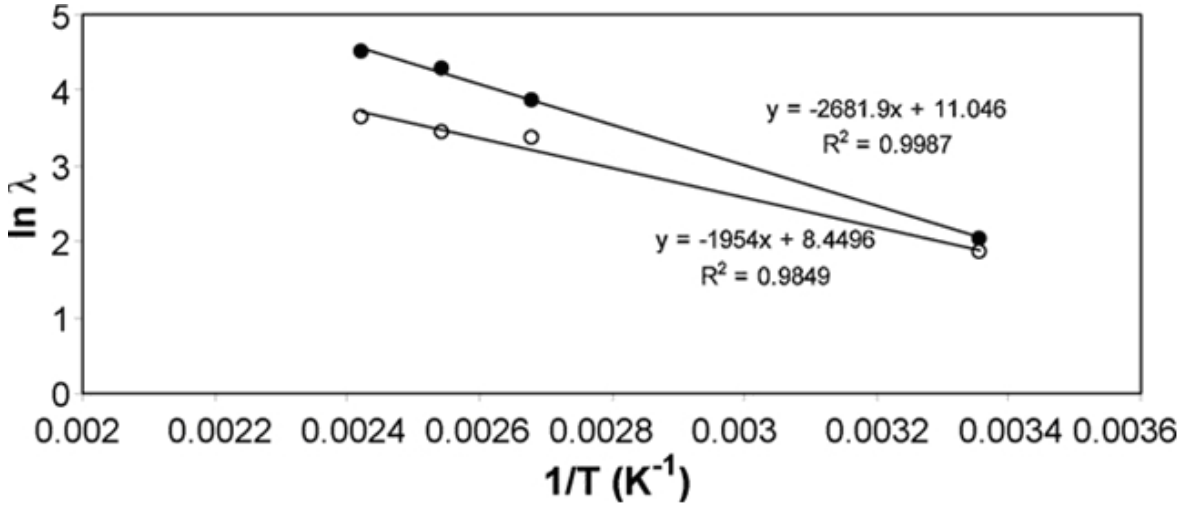

Figure 3.18 Temperature dependence of the water uptake coefficients of blends: S-PEEK

3.2.4. Electrical Properties

3.2.4.1 Dielectric Analysis

Figure 3.19 shows the AC conductivity of a S-PEEK(0.75)/Si-PPSU composite thermally treated at 140°C for 64 hours and a full heating/cooling cycle at fixed frequency 10 kHz. The comparison with the untreated membrane was impossible because the sample bonded to the electrodes during the experiment.

In **Figure 3.19 (a) and (b)** is shown the temperature dependence of the AC conductivity. During heating, the ionic conductivity decreases until reaching a relative minimum at around 130°C. This drop is probably due to the water loss. Above 150°C an increase of ionic conductivity is observed. The polymer is becoming soft, because the temperature is approaching the glass transition and the movements of the macromolecular chains can support the ion hopping. During cooling, the conductivity decreases monotonically with the temperature and below the glass transition follows an Arrherinus law (**Figure 3.20.**). The apparent activation energy obtained is about 30 kJ mol^{-1} [20].

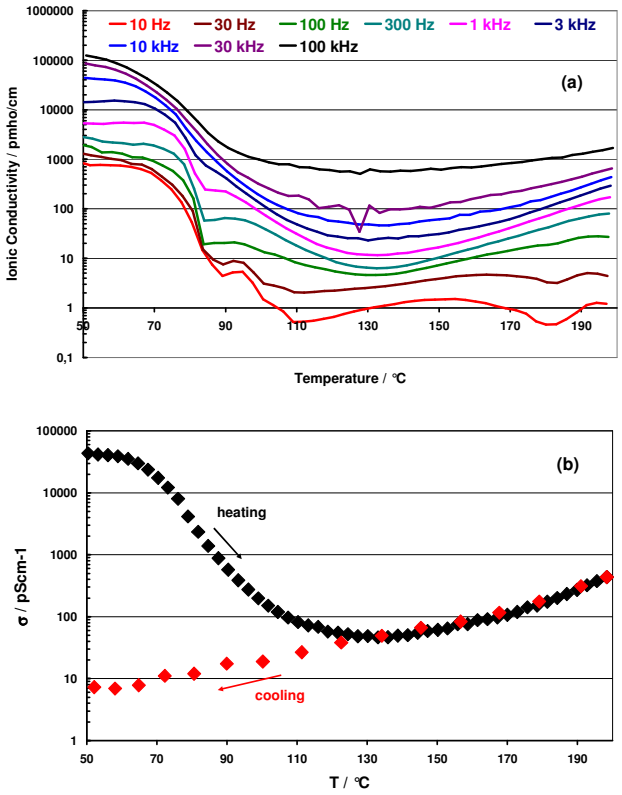

Figure 3.19 AC conductivity of a S-PEEK(0.75)/Si-PPSU blend membrane as function of temperature (a) at all frequencies between 10 Hz and 100 kHz and (b) at 10 kHz during a complete heating and cooling cycle (membrane cured at 140°C for 64 hours).

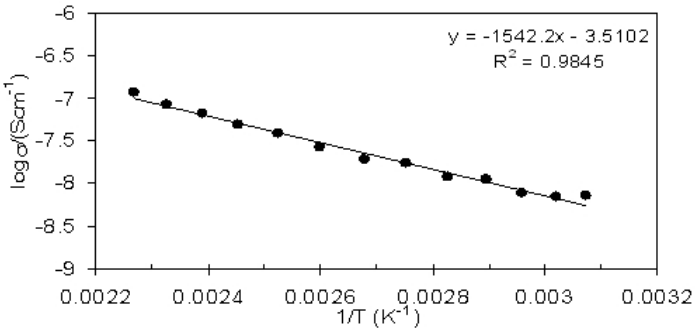

Figure 3.20. Arrhenius plot of AC conductivity of anhydrous S-PEEK(0.75)/Si-PPSU blend from DEA measurements.

3.2.4.2 Proton conductivity measurements

Figure 3.21 shows the proton conductivity (σ) of S-PEEK (0.9) blend thermally treated at 140°C for 64 hours. The membrane conductivity was evaluated at 100°C, as function of relative humidity, using impedance spectroscopy. In **Figure 3.21** were inserted data of neat S-PEEK (0.9) as reported in Ref. [21]. The blend conductivity is nearly equivalent to the conductivity of

pure S-PEEK up to about 80% RH. At higher RH values, the S-PEEK membrane becomes unstable and the conductivity decreases drastically due to membrane swelling. The conductivity of the blend turns out to be stable up to at least 90% of relative humidity [20]. This is obviously a very significant advantage for eventual use in fuel cells at high humidification.

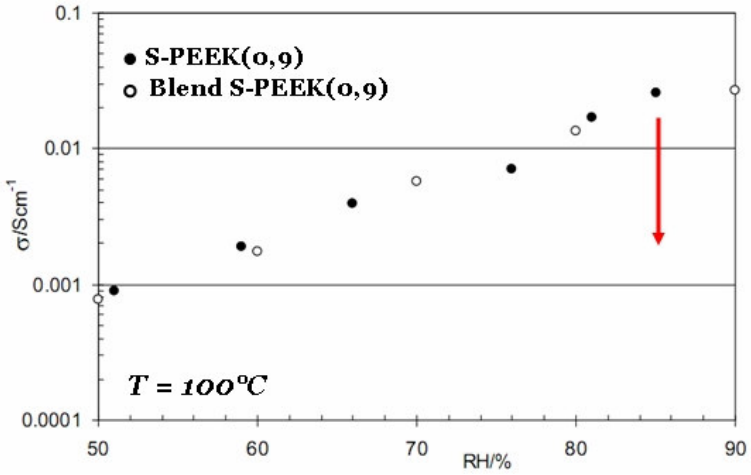

Figure 3.21 Proton Conductivity at 100°C vs Relative Humidity for a S-PEEK (0.9)/Si-PPSU membrane cured at 140°C for 64 hours and S-PEEK (0.9)

3.2.5. Discussion

PEEK and PPSU were chosen for their complementary chemical and morphological properties. Being fully aromatic, these polymers have excellent thermal oxidation resistance with a high glass transition temperature (T_g). The value of T_g depends on macromolecular characteristics affecting chain stiffness. Chain flexibility is diminished and glass transition temperature increased by presence of bulky side groups, polar side groups, aromatic chain groups, which tend to stiffen the molecular backbone.

An important aspect regards their conformational characteristics: the polymeric backbone of PEEK is more flexible while the molecular chain of PPSU is rather rigid. Both the direct linkage between the aromatic rings and the resonance effects due to the sulfonyl group contribute to its reduced flexibility. A more rigid polymer in which chain segments are unmoving in fixed positions has stronger intermolecular interactions. This behaviour is reflected in the T_g of the two polymers: 208°C and 143°C for PPSU and PEEK, respectively. Thus, the relatively linear conformation of Si-PPSU, as previously discussed, can be correlated to the rigidity of the polymer and to the bulky phenyl side group bonded to silicon that is stiff and near to the backbone and can cause steric hindrance, decreasing chain mobility. Depending on the molecular

structure and on the flexibility and conformation of macromolecules, different intermolecular bonding forces act among polymeric systems.

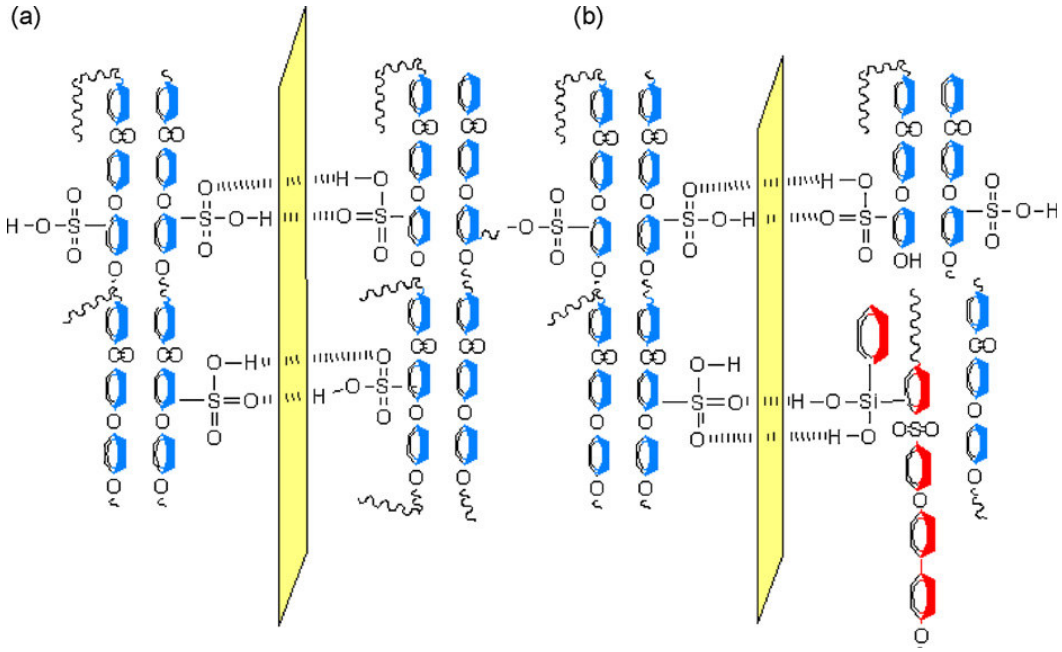

Figure 3.22 Schematic representation of the interface between (a) SPEEK polymer chains and (b) SPEEK and SiPPSU chains

In the arylen-based systems, different types of interactions between the polymer chains are always present: London-type interactions between the backbones, dipole–dipole interactions between the carbonyl or sulfonyl groups, hydrogen bridges and electrostatic interactions connected with the acidic groups present when the polymers are sulfonated [2]. The nature and quantity of these interactions determine the molecular aggregation of the system leading to different tertiary structures. The type of self assembly plays a fundamental role in the polymer properties and determines the membrane behaviour [22]. Consequently the introduction of the second phase in S-PEEK can lead to the formation of specific interactions between the polymer chains modifying the hydrophilic/hydrophobic domains and reinforcing the mechanical strength. The larger temperature range for loss of sulfonate groups, in comparison with pure S-PEEK, indicates that interactions at the interface between the two polymers modify the intermolecular bond energetics, as schematically represented in **Figure 3.22**, and lead to a larger distribution of decomposition temperatures. The interface represents also a region, where water molecules are preferably located, leading at high water partial pressure to the formation of hydrophilic conduction pathways. The symmetry break between the two polymer chains in the blend is clearly seen (**Figure 3.22 (b)**). The introduction of Si-PPSU chains increases the hydrophobicity

of the polymer blend and induces specific interactions in the system modifying the hydrophilic/hydrophobic domains. This model justifies the significant changes of water uptake and mechanical properties observed in the blends.

We can conclude this part by stating that the preparation of composite materials, including a majority proton conducting polymer and a minority "anchor" polymer with high mechanical strength is a promising strategy for membrane improvement, especially if combined with an optimized annealing treatment.

3.3. SPEEK-Organically Modified TiO_2 Composites

In this part, two different TiO_2 particles with organically modified surface are used as filler. The hybrid membranes are characterized and compared with pure S-PEEK membranes. The swelling and thermal behaviour, mechanical strength, and electrical properties are discussed.

3.3.1. Structure and Microstructure

The X-Ray diffraction pattern of a composite membrane is reported in **Figure 3.23**. Composite membranes show a clear amount of crystalline anatase phase within the majority amorphous polymer, as can be immediately concluded from the reflections in the diffraction pattern. The presence of crystalline TiO_2 is expected to influence the mechanical and electrical properties of the hybrid membranes.

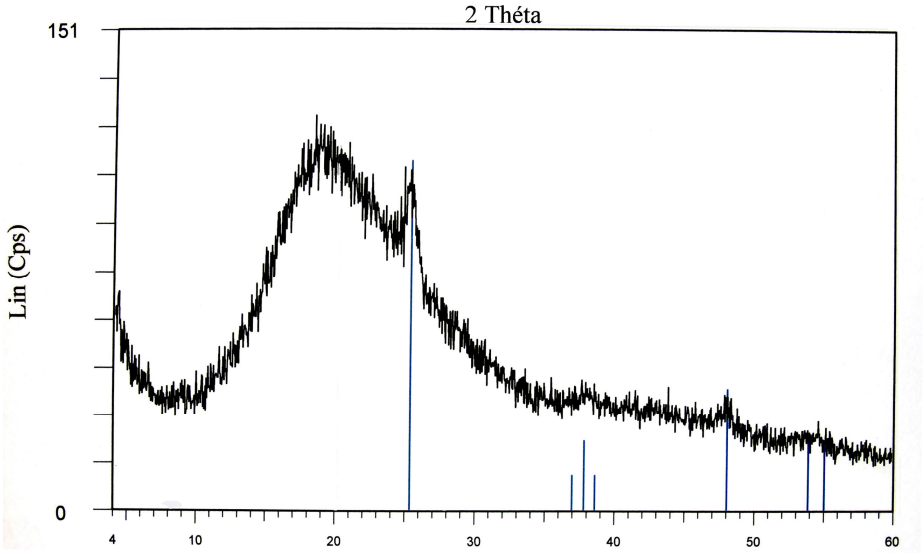

Figure 3.23 Ray diffraction pattern of S-PEEK/TiO_2 composite

The following SEM images show typical microstructures of S-PEEK/TiO_2 composites. Left image (**Figure 3.24 (a)**) shows a membrane with hydrophilic TiO_2: the important agglomeration of titania particles leads to an inhomogeneous membrane. The right image (**Figure 3.24 (b)**) shows a membrane with hydrophobic TiO_2, which is much more homogenous, due to smaller interaction between TiO_2 particles. The corresponding EDX (see **Figure 3.25**) analysis shows clearly the presence of S, due to sulfonic acid groups, and Ti from the inorganic oxide.

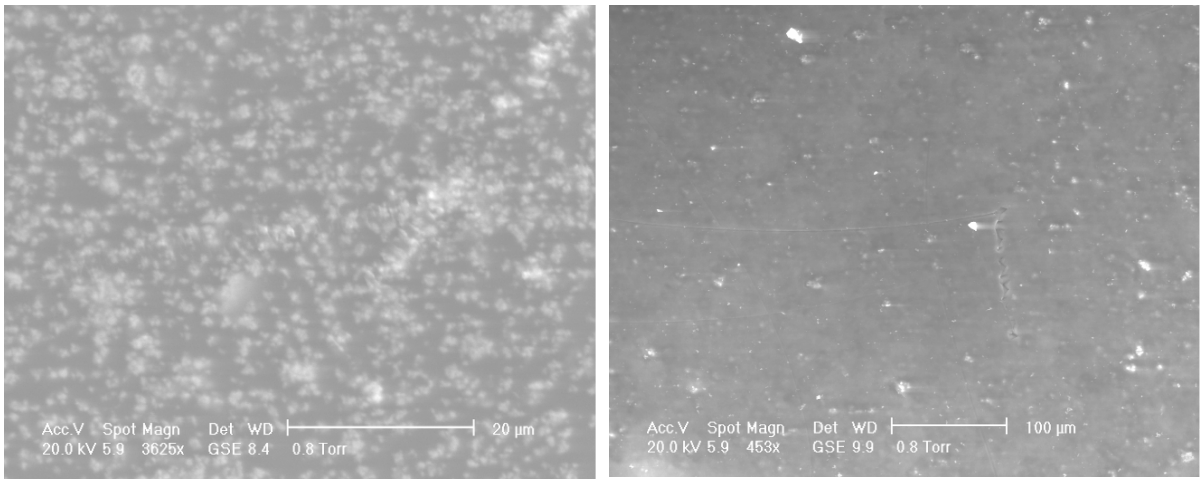

(a) (b)

Figure 3.24 SEM image of (a) S-PEEK(0.75)/hydrophilic TiO_2 and (b) S-PEEK(0.75)/hydrophobic TiO_2 composites

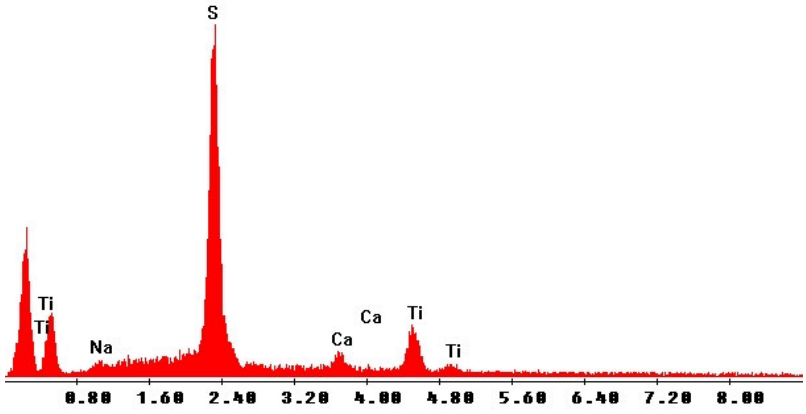

Figure 3.25 EDX analysis of S-PEEK/TiO_2 membrane

The following AFM images (**Figure 3.26**) show the characteristics of S-PEEK(0.75)/F-TiO_2 composites annealed at 140°C for 64 hours and untreated. All the surfaces are without pores, but the presence of the second phase makes the surfaces inhomogeneous with a higher mean roughness for the annealed membranes (R_{ms} = 49 nm for annealed and R_{ms} = 15 nm non annealed hydrophilic TiO_2 composites; R_{ms} = 20 nm for annealed and R_{ms} = 15 nm non annealed hydrophobic TiO_2 composites). The two functionalized TiO_2 composites do not show the same roughness when they are annealed: with hydrophilic TiO_2 the membrane has a higher R_{ms}. The annealing seems to enhance the inhomogeneity of membranes.

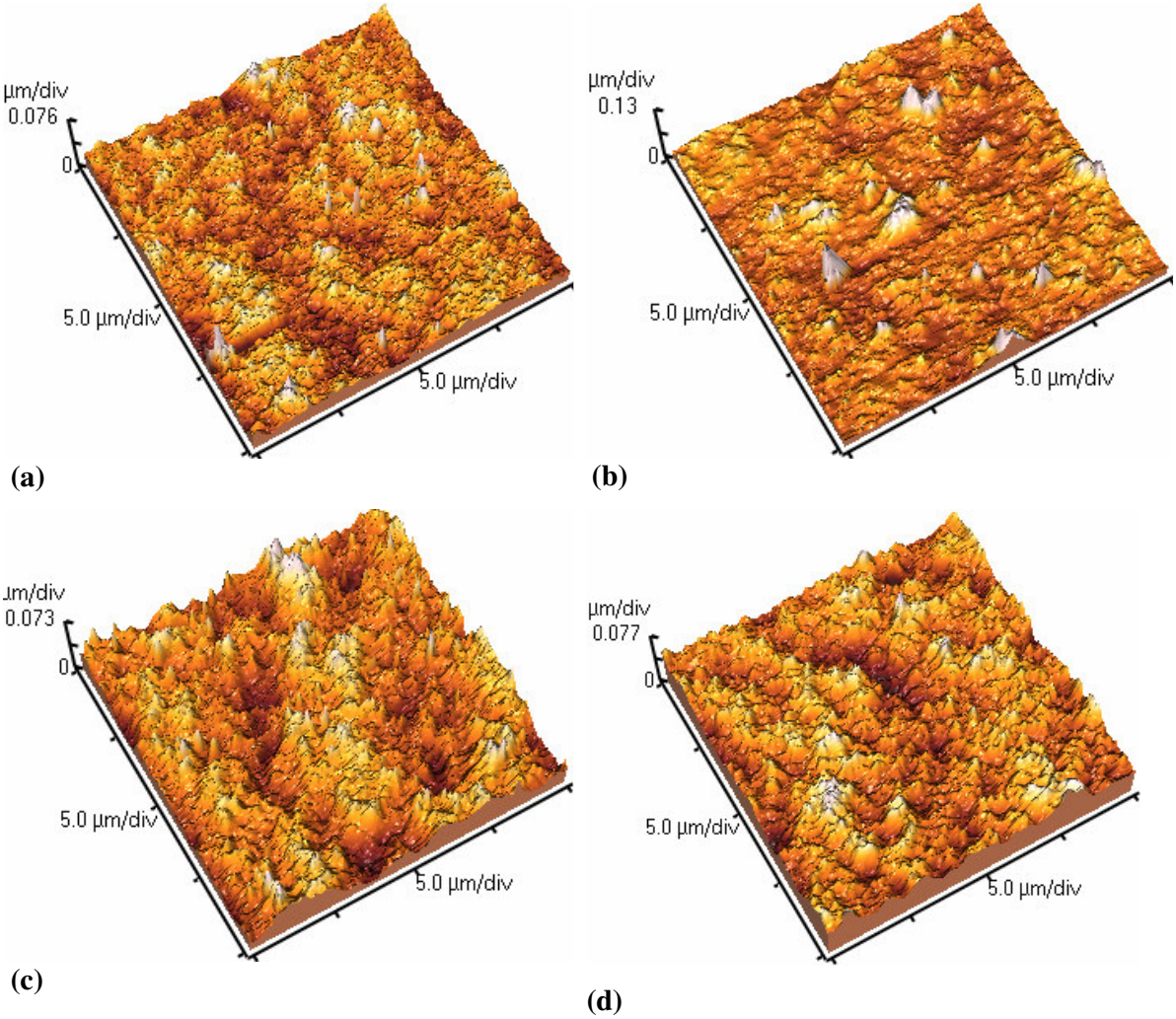

Figure 3.26 AFM images of S-PEEK(0.75)/hphi TiO_2 (a) annealed at 140°C for 64 hours and (b) untreated and S-PEEK(0.75)/hpho TiO_2 (c) annealed at 140°C for 64 hours and (d) untreated.

Figure 3.27 shows a comparison between typical FTIR spectra of S-PEEK(0.75) membrane and of S-PEEK(0.75)/hphi TiO_2 and S-PEEK(0.75)/hpho TiO_2 composites. In all

spectra, aromatic groups from PEEK backbone and sulfonic acid groups are observed. The hydrophobic composite exhibits some differences around 2350 cm^{-1}. There is also a clear difference between these spectra around 3500 cm^{-1}, the region of OH absorption. Furthermore, the transmittance between 800 cm^{-1} and 400 cm^{-1} is lower in composites, where cation-ligand interactions can be observed.

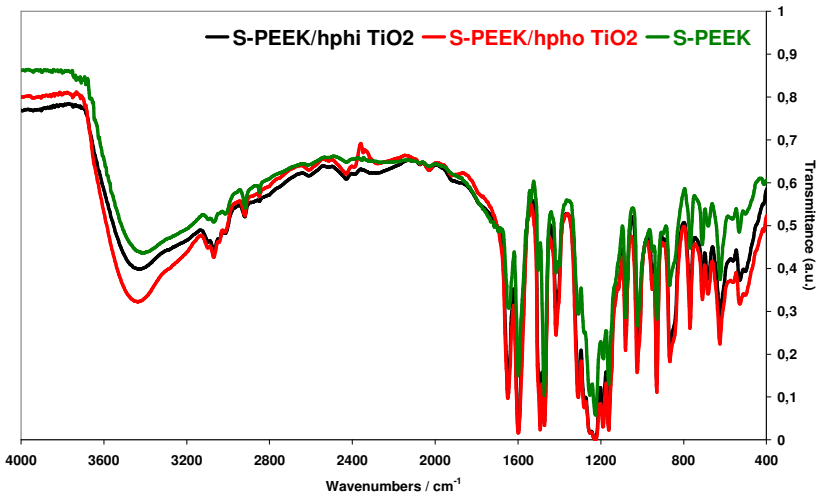

Figure 3.27 FTIR spectra of SPEEK/hydrophilic titania (black line) SPEEK/hydrophobic titania (red line) and S-PEEK (green line).

3.3.2. Thermochemical Properties

The thermogravimetric analysis (**Figure 3.28**) shows that S-PEEK/F-TiO_2 composite membranes have the same decomposition profile. At low temperature, two mass losses can be observed for all samples corresponding to about 7% of their initial mass. The first loss (around 120°C - 150°C) can be attributed to water molecules sorbed by hydrophilic groups and lost until the dry state of the sample is reached [9, 23] and to residual casting solvent DMSO removal [7]. The second loss (around 200°C - 210°C) can be attributed to cross-linking of macromolecular chains.

The main mass loss starts approximately at 210°C and is attributed to the decomposition of the sulfonic acid groups of S-PEEK. The whole weight loss can be evaluated knowing the degree of sulfonation of S-PEEK. It is expected to be around 16% and **Figure 3.28** confirms a weight loss close to this value for all membranes. The presence in the membranes of titanium dioxide slightly modifies the temperature range in which the decomposition of sulfonic groups occurs. The loss of sulfonic acid groups for S-PEEK/TiO_2 composites was observed between 210°C and

330°C. The last mass loss is attributed to PEEK main chain decomposition. For S-PEEK membranes it is observed between 400°C - 500°C, while for S-PEEK/TiO_2 it is recorded in the temperature range 325°C - 465°C.

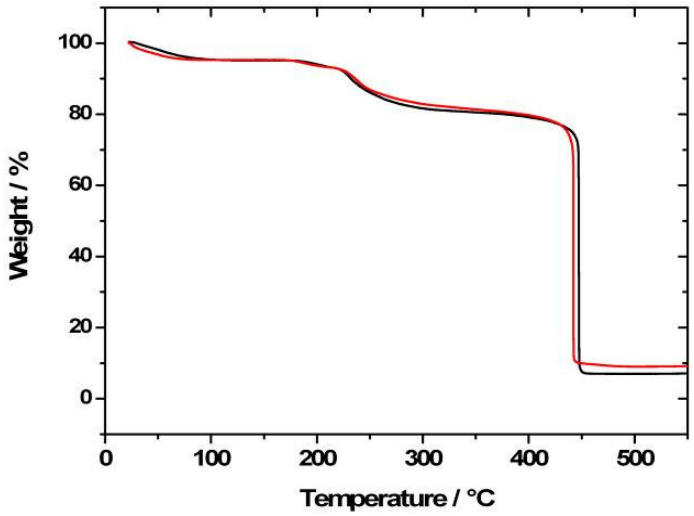

Figure 3.28 HR-TGA of S-PEEK(0.75)/hydrophobic TiO_2 (red line) and S-PEEK(0.75)/hydrophilic TiO_2 (black line).

3.3.3. Water Uptake

Figure 3.29 shows λ values obtained after 1 hour of full immersion in water at different temperatures for the three membranes. **Table 3.5** reports the values reached by the samples at equilibrium. We can observe that at 25°C the values of the water uptake coefficient are not influenced by the presence of F-TiO_2 in the matrix. The presence of functionalized titanium dioxide is instead of fundamental importance at higher temperature; it enhances the stability of the membranes reducing their tendency to absorb water. While S-PEEK is soluble after 1 hour at a temperature higher then 75°C, the two composites reach a stable value. Another aspect that could be noted is that the nature of the chemical modification influences the behaviour of the membranes. Even if the percentage of TiO_2 added to S-PEEK is the same, the water uptake values are higher if the surface additive is hydrophilic, confirming an expected tendency.

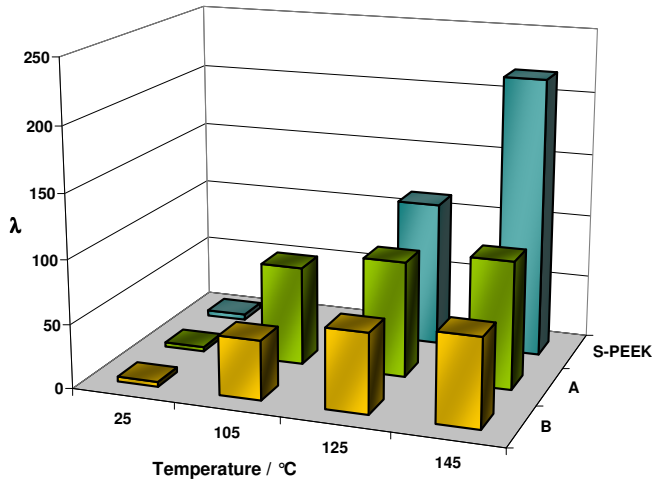

Figure 3.29 Maximum water uptake coefficient (λ) obtained for S-PEEK/hphi-TiO_2 (label A) and S-PEEK/hpho-TiO_2 (label B) composites

Water Temperature (°C)	*S-PEEK(0,75)/hphi TiO_2*	*S-PEEK(0,75)/hpho TiO_2*
25	4	4
105	77	46
125	90	62
145	100	69

Table 3.5 Water Uptake coefficients of F-TiO_2 composites annealed at 140°C for 64 hours measured in full immersion in liquid water.

The results obtained in water vapour sorption at 25°C are shown in **Figure 3.30**. The water uptake obtained is consistent with those obtained by immersion in liquid water (IEC = 2.2 mequiv/mol).

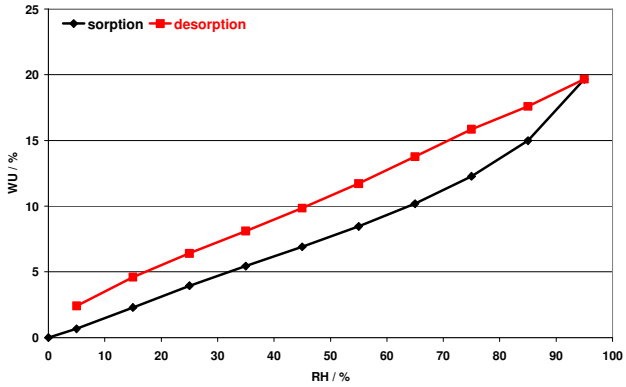

Figure 3.30 Water sorption isotherm at 25°C for S-PEEK(0.75)/hphi TiO_2 composite annealed at 140°C for 64 hours

3.3.4. Mechanical Properties

Figure 3.31 shows typical stress-strain curves for composite membranes and comparison with single-phase S-PEEK. The static mechanical properties of S-PEEK and S-PEEK with hydrophobic TiO_2 are very reproducible, which is in accordance with a very homogenous membrane. On the contrary, the mechanical properties determined for the membrane with hydrophilic TiO_2 show a large scatter, probably related to the inhomogenous nature of the membrane, as shown in the SEM image. The data reported in **Table 3.6** have therefore considerably different standard deviations. Provided this limitation, it seems that the composite with hydrophilic titania shows the highest strength and lowest ductility. Both composite are considerably less ductile than pure S-PEEK.

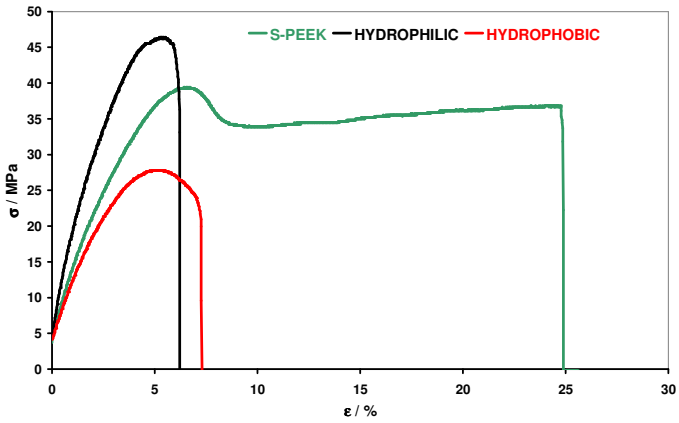

Figure 3.31 Stress Strain curves of S-PEEK(0.75)/hydrophobic TiO_2 (red line) and S-PEEK(0.75)/hydrophilic TiO_2 (black line) and SPEEK(0.75) (green line) annealed at 140°C for 64 hours

Membrane	*E [MPa]*	*σ [MPa]*	*ε [%]*
S-PEEK(0.75)/hphi TiO_2	1400±500	41±13	7±4
S-PEEK(0.75)/hpho TiO_2	880±20	27±2	8±2

Table 3.6 Young's Modulus (E), Ultimate Strength (σ) and Elongation at the Rupture (ε) of SPEEK(0.75)/F-TiO_2 composites annealed at 140°C for 64 hours.

Figure 3.32 shows DMA experiments made on annealed and non annealed S-PEEK(0.75)/F-TiO_2 composites. The adding of functionalized TiO_2 with annealing increases the glass transition temperature importantly. The composites made using hydrophobic TiO_2 have a slightly higher glass transition that the ones made using hydrophilic TiO_2. The functionalization of TiO_2 seems influence the T_g after the annealing: the composite made using the hydrophobic TiO_2 has a higher glass transition that the one made using hydrophilic TiO_2.

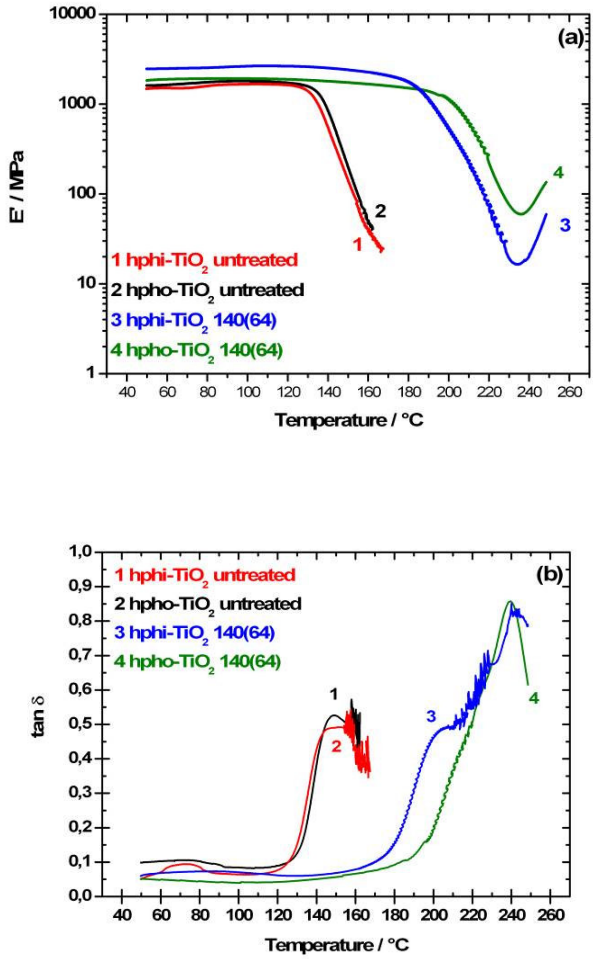

Figure 3.32 (a) Storage Modulus (E') and (b) tan δ of S-PEEK(0.75)/F-TiO_2 composites as function of temperature from DMA experiments.

Thermal Treatment Temperature (time)	***T_g (°C)***
	hydrophobic TiO_2
Untreated	135
140(64)	200
	hydrophilic TiO_2
Untreated	140
140(64)	185

[(a)]Thermal Treatment temperature in °C and time in hours

Table 3.7 Glass transition temperatures of S-PEEK(0.75)/F-TiO_2 composites annealed and non annealed.

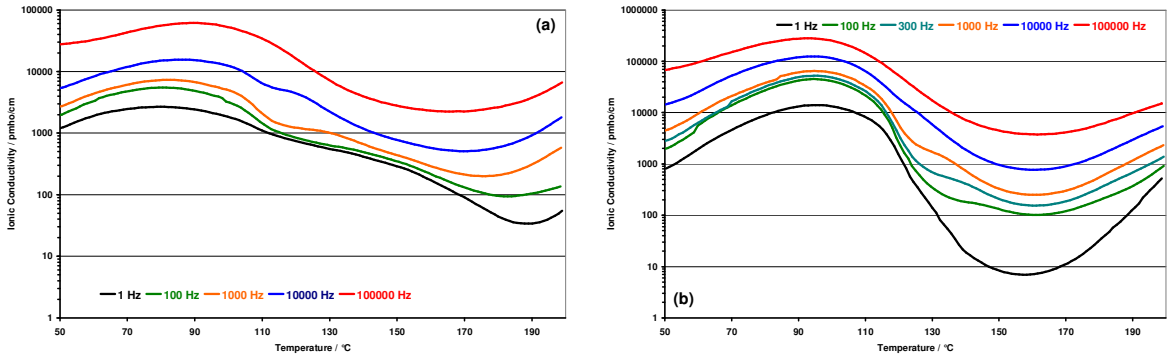

Figure 3.33 AC conductivity of (a) S-PEEK(0.75)/hphi TiO_2 and (b) S-PEEK(0.75)/hpho TiO_2 composites annealed at 140°C for 64 hours

3.3.5. Electrical Properties

Figure 3.33 shows the AC conductivity of S-PEEK(0.75)/F-TiO_2 composites annealed at 140°C for 64 hours. During heating, an increase of ionic conductivity was observed in both samples until reaching a maximum around 70°C - 90°C for composites with hydrophobic TiO_2 and around 100°C with hydrophilic TiO_2. Probably the hydrophilic nature of the second phase allows reaching a higher ionic conductivity. Above 110°C the ionic conductivity decreases until to reach a minimum at around 150°C for hpho-TiO_2 and at 170°C for hphi-TiO_2. The lower temperature of the minimum of hydrophobic TiO_2 composite can be related to its lower T_g revealed by DMA. Above this temperature an increase of ionic conductivity was observed because the glass transition is approaching.

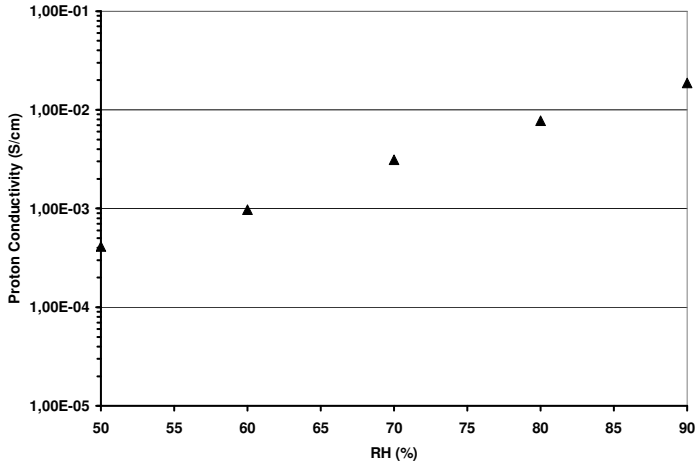

Figure 3.34 Proton conductivity of S-PEEK(0.75)/hpho TiO_2 composite annealed at 140°C for 64 hours

The proton conductivity of S-PEEK(0.75)/hphi TiO_2 (**Figure 3.34**) is lower than that of pure S-PEEK, because of the hydrophobic nature of the composite. the ionic conductivity of this membrane can be compared with values reported in Chapter 4 for double-treated S-PEEK(0.9) membrane. In that case, the cause of the low ionic conductivity was the reduced number of sulfonic groups due to the cross-link reaction. Here, the reduced ionic conductivity was due to the lower degree of sulfonation of S-PEEK used (DS = 0.75) and to the hydrophobic functionalization of TiO_2. In both cases the low content of sulfonic acid groups reduces the conductivity of membranes.

3.3.6. Discussion

The reported data show the influence of surface functionalization of the inorganic particles on the properties of the composite material: whereas a hydrophilic surface improves the proton conductivity, but reduces the homogeneity of the membranes, the hydrophobic surface gives an excellent homogeneity, but with low ionic conductivity. There is clearly room for optimization of the surface treatment, by choosing molecules with intermediate properties that could lead to a good compromise between homogeneity (and therefore reproducibility) and proton conductivity. Future experiments will be made in this direction.

3.4. References

[1] J. Kerres, W. Zhang and W. Cui, *Journal of Polymer Science Part a-Polymer Chemistry* **1998**, *36*, 1441-1448.

[2] J. A. Kerres, *Fuel Cells* **2005**, *5*, 230-247.

[3] M. L. Di Vona, A. D'Epifanio, D. Marani, M. Trombetta, E. Traversa and S. Licoccia, *Journal of Membrane Science* **2006**, *279*, 186-191.

[4] D. I. Bower, *An Introduction to Polymer Physics*, Cambridge University Press, **2002**, p. 117-161.

[5] M. L. Di Vona, E. Sgreccia, S. Licoccia, M. Khadhraoui, R. Denoyel and P. Knauth, *Chemistry of Materials* **2008**, *20*, 4327-4334.

[6] S. M. J. Zaidi, S. D. Mikhailenko, G. P. Robertson, M. D. Guiver and S. Kaliaguine, *Journal of Membrane Science* **2000**, *173*, 17-34.

[7] G. P. Robertson, S. D. Mikhailenko, K. P. Wang, P. X. Xing, M. D. Guiver and S. Kaliaguine, *Journal of Membrane Science* **2003**, *219*, 113-121.

[8] M. L. Di Vona, D. Marani, C. D'Ottavi, M. Trombetta, E. Traversa, I. Beurroies, P. Knauth and S. Licoccia, *Chemistry of Materials* **2006**, *18*, 69-75.

[9] D. Marani, M. L. Di Vona, E. Traversa, S. Licoccia, I. Beurroies, P. L. Llewellyn and P. Knauth, *Journal of Physical Chemistry B* **2006**, *110*, 15817-15823.

[10] M. L. Di Vona, D. Marani, A. D'Epifanio, S. Licoccia, I. Beurroies, R. Denoyel and P. Knauth, *Journal of Membrane Science* **2007**, *304*, 76-81.

[11] I. Merdas, F. Thominette, A. Tcharkhtchi and J. Verdu, *Composites Science and Technology* **2002**, *62*, 487-492.

[12] I. Merdas, F. Thominette and J. Verdu, *Journal of Applied Polymer Science* **2000**, *77*, 1439-1444.

[13] E. Sgreccia, M. Khadhraoui, C. de Bonis, S. Licoccia, M. L. Di Vona and P. Knauth, *Journal of Power Sources* **2008**, *178*, 667-670.

[14] G. Ye, C. M. Mills and G. R. Goward, *Journal of Membrane Science* **2008**, *319*, 238-243.

[15] S. Kaliaguine, S. D. Mikhailenko, K. P. Wang, P. Xing, G. Robertson and M. Guiver, *Catalys Today* **2003**, *82*, 213-222.

[16] A. Kumar and R. K. Gupta, *Fundamentals of Polymer Engineering*, Marcel Dekker Inc., **2003**, p. 45-47.

[17] C. A. Daniels, *Polymers: Structure and Properties*, CRC Press, **1989**, p. 17-19.

[18] K. P. Menard, *Dynamic Mechanical Analysis: a Practical Introduction*, CRC Press, **1999**, p. 88-120.

[19] K. Kidena, *Journal of Membrane Science* **2008**, *323*, 201-206.

[20] E. Sgreccia, M. L. Di Vona, S. Licoccia, M. Sganappa, M. Casciola, J. F. Chailan and P. Knauth, *Journal of Power Sources* **2009**, *192*, 353-359.

[21] G. Alberti, M. Casciola, L. Massinelli and B. Bauer, *Journal of Membrane Science* **2001**, *185*, 73-81.

[22] G. Alberti, R. Narducci and M. Sganappa, *Journal of Power Sources* **2008**, *178*, 575-583.

[23] A. Carbone, R. Pedicini, G. Portale, A. Longo, L. D'Ilario and E. Passalacqua, *Journal of Power Sources* **2006**, *163*, 18-26.

Chapter 4: Cross-Linked Sulfonated Aromatic Polymers

4.1. S-PEEK Membranes

Thermal treatments significantly modify the performance of SAP membranes. This behaviour can be ascribed to two main effects; the first one of minor influence is due to the annealing of the polymer and related to conformational changes, the second one is related to the formation of cross-linking by SO_2 bridges between macromolecular chains. An important role is played by the casting solvent: among the investigated solvents, (mainly DMAc and DMSO) dimethylsulfoxide is the only one that allowed the formation of cross-linked SAP. In this part, the effect of the thermal treatment carried out with membranes casted with the two solvents will be discussed separately for clarity reasons. At the end of the results section the data will be compared and discussed.

4.1.1. Membranes synthesized using DMAc as solvent

In this section the results obtained for membranes of sulfonated PEEK with a degree of sulfonation of 0.6 or 0.9 are reported. All the membranes were obtained using N,N-dimethylacetamide as solvent. Subsequent thermal treatments of membranes were performed at temperatures between 90°C and 210°C for times between 48 hours and 168 hours. Some of these samples, called double-treated membranes, were heated for 64 hours at 120°C and then 64 hours at 160°C.

4.1.1.1. X-Ray Diffraction

All membranes obtained by this casting technique are completely amorphous. The thermal treatments do not change their structure, even if the temperature and the time of the cure are changed. **Figure 4.1** shows the XRD patterns obtained for S-PEEK(0.6) membranes cured at temperatures between 90°C and 210°C for 48 hours. The broad signal observed for all samples around the reflections of crystalline S-PEEK confirm the absence of significant crystalline domains in the membranes [1].

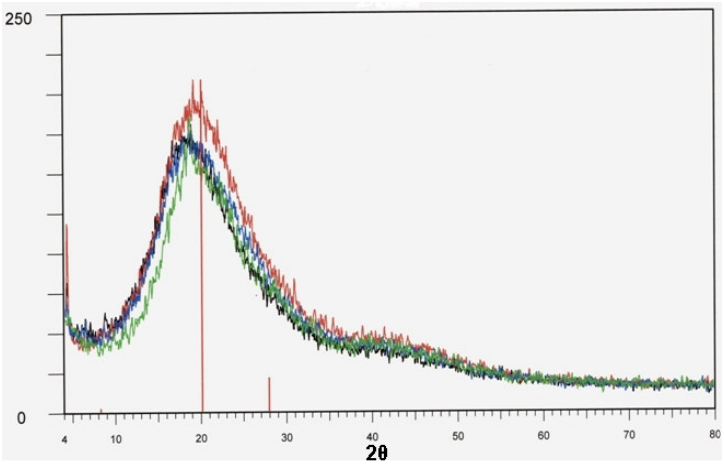

Figure 4.1 X-Ray diffractogram of S-PEEK(0.6) in DMAc treated at 90°C (black line), 120°C (red line), 160°C (blue line) and 210°C (green line) for 48 hours

4.1.1.2. Thermogravimetric Analysis

Figure 4.2 shows typical thermogravimetric curves obtained with a heating rate of 5 K/min between 25°C and 800°C.

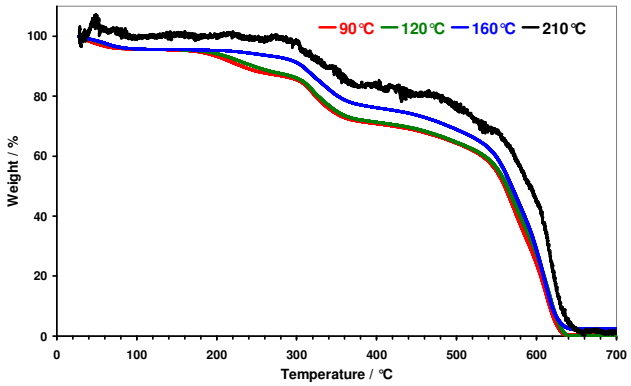

Figure 4.2 Thermogravimetric Analysis of S-PEEK(0.6) thermally treated at 90°C (red line) 120°C (green line) 160°C (blue line) and 210 °C (black line) for 48 hours.

The samples cured at 90°C and 120°C have the same thermal behaviour. For both samples two main weight losses were observed. The first weight loss comprises two sublosses: the first at 150°C - 160°C can be attributed to solvent removal The second between 250°C and 350°C is due to the loss of sulfonic acid groups [2, 3]. The complete decomposition of polymer membranes is observed above 450°C. A different behaviour is observed for samples cured at 160°C and 210°C. The first decrease of the weight is observed between 250°C and 350°C and can be attributed to the thermal degradation of sulfonic groups. The second and last weight loss, due to the complete

pyrolysis of the polymer, is observed at approximately 450°C. The lack of the first subloss (above 150°C - 160°C) observed for samples treated at 160°C and 210°C indicates absence of residual solvent in the membranes. The high temperature of treatment, near or higher than the boiling temperature of the casting solvent (DMAc, b.p. 165 °C), is responsible for the loss of free solvent. It is also possible to remove the casting solvent at lower temperatures, using long annealing time. **Figure 4.3** shows the thermal behaviour of a S-PEEK(0.6) membrane cured at 120°C for 168 hours (1 week). The subloss at around 150°C is still observed.

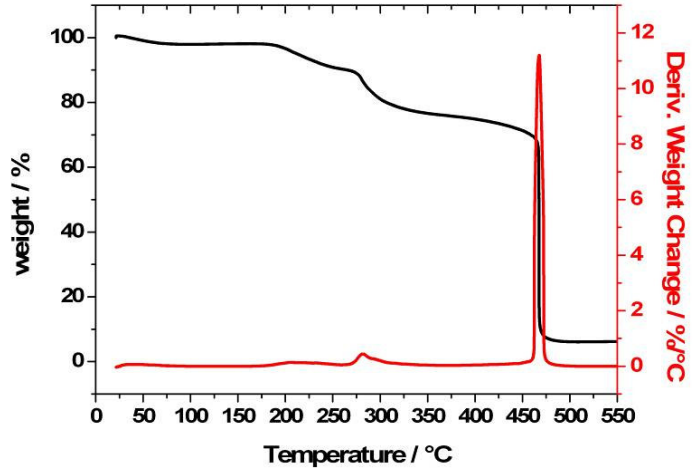

Figure 4.3 HR-TGA of S-PEEK(0.6) membrane cured at 120°C for 168 hours

4.1.1.3 Water Uptake

Table 4.1 shows the water uptake coefficients of S-PEEK(0.6) membranes (IEC = 1.81 meq/g) obtained by immersion in liquid water at different temperatures. The comparison of membranes treated for 48 hours at different temperatures shows that the cure temperature influences the capability of samples to absorb water. While the sample heated at 90°C dissolved in water at a temperature of 45°C samples treated at 120°C and 160°C dissolved at 75°C; at lower temperatures the first specimen had a water uptake coefficient more than twice that obtained for the latter.

The double thermal treatment (48 hours at 120°C followed by 48 hours at 160°C) did not enhance the membrane performances. The values of the water uptake coefficient obtained at different temperatures for the double treated sample was between that obtained for samples

treated at 120°C (48 hours) and that obtained for samples treated at 160°C (48 hours). Furthermore, the membrane dissolved at 75°C.

The thermal treatment at 160°C for 64 hours allowed a control of water uptake up to 65°C, but the extending of the cure by 64 hours did not prevent the sample dissolving at 75°C. The results obtained for the sample heated at 120°C for 168 hours (1 week) indicate that longer treatments improve the properties. A better control of the water uptake was achieved in comparison with a membrane treated at 120°C for only 48 hours. Moreover, it dissolved at a higher water temperature.

Thermal Treatment Temperature (time/h)[a]	Water Temperature (°C)							
	25	45	55	65	75	105	125	145
90(48)	5	∞						
120(48)	5	8	11	140	∞			
120(168)	7	---	---	58	550	∞		
160(48)	5	9	9	49	∞			
210(48)	3	---	---	---	---	---	33	47
120(48)+160(48)	5	---	---	73	∞			

[a] Thermal treatment temperature in °C and time in hours; ∞ means that the membranes completely dissolved

Table 4.1 Water Uptake Coefficient (λ) of S-PEEK(0.6) membranes (synthesized using DMAc as solvent) measured by immersion in liquid water at different temperatures (λ was calculated using IEC = 1.81 mequiv/g)

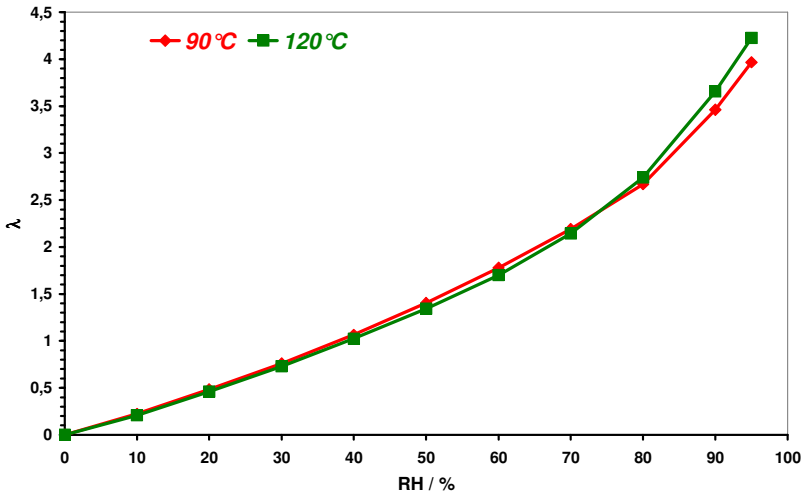

Figure 4.4 Water Uptake Coefficient obtained during the water sorption isotherm at 25°C for S-PEEK(0.6) membranes treated at 90°C (red line), 120°C (green line) for 48 hours.

Figure 4.4 shows the water uptake coefficients obtained at different RH during water vapour sorption experiments at 25°C. The two samples have apparently the same behaviour at all RH values. The thermal treatment has no great influence on the water vapour sorption. For all samples, the water uptake coefficient obtained at 95% of relative humidity is slightly lower than the one obtained by immersion in water, which is fully consistent.

Starting from the water sorption isotherms, it was possible to evaluate the chemical Diffusion Coefficient of water (*D*), calculated using Eq.(3.1). The obtained results for three samples at different relative humidity are summarized in **Figure 4.5**.

The sample treated at 90°C shows a higher diffusion coefficient at all RH values. At high relative humidity a peak of *D* coefficient is observed. It is an artefact due to membrane swelling as discussed for S-PEEK(0.9)/SiS-PPSU and S-PEEK(0.9)/S-PPSU blends. The proportionality of D with L^2 gives as result an apparently higher diffusion coefficient.

S-PEEK(0.6) membranes treated at 120°C and 160°C show a lower water diffusion coefficient at all RH values. Their values are around half of that calculated for the sample heated at 90°C. Enlarging **Figure 4.5 (a)** and eliminating the data of S-PEEK(0.6) cured at 90°C, it is possible to notice that the peak of water diffusion coefficient is observed in both samples cured at 120°C and 160°C respectively (see **Figure 4.5 (b)**). A higher temperature of thermal treatment allows the shift of the diffusion coefficient peak towards a lower value of RH. The RH dependence of chemical diffusion coefficient of sample treated at 160°C is very close to the curve obtained for S-PEEK(0.9)/Si-PPSU blend: it increases with RH up to a maximum at 60% of RH and decreases at high RH [4]. This behaviour is due to the change of the thermodynamic factor, including the water activity coefficient, as discussed in Ref. [5].

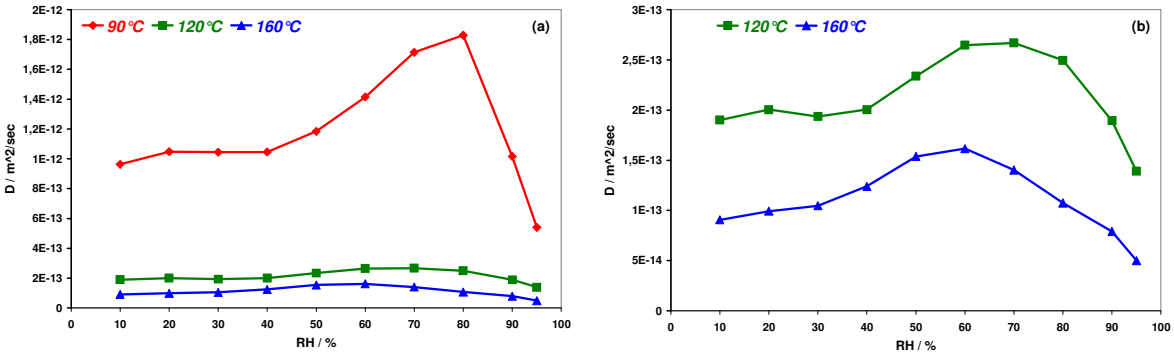

Figure 4.5 (a) Water Diffusion Coefficient of S-PEEK(0.6) (membranes synthesized using DMAc as solvent) thermally treated at 90°C (red line), 120°C (green line) 160°C (blue line) for 48 hours (T = 25°C) and (b) Water Diffusion Coefficient without the data of the sample treated at 90°C for 48 hours.

4.1.1.4. Mechanical Properties

4.1.1.4.1 Stress-Strain Tests

Figure 4.6 shows typical stress-strain curves obtained for S-PEEK(0.6) membranes thermally treated at 90°C, 120°C and 160°C. The corresponding mechanical parameters are resumed in **Table 4.2**. No curve is reported for the sample heated at 210°C, due to its extreme brittleness which did not allow the evaluation of parameters such as Ultimate Strength (σ) and Elongation at the Rupture (ε).

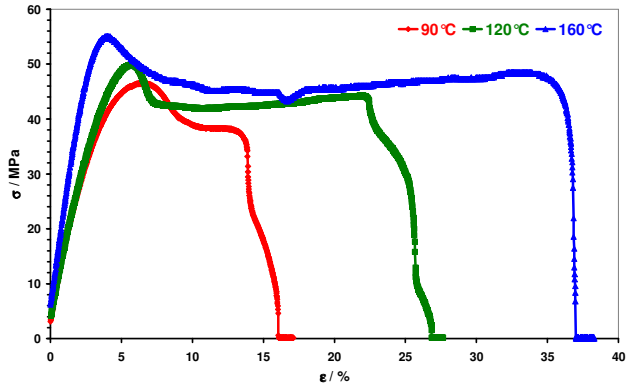

Figure 4.6 Typical stress-strain curves obtained for S-PEEK(0.6) membranes thermally treated casted from DMAc.

Thermal Treatment Temperature (time)[(a)]	*E [MPa]*	*σ [MPa]*	*ε [%]*
90 (48)	1200 ± 250	37 ± 8	12 ± 2
120 (48)	1500 ± 240	50 ± 6	26 ± 6
160 (48)	1970 ± 120	51 ± 11	37 ± 9

[a] Thermal treatment temperature in °C and time in hours

Table 4.2 Young's Modulus (E), Ultimate Strength (σ) and Elongation at Rupture (ε) of thermally treated S-PEEK(0.6) membranes. The data for the membrane treated at 210°C were impossible to exploit, because the membrane broke immediately.

As shown in **Figure 4.6**, thermal treatment influences mechanical properties. The comparison of Young's Modulus values obtained for the four samples shows that a higher temperature of thermal treatment increases that parameter. But when the cure is made at too high temperature, such as 210°C, it leads to a general degradation of mechanical properties.

The main change is the large increase of ductility, parameter ε, of three thermally treated membranes, as can be observed on **Figure 4.6**. The membrane strength, evaluated by σ, increases

also by thermal treatments. As shown in **Table 4.2** mechanical properties are generally enhanced by thermal treatment until to reach an optimal value and then degrade.

4.1.1.4.2. Dynamic Mechanical Analysis

Figure 4.7 shows typical DMA curves in dry conditions presenting the storage modulus (*E'*) and tan δ vs. temperature of S-PEEK(0.9) membranes thermally treated at 160°C for 64 hours and untreated. The experiments were performed using a variable force, producing a strain of 125% of the initial length of specimens. It is possible to observe the different behaviour of the two samples with the temperature. The decrease of storage modulus observed above 110°C for the untreated sample and above 190°C for the 160°C heated sample is due to the glass transition [6, 7].

The glass transition temperature, evaluated at the peak of tan δ [8] (**Figure 4.7 (b)**), is strongly influenced by thermal treatment: the untreated sample had a T_g at 130°C, while the 160°C heated sample had a T_g at 217°C.

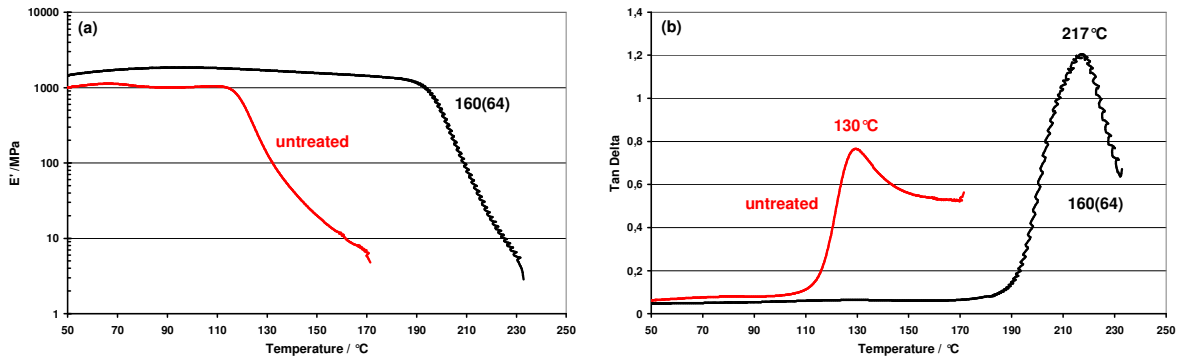

Figure 4.7 Dynamic Mechanical Analysis curves of S-PEEK(0.9) membranes untreated (red line) and heated at 160°C for 64 hours; (a) Storage Modulus and (b) Tan δ.

4.1.2. Membranes synthesized using DMSO as solvent

In this section the membranes of sulfonated PEEK with a degree of sulfonation between 0.6 and 0.9 obtained using dimethylsulfoxide as casting solvent are studied. Subsequent thermal treatments of membranes were performed at temperatures between 120°C and 180°C for times between 64 hours and 168 hours. Some of these samples, called double-treated membranes, were heated for 64 hours at 120°C and then 64 hours at 160°C.

4.1.2.1. Structure and Microstructure

4.1.2.1.1. Infrared Spectroscopy

Figure 4.8 (a) shows typical FTIR spectra of S-PEEK (0.9) membrane untreated (black line) and heated at 160°C for 64 hours (red line).

The analysis of membranes by FTIR spectroscopy allows studying any macromolecular changes due to thermal treatment. In both spectra PEEK adsorption is observed: 1600 cm^{-1} $\nu_{C=O}$, 1217 cm^{-1} $\nu_{Ph\text{-}CO\text{-}Ph}$, 1025 cm^{-1} $\nu_{C\text{-}O\text{-}C}$ or $\nu_{C\text{-}O}$ and 929 cm^{-1} $\nu_{sy\ Ph\text{-}(C=O)\text{-}Ph}$ [9-11]. Adsorption due to aromatic sulfonic groups are observed for both samples at 1185 cm^{-1} (ν_{as}-SO_3H), 1020 cm^{-1} (ν_{sym}-SO_3H), and 965 cm^{-1} (δ-SO_3H) [3].

Figure 4.8 (b) shows the subtraction of the spectrum of untreated membrane from that of 160°C treated one. The results of that subtraction shows signals due to 1:2:4-substituted phenyl rings at 1225 cm^{-1} and 1080 cm^{-1}. Bands of aromatic sulfone moieties at 1210 cm^{-1} and 1065 cm^{-1} are observed too. The S=O stretching vibration of $PhSO_2Ph$ is present at 1165 cm^{-1}. These results indicate that sulfone cross-links are formed between macromolecular chains [3, 12].

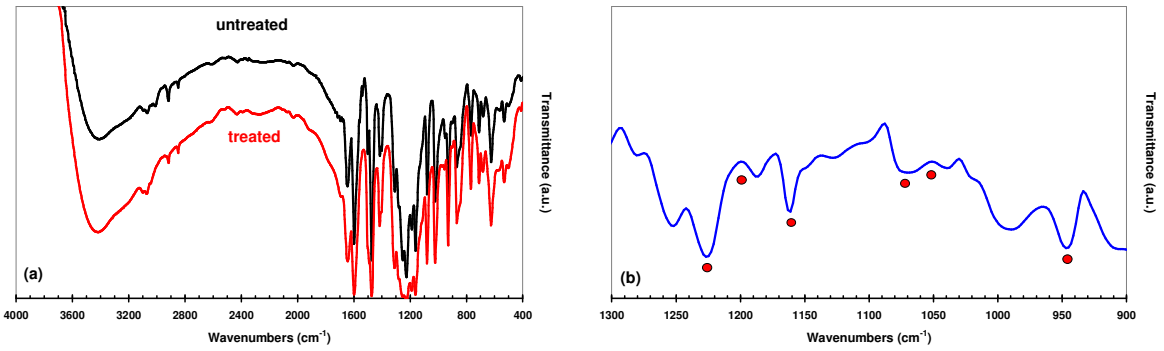

Figure 4.8 FTIR spectra of (a) S-PEEK(0.9) DMSO, untreated sample (black line) and S-PEEK(0.9) DMSO treated at 160°C for 64 hours (red line). (b) difference spectrum [(red line)-(black line)]

4.1.2.1.2. X-Ray Diffraction

The membranes are fully amorphous according to XRD without any change during heat treatment. Significant modifications of crystallinity can be excluded as origin of the important property changes observed on thermally treated membranes.

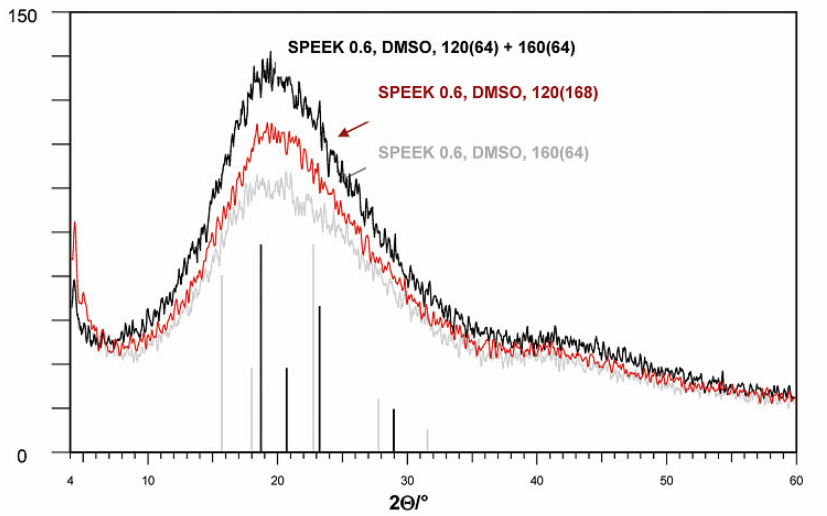

Figure 4.9 X-Ray diffractogram of S-PEEK(0.6) in DMSO treated at 160°C for 64 hours (grey line), 120°C for 1 week (red line), 120°C for 64 hours followed by 160°C for 64 hours (black line).

4.1.2.1.3. Atomic Force Microscopy

Figure 4.10 shows the microstructure image of untreated (**Figure 4.10 (a)**) and thermally treated S-PEEK membrane (**Figure 4.10 (b)**). As explained in Ref. [13] and Ref. [14], the dark regions are related to zones that contain a large amount of hydrophilic sulfonic groups (softer region), while the light regions are related to zones that contain a little amount of sulfonic groups (harder region). In both membranes, homogeneous and smooth surfaces without pores are observed (R_{ms} = 1.6 nm for untreated sample and R_{ms} = 4.2 nm for 160°C heated sample).

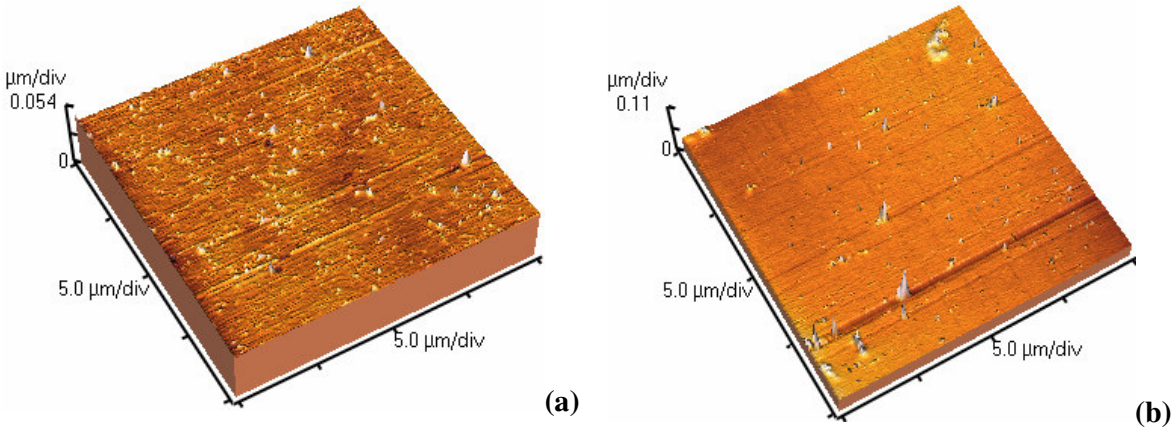

Figure 4.10 AFM images of S-PEEK(0.9) (a) untreated and (b) treated at 160°C for 64 hours

4.1.2.1.4. Contact Angle

Figure 4.11 shows a drop of water (1 μl) deposited on the surface of untreated S-PEEK (0.9) membrane. The measure of contact angle was instead no possible because the membrane under the drop swelled and assumed the same shape of the drop. A different behaviour was observed for a thermally treated S-PEEK (0.9) membrane: no swelling was observed.

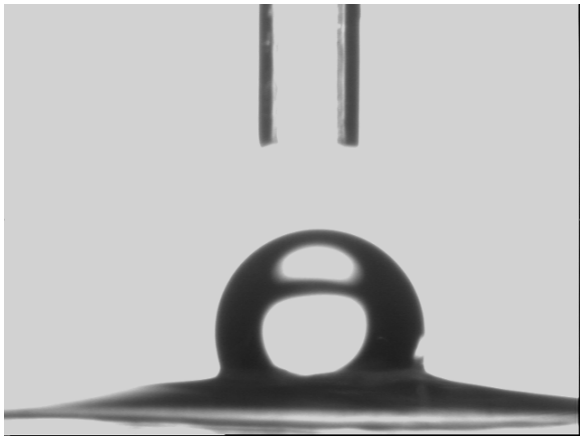

Figure 4.11 Drop of water deposited on the surface of untreated S-PEEK(0.9) membrane

A preliminary study, that needs further confirmations, gave as result: 40 mJ/m^2 for the surface free energy of heated S-PEEK(0.9).

4.1.2.2. Thermogravimetric Analysis

Figure 4.12 shows typical high resolution thermogravimetric curves of S-PEEK (0.9) membrane thermally treated at 120°C for 1 week (**Figure 4.12 (b)**), double treated (**Figure 4.12 (c)**) and untreated (**Figure 4.12 (a)**).

A different thermal behaviour was observed for the three samples, especially below 300°C. **Figure 4.13** shows the comparison of samples at temperatures between 25°C and 300°C. The initial weight loss revealed at the beginning of the measurement of the untreated sample (black line) can be attributed to the evaporation of the water remained in the sample which was in equilibrium with the ambient. The following weight loss revealed for the untreated sample comprises two sublosses: the first of about 10% between 130°C and 195°C can be attributed to the residual solvent removal. The second, between 200°C and 300°C, of approximately 30%, is

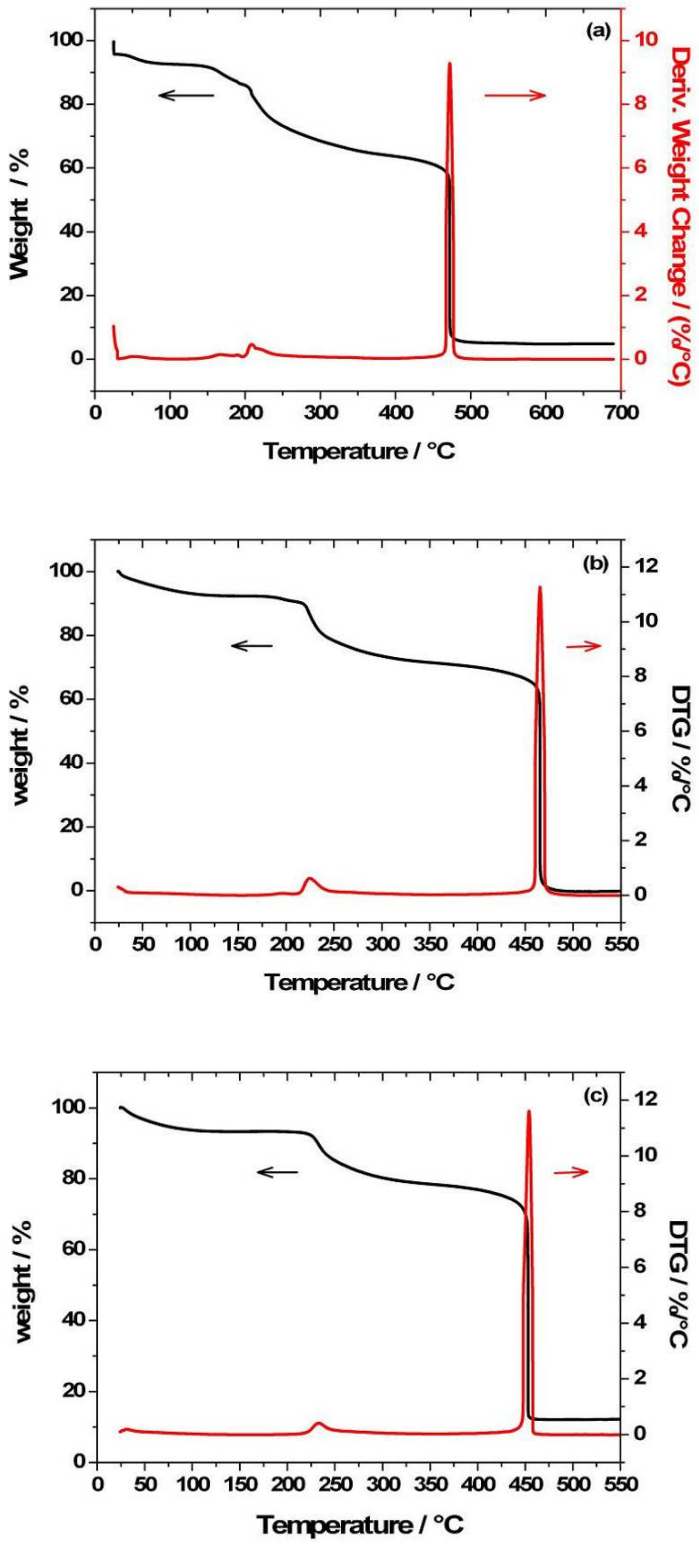

Figure 4.12 HR-TGA curves for (a) S-PEEK (0.9), DMSO untreated, (b) S-PEEK (0.9), DMSO thermally treated at 120°C for 1 week (168 hours) and (c) S-PEEK (0.9) DMSO double treated (120°C for 64 hours followed by 160°C for 64 hours)

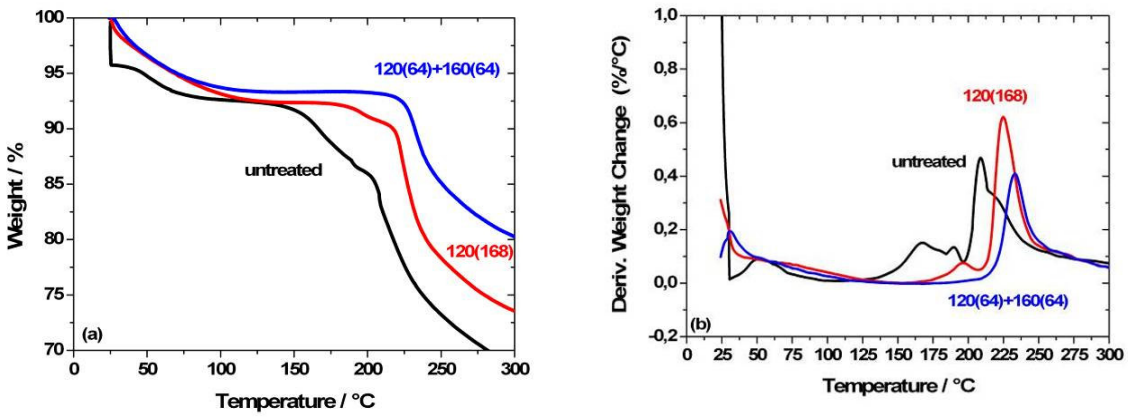

Figure 4.13 Superimposition of HR-TGA curves obtained for S-PEEK (0.9), DMSO membranes thermally treated. (a) weight change, (b) derivate weight change

related to the decomposition of sulfonic acid groups. The same behaviour of the untreated sample was observed for the membrane heated at 120°C for 1 week (168 hours) (red line), but the reduction of the weight due to the evaporation of the residual solvent was less that the 10%. On the double treated sample measure was observed the initial weight loss due to the water vapour evaporation and the decomposition of sulfonic acid groups between 200°C and 300°C [2, 3, 15, 16].

Thermal Treatment Temperature (time)[a]	Degree of Cross-Linking[b]	Degree of Sulfonation[b]	IEC[c] (meq/g)
	S-PEEK(0.6)		
120(64)	0	0.6	1.79
120(64)+160(64)	0.15	0.45	1.33
	S-PEEK(0,9)		
120(64)	0	0.9	2.50
120(168)	-	-	2.50
160(64)	-	-	1.96
120(64)+160(64)	0.24	0.66	1.90

[a] Treatment temperature in °C and time in hours; [b] from TGA; [c] from titration

Table 4.3 Thermogravimetric Analysis (TGA) and titration of S-PEEK membranes

The comparison of the derivate weight change of the three samples (**Figure 4.13 (b)**) shows that the peak due to the degradation of sulfonic acid groups shifts towards higher temperatures when the membranes are thermally cured at higher temperature. A different shape

of the untreated sample peak was observed between 200°C and 300°C. That peak seems to be a merging of two peaks: one related to the decomposition of sulfonic groups and one probably associated to an in situ cross-link reaction. As shown in both **Figure 4.12** and **Figure 4.13**, a different reduction of weight due to the degradation of sulfonic acid groups was observed for the sample thermally heated at higher temperature. From the peak area a modified degree of sulfonation can be calculated. The values calculated from such thermogravimetric experiments are reported for different membranes in **Table 4.3**.

Table 4.3 shows that the results obtained by thermogravimetric analysis and titration are very in good agreement: membranes thermally treated at 160°C lose about 30% of sulfonate groups [12].

The complete decomposition of polymer main chain is revealed for all samples between 400°C and 500°C (**Figure 4.12 (a)**, **(b)** and **(c)**) [2, 3, 15, 16]. As reported in literature [17], cross linking $–SO_2$ bridges decomposed together with the main polymer chains [12].

4.1.2.3. Water Uptake

Figure 4.14 shows the water uptake kinetics of S-PEEK (0.6) membranes treated at 160°C for 64 hours after immersion in deionized water of different temperatures. In order to reach a constant value of the water uptake coefficient at 25°C, immersion times of several days were required.

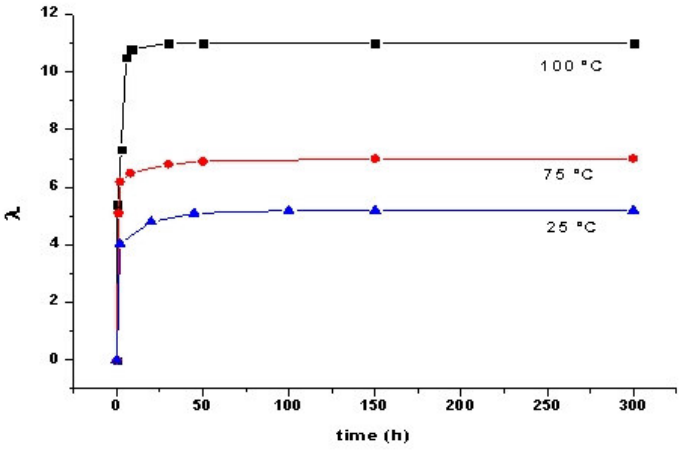

Figure 4.14 Water Uptake kinetics of S-PEEK(0.6) membranes treated for 64 hours at 160°C after immersion in deionized water of different temperatures

It is noteworthy that even at 100°C, the water uptake coefficient of this thermally treated membrane reached a value of only 11, whereas an untreated membrane dissolved completely [12].

Water uptake coefficients determined after full immersion in water at different temperatures are reported in **Table 4.4**.

Thermal Treatment temperature (time)[a]	Water Temperature (°C)					
	25	65	75	105	125	145
	S-PEEK (0.6) (IEC = 1.81 mequiv/g)					
120(64)	8.0	17.3	∞			
120(168)	7.0	20.0	124	∞		
160(64)	5.2	---	7.0	11.0	16.0	19.3
120(64)+160(64)	3.6	---	5.0	6.0	6.7	---
	S-PEEK (0.7) (IEC = 2.03 mequiv/g)					
120(64)	10.0	---	∞			
120(64)+160(64)	3.8	---	---	10.0	---	---
	S-PEEK (0.75) (IEC = 2.20 mequiv/g)					
140(64)	4.4	---	7.9	118.7[1]	123.6[1]	218.8[1]
160(64)	3.4	---	6.3	11.2	13.2	12.9
	S-PEEK (0.9) (IEC = 2.43 mequiv/g)					
120(64)	33.0	∞				
120(168)	17.0	∞				
160(64)	6.2	10.5	---	16.1	21.6	27.3
120(64)+160(64)	5.0	8.0	10.0	14.0	22.9	24.7
180(64)	2.9	2.2	---	2.8	4.1	3.9

[a] Thermal treatment temperature in °C and time in hours; [1] after 1 hour of full immersion

Table 4.4 Water Uptake Coefficients (λ) of membranes measured by immersion in liquid water at different temperatures

All membranes thermally treated at 120°C solved at low water temperatures and as expected, the samples made using S-PEEK with higher degree of sulfonation solved at lower water temperatures. The stability of membranes seems enhanced when they are heated at 140°C, but the high water uptake coefficient obtained after 1 hour of immersion in water heated at temperatures above 100°C indicate that the samples dissolve at such temperatures. Water uptake

coefficients remain instead at reasonable values even up water temperature of 145°C, when the samples are thermally cured at 160°C for 64 hours. The so-called double treated sample (thermally treated at 120°C for 64 hours followed by 160°C for 64 hours) have a non homogeneous behaviour: for S-PEEK(0.6) membranes a very low λ values was obtained up to 120°C of water temperature; for S-PEEK(0.9) membranes, instead was obtained a behaviour very close to the one observed for the sample heated at 160°C for 64 hours. Thermal treatment performed at 180°C further reduces the water uptake coefficient, but no major changes were observed at all water temperatures.

Figure 4.15 shows the water vapour sorption isotherms of different membranes. The water uptake coefficient obtained are consistent with those obtained by immersion in liquid water and confirm that the thermal treatment of 160°C (64 hours) is more efficient in reducing the amount of sorbed water [12].

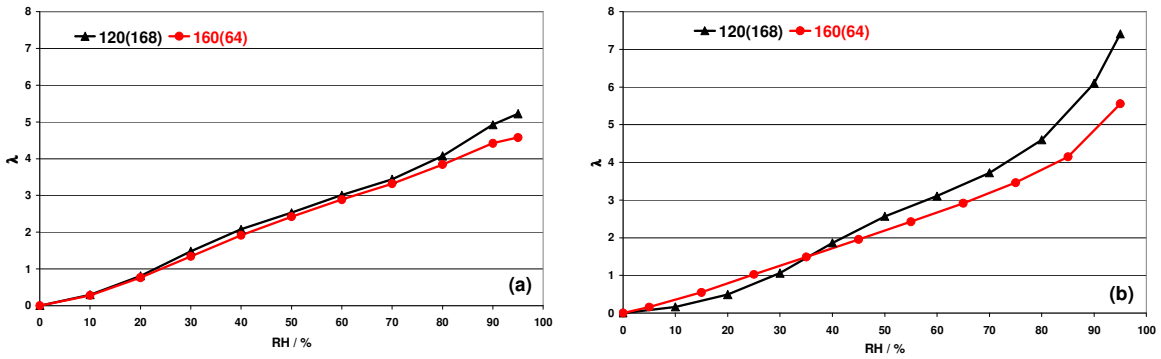

Figure 4.15 Water sorption isotherms at 25°C for (a) S-PEEK (0.6) in DMSO treated at 120°C for 1 week (black line) and treated at 160°C for 64 hours (red line) and (b) S-PEEK (0.9) in DMSO treated at 120°C for 1 week (black line) and treated at 160°C for 64 hours (red line)

4.1.2.4. Mechanical Properties

4.1.2.4.1. Stress-Strain Tests

Figure 4.16 shows typical stress strain curves obtained for S-PEEK (0.9) membranes thermally treated at different temperatures and for different times. The related mechanical parameters are resumed in **Table 4.5**. As shown in **Figure 4.16**, mechanical properties are strongly influenced by thermal treatments. Young's modulus values obtained for the samples show that higher temperatures of thermal treatments increase that parameter. Anyway for all samples a Young's Modulus above 1 GPa was measured [18]. The strength of membranes,

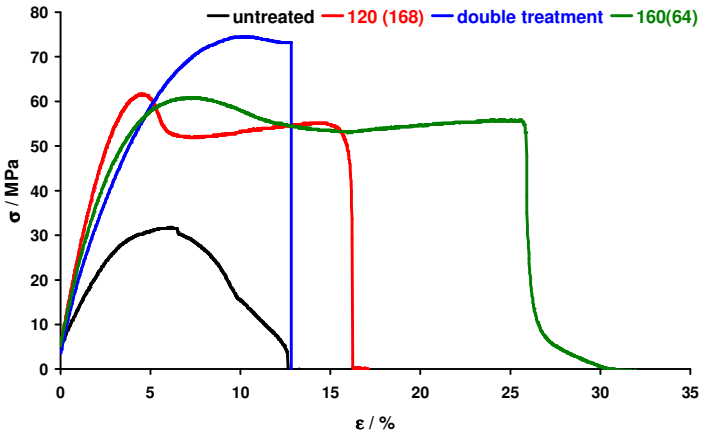

Figure 4.16 Typical Stress-Strain curves of S-PEEK(0.9) membranes thermally treated

Thermal Treatment Temperature (time)[a]	***E [MPa]***	***σ_{max} [MPa]***	***ε_{max} [%]***	***ε_r [%]***	***T_g [°C]***
			S-PEEK (0.9)		
untreated	1010±80	32±1	5±1	7±1	105
120 (168)	1590±260	56±11	5±1	12±4	
140 (64)	1760±40	58±4	6±1	22±10	190
160 (64)	2020±170	64±8	7±1	17±10	205
120 (64) + 160 (64)	2305±250	75±5	8±1	10±3	
			S-PEEK (0.75)		
untreated					140
140 (64)	1240±120	43±4	7±1	29±13	
			S-PEEK (0.6)		
untreated					140
120 (168)	1410±240	34±9	5±2	48±10	

[a] Thermal treatment temperature in °C and time in hours

Table 4.5 Young's Modulus (e), Ultimate Strength (σ_{max}), Elongation at the ultimate strength (ε_{max}), elongation at the rupture (ε_r) and Glass Transition Temperature (T_g) of S-PEEK membranes thermally treated.

evaluated by σ_{max}, is increased by thermal treatments: higher is the temperature of heating cure, higher is the strength of membrane. A different behaviour was observed for the ductility (ε_r); this parameter was increased by 120°C thermal heating (see **Table 4.5**), but at higher temperatures of thermal treatment samples became less ductile and more brittle. The ductility of membranes is enhanced by higher temperature of thermal treatment, until to reach a maximum and then

decreases if the temperature is further increased. The yield point, evaluated by ε_{max}, is below 10% in all cases [18]. The performed thermal treatments generally increase the elastic modulus and tensile strength of the membranes and reduce the ductility [18].

The comparison of polymers with similar heat treatment, but different degree of sulfonation, shows that the membranes made using a polymer with larger degree of sulfonation show a lower ductility but a higher strength, probably due to the stronger intermolecular forces between macromolecular chains by a greater amount of hydrogen bonds [18]. Apparently, the higher DS gives higher mechanical strength, probably because of ionic interactions between macromolecules.

4.1.2.4.2. Dynamic Mechanical Analysis

Figure 4.17 shows typical DMA curves in dry conditions presenting the storage modulus (E') and tan δ vs. temperature of S-PEEK membranes with and without annealing. **Figure 4.17 (a)** present the variation of storage modulus (E') with temperature for S-PEEK membranes without and with annealing. At the beginning of the measurement, an increase of storage modulus, probably due to the removal of residual casting solvent and water, is observed for all membranes. The strong decrease of storage modulus observed at higher temperatures is due to the change of materials properties because the temperature is approaching the glass transition [6, 7].

The glass transition temperature was evaluated at the peak of tan δ [8] (**Figure 4.17 (b)**). As reported in **Table 4.5**, T_g is strongly influenced by thermal treatments. An example is represented by S-PEEK (0.9) membrane: when it is thermally treated at 160°C for 64 hours, an increase of glass transition temperature of about 100°C is observed. Reducing the temperature of the annealing a lower increase of T_g is observed.

The comparison of glass transition temperatures of S-PEEK (0.6) and S-PEEK (0.9) membranes annealed and non annealed, show that before thermal treatment T_g is strongly influenced by DS of polymers. After the annealing, DS seems do not influence this parameter [18].

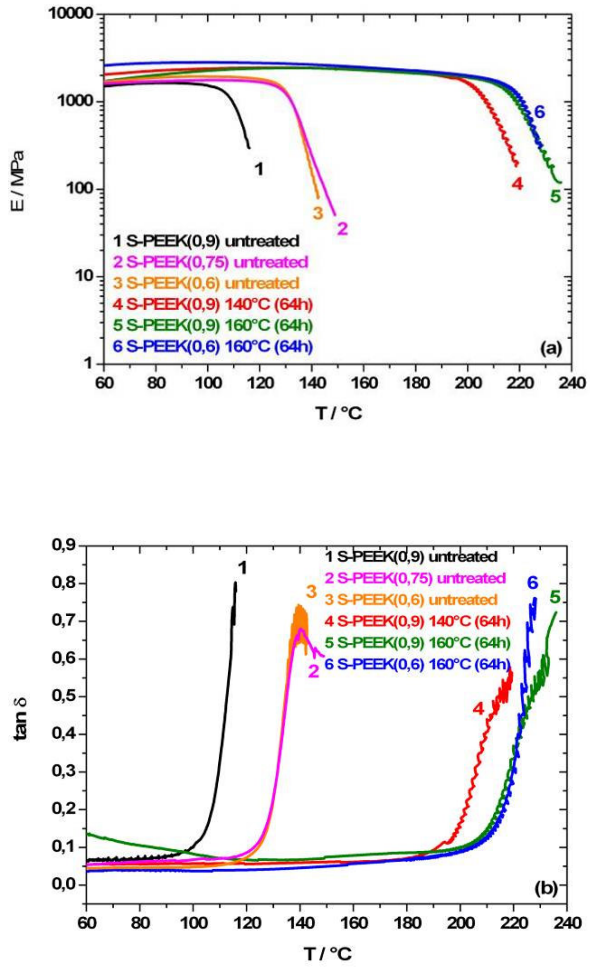

Figure 4.17 (a) Storage modulus and (b) tan δ of various S-PEEK membrane as function of temperature from DMA experiments

4.1.2.5. Electrical Properties

4.1.2.5.1. Dielectric Analysis

Figure 4.18 shows the AC conductivity of a S-PEEK (0.9) membrane annealed at 160°C for 64 hours (**Figure 4.18 (a)**) and of a S-PEEK (0.75) membrane heated at 140°C for 64 hours (**Figure 4.18 (b)**). The comparison with the untreated membranes was not possible because the samples bonded to the electrodes during the experiments.

Even if in S-PEEK (0.9) membrane there are a reduced number of sulfonic acid groups (because cross-linked each other), its AC conductivity is remarkably higher than that of not cross-linked S-PEEK (0.75) membrane. Moreover at around 200°C, when both samples are completely dry, the AC conductivity of S-PEEK (0.9) is still higher than that of S-PEEK (0.75).

During heating, in both samples an increase of ionic conductivity was observed until to reach a maximum at around 90°C - 110°C. Above 110°C a decrease of ionic conductivity, probably due to the water loss, was observed. A minimum of ionic conductivity was observed at around 170°C in both samples. Above this temperature an increase of the AC conductivity was observed. The polymer is becoming soft because the temperature is approaching the glass transition and the movements of the macromolecular chains can support the ion hopping.

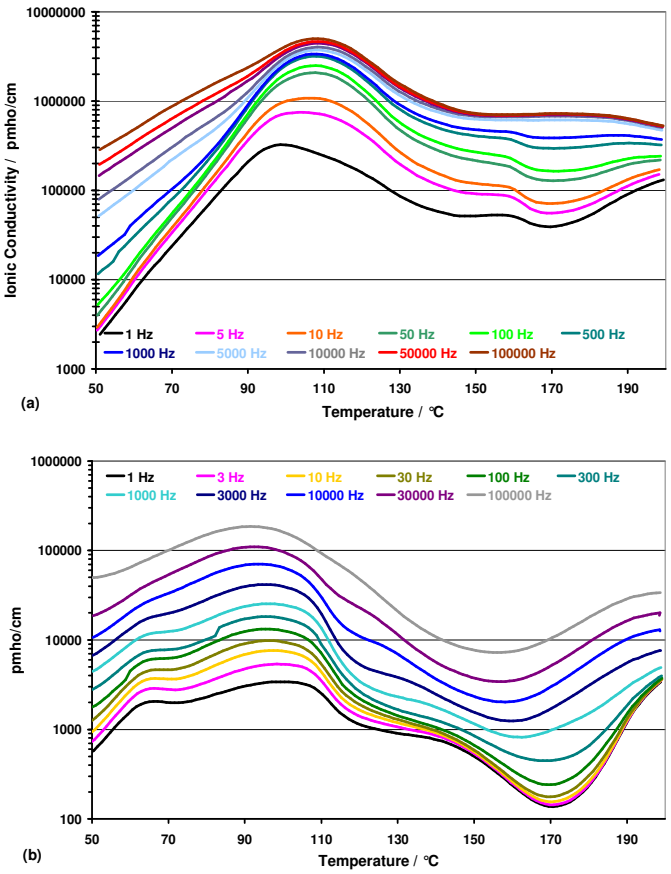

Figure 4.18 AC Conductivity of (a) S-PEEK(0.9) membrane thermally treated at 160°C for 64 hours and (b) S-PEEK(0.75) membrane annealed at 140°C for 64 hours

4.1.2.5.2. Proton Conductivity Measurements

Figure 4.19 shows the proton conductivity (σ) of S-PEEK(0.9) membrane double thermally treated (120°C for 64 hours followed by 160°C for 64 hours). The membrane conductivity was evaluated at 100°C, as function of relative humidity, using impedance spectroscopy. The comparison of data obtained for this membrane with S-PEEK membranes presented in literature (Ref. [19]) shows that S-PEEK (0.9) sample double treated has a lower

conductivity. These results can be explained by the reduced number of sulfonic groups in the membrane due to cross-link (see **Table 4.3**) [12]. The disadvantage of the low content of sulfonic groups in the membrane is compensated by the stability of membrane: S-PEEK (0.9) double treated remains stable up to the 90% of RH. Usually S-PEEK membranes cannot be used at these temperatures and relative humidity because the high hydration leads to a large swelling of the sample and impede its use at these conditions [19].

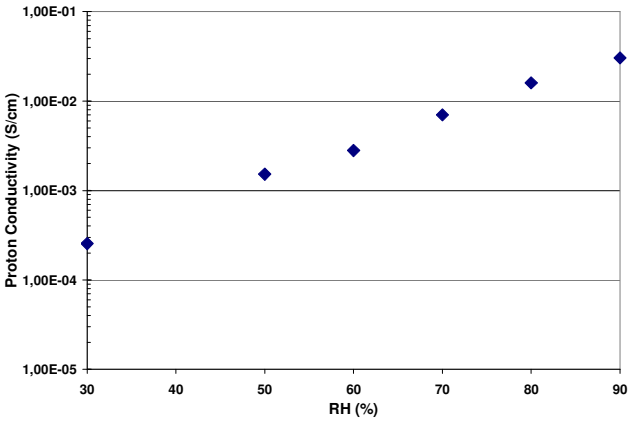

Figure 4.19 Proton conductivity vs. relative humidity at 100°C for S-PEEK(0.9) thermally treated at 120°C for 64 hours and then at 160°C for 64 hours (double treated).

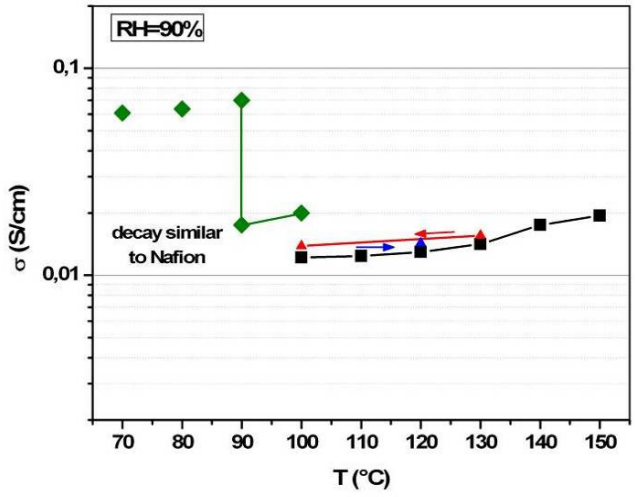

Figure 4.20 Proton conductivity vs. temperature at 90% RH for S-PEEK(0.9) thermally treated at 160°C for 64 hours during heating (black line) and cooling (red line), and untreated (green line).

In order to test the stability of annealed S-PEEK membranes, the proton conductivity was measured fixing the relative humidity at 90% and changing the temperature of the test cell. **Figure 4.20** shows the results obtained for untreated and annealed S-PEEK membranes. The

untreated membrane has a higher conductivity, but at 90°C it becomes unstable and σ decades; it has the same behaviour of Nafion [20, 21]. The annealed membrane has a lower conductivity, but the sample was stable up to 150°C. During the cooling just a small hysteresis was observed.

4.2. S-PES Membranes

Polyethersulfone (PES) belong to a class of high glass transition temperature polymers of high mechanical, thermal and chemical resistances. It consists of repeated phenyl groups and ether and sulfone groups (see **Figure 4.21**) [22, 23].

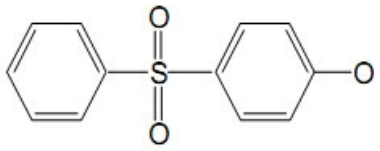

Figure 4.21 The strucure of PES

Although PES has an excellent physical performance characteristic, the hydrophobicity of this material has limited its application sometimes. In order to improve its properties, such as hydrophilicity, permeability and proton conductivity it is frequently sulfonated [23]. The sulfonation of PES is not easy, because the electron withdrawing effect of the sulfone linkages that deactivate the adjacent aromatic rings for electrophilic substitution and its sulfonation required stronger reagents or/and longer time [17, 23]; under these conditions, up to two sulfonic groups can however be inserted per repeat unit. S-PES is more hydrophilic than other SAP membranes due to its short and polar repeat unit. Its low molecular weight (312 g/mole) leads to high IEC values even for relatively low degree of sulfonation (DS = 1 corresponds to 3.2 meq/g) and it reaches conductivity values similar to highly sulfonated S-PEEK. On the other hand, S-PES membranes with suitable DS dissolve easily in water.

In this section results obtained for membranes of sulfonated PES with a high degree of sulfonation are reported. All the membranes were obtained using dimethylsulfoxide as solvent. Subsequent thermal treatments of membranes were performed at 160°C for 64 hours.

4.2.1. Structure and Microstructure

Figure 4.22 shows ^{1}H NMR of PES and S-PES in DMSO. The presence of a sulfonic acid group causes a significant down-field shift of the hydrogen located in the *o*-position at the aromatic ring. From the spectrum, one can calculate the degree of sulfonation, according to Ref. [24]; furthermore, it is possible to exclude the degradation of the polymer during sulfonation.

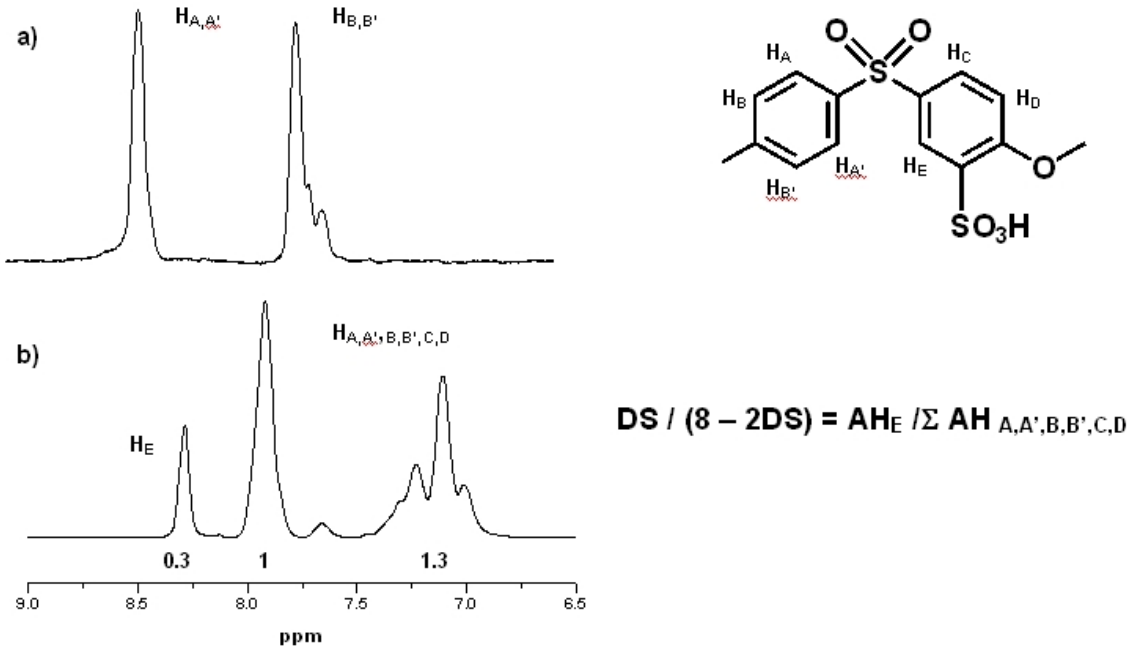

Figure 4.22 ^{1}H NMR of a) unsulfonated PES and b) sulfonated PES in d_6 DMSO

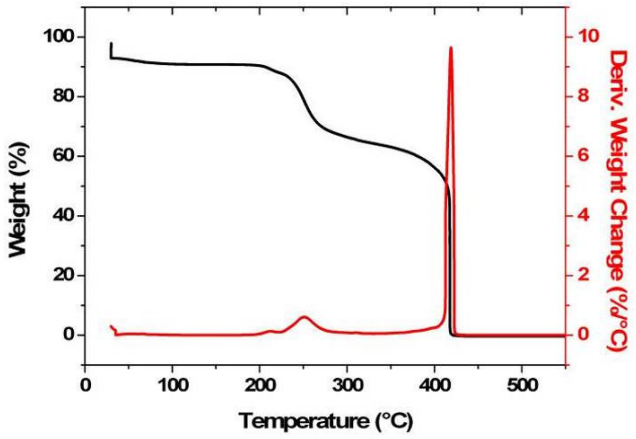

Figure 4.23 HR-TGA of S-PES membrane thermally treated at 160°C for 64 hours

Figure 4.23 show a typical high resolution thermogravimetric curves of S-PES membrane thermally treated at 160°C for 64 hours. The initial weight loss observed at the beginning of the measure can be attributed to the evaporation of the water remained inside the sample which was in equilibrium with the ambient. For the sample two main weight losses are observed. The first, revealed at 200°C can be attributed to the degradation of sulfonic acid groups. The second loss of mass, which correspond to the complete decomposition of polymer main chain, is revealed between 400°C and 450°C [2, 3, 15, 16].

4.2.3. Water Uptake

Figure 4.24 shows the water sorption isotherm at 50°C. Unfortunately no comparisons were possible with water uptake obtained in full immersion in water because the membrane dissolved at 25°C after few minutes.

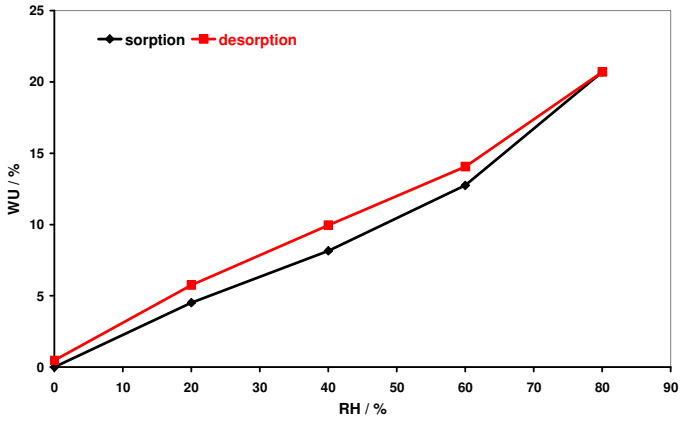

Figure 4.24 Water sorption/desorption isotherm at 50°C of S-PES membrane thermally treated at 160°C for 64 hours

4.3. S-PPSU Membranes

In this section results obtained for membranes of sulfonated PPSU with a high degree of sulfonation are reported. All membranes were obtained using dimethylsulfoxide as solvent.

Subsequent thermal treatments of membranes were performed at temperatures between 160°C and 170°C for 48 hours or 64 hours.

4.3.1. Structure and Microstructure

4.3.1.1. Infrared Spectroscopy

Figure 4.25 (a) shows typical FTIR spectra of S-PPSU membrane thermally untreated (black line) and heated at 170°C for 64 hours (red line). S-PPSU adsorption is evident in both spectra. No significant differences are pointed out, because cross-link reaction leads to the formation of sulfone groups already present in the backbone of the polymer. However the subtraction of normalized spectrum of untreated S-PPSU from that of 170°C treated S-PPSU (**Figure 4.25 (b)**) evidences at 1165 cm^{-1} the S-O stretching vibration due to $PhSO_2Ph$ generated in the cross-link reaction. Signals due to 1:2:4-substituted phenyl rings are also present at 1080 cm^{-1}. it is also possible to observe bands of aromatic sulfone moieties at 1210 cm^{-1} (shoulder) and 1065 cm^{-1} (tail) [3, 12].

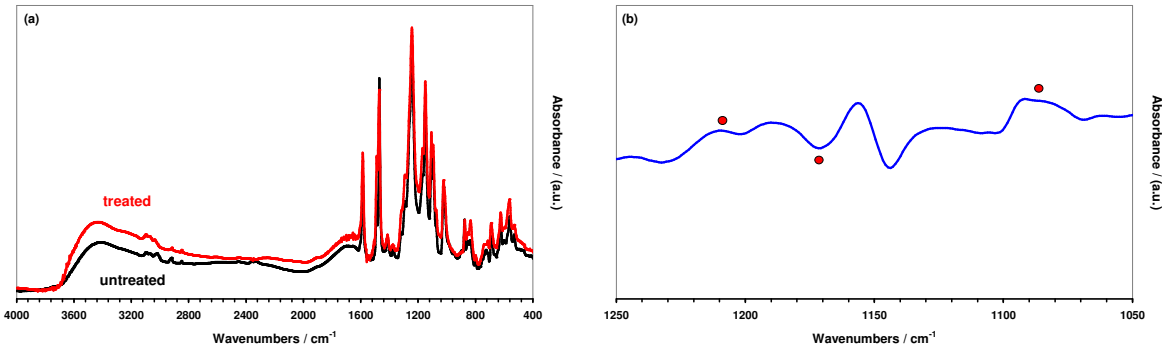

Figure 4.25 FT-IR spectra of S-PPSU(2.0) (a) Black: untreated membrane, red: membrane treated at 170°C for 64 hours. (b) difference spectrum [(black line)-(red line)]

4.3.1.2. Atomic Force Microscopy

Figure 4.26 shows the microstructure image of untreated (**Figure 4.26 (a)**) and annealed S-PPSU membrane (**Figure 4.26 (b)**). Wang et al. in Ref.[13] and Wu et al. in Ref. [14] affirm that the dark regions in AFM images can be associated to a large amount of hydrophilic sulfonic groups (softer regions), while the light regions to a little amount of such groups (harder regions). In both membranes homogeneous and smooth (R_{ms} = 2.2 nm for untreated sample and R_{ms} = 1.4 nm for 160°C heated sample) surfaces without pores are observed.

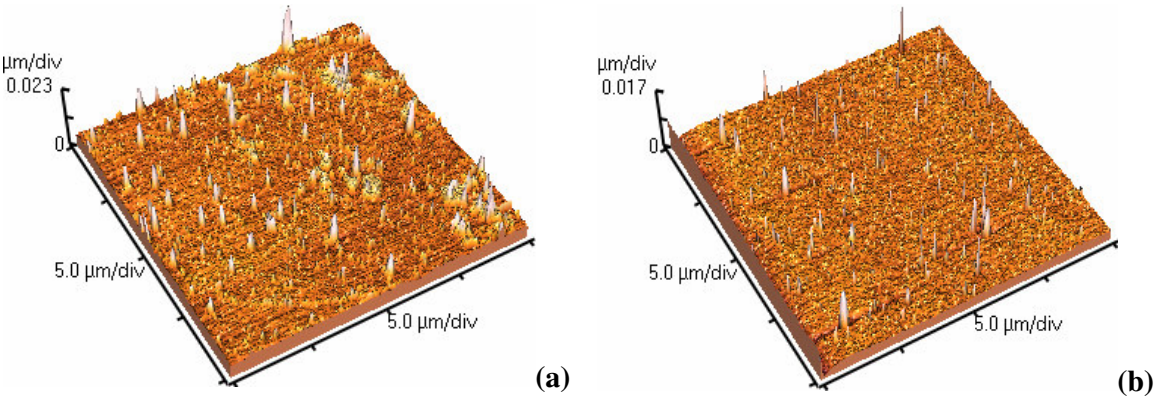

Figure 4.26 AFM images of S-PPSU(2.0) (a) untreated and (b) treated at 170°C for 64 hours

4.3.1.3. Contact Angle

The wettability of the surface of S-PPSU membrane can be evaluated depositing a drop (1 µl) of water and measuring the contact angle. The measurement was not possible for untreated samples, because the membranes swelled under the drop (**Figure 4.27**). A different behaviour was observed for annealed S-PPSU membrane: no swelling was observed.

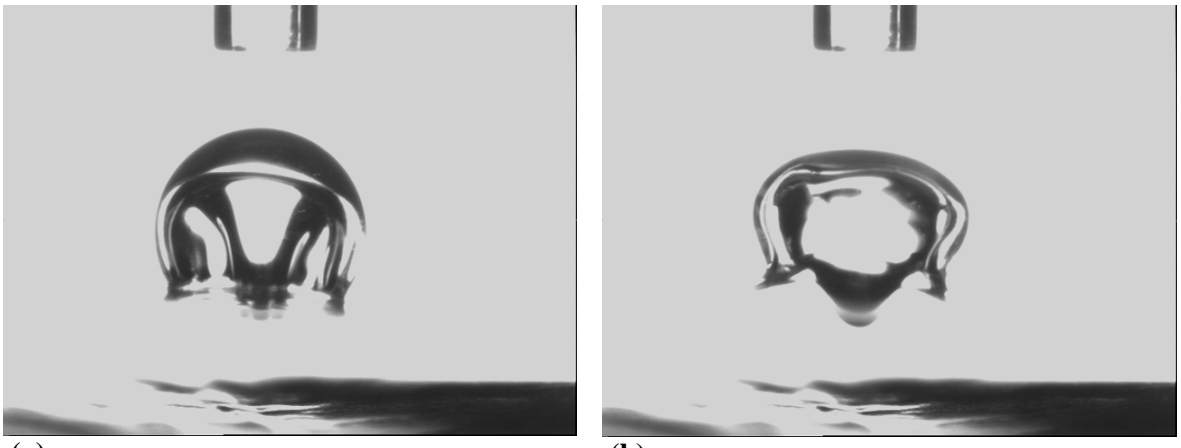

Figure 4.27 Drop of water deposited on the surface of untreated S-PPSU membrane (a) immediately after deposition (b) after 30 s

A preliminary study gave as surface free energy of heated S-PPSU 35 mJ/m^2 very similar to the value determined for S-PEEK.

4.3.2. Thermogravimetric Analysis

Figure 4.28 shows typical high resolution thermogravimetric curves of S-PPSU membrane untreated (**Figure 4.28 (a)**) and thermally treated at 170°C for 48 hours (**Figure 4.28 (b)**) and 64 hours (**Figure 4.28 (c)**).

A different thermal behaviour was observed for the three samples, especially below 300°C. **Figure 4.29** shows the comparison of the samples at temperatures below 300°C. Both annealed samples (170(48): red line and 170(64): blue line) have the same thermal behaviour: the initial weight loss observed at the beginning of the measurement can be attributed to the evaporation of the water remained inside the samples which were in equilibrium with the ambient. The weight loss observed between 200°C and 300°C is instead related to the decomposition of sulfonic acid groups [2, 3, 15, 16]. The untreated sample (black line in **Figure 4.29**) reveals a different thermal behaviour. After the initial weight loss observed at the beginning of the measurement which can be associated to the evaporation of water remained inside the membrane, a weight loss was observed between 125°C and 300°C. This weight loss comprises two sublosses, the first between 125°C and 175°C and of about 3%, can be attributed to the evaporation of residual water still remained inside the membrane. The latter subloss, observed between 175°C and 300°C can be attributed to the degradation of sulfonic acid groups. Comparing the starting point of the degradation of sulfonic groups, it can be noted that in the untreated sample the deterioration of sulfonic groups starts at lower temperature. Probably the cross-link reaction, with consequent weight reduction, starts at temperatures above 175°C. The derivative weight change is particularly instructive: the starting cross-linking reaction can be well observed before the leading edge of the main peak. The difference between the two heated samples is also clearly seen.

The complete decomposition of polymer main chain is revealed for all samples between 375°C and 500°C (**Figure 4.28 (a)**, **(b)** and **(c)**) [2, 3, 15, 16]. As reported in literature [17], cross linking $–SO_2$ bridges decompose together with the main polymer chains of sulfone-containing polymers [12].

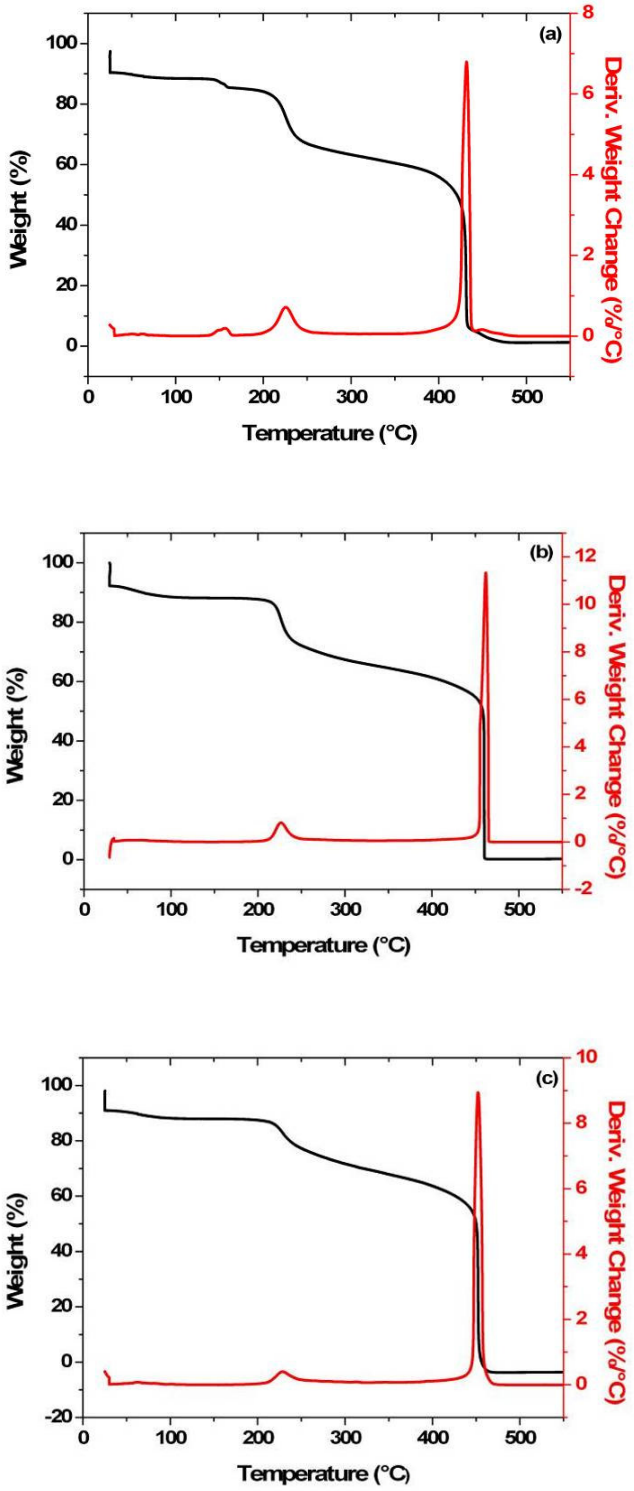

Figure 4.28 HR-TGA curves for S-PPSU, DMSO (a) untreated, (b) thermally treated at 170°C for 48 hours and (c) thermally treated at 170°C for 64 hours

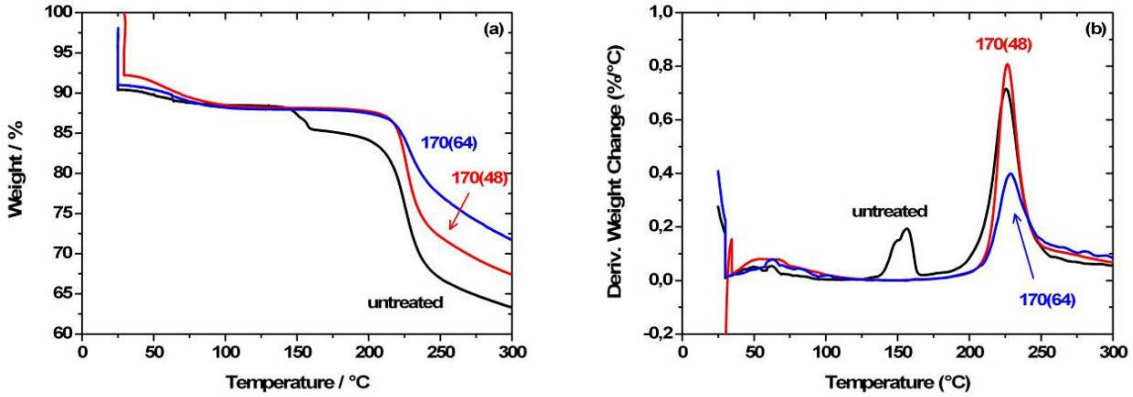

Figure 4.29 Superimposition of HR-TGA curves obtained for S-PPSU, membranes thermally treated and untreated. (a) weight change and (b) derivate weight change

4.3.3 Water Uptake

Figure 4.30 shows the water uptake kinetics obtained for S-PPSU membrane thermally treated at 170°C for 64 hours in liquid water at various temperatures. It is noteworthy that even at temperatures as high as 145°C, the water uptake remains at very reasonable values. It also observed that the water sorption is a fast process. Alberti et al. [25] discussed the decrease of water uptake rate with the temperature as result of two distinct processes, the first very fast and the second very slow. The fast process was attributed to the equilibration necessary for the water diffusion within the thin membrane, while the slow process was associated with a modification of the polymer conformation with the temperature. Similar mechanisms seem to be applicable also to SAP.

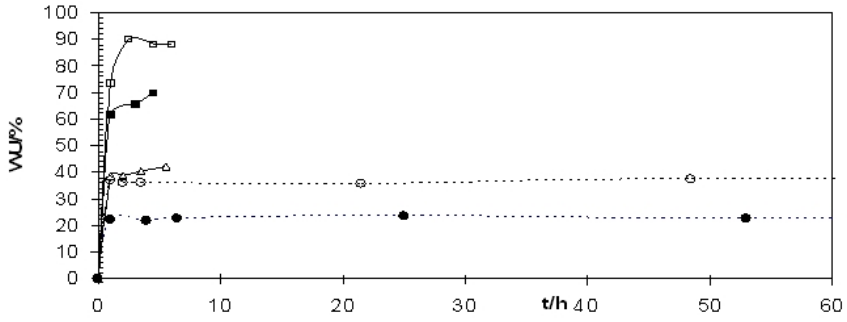

Figure 4.30 Water uptake kinetics by immersion in liquid water of a SPPSU membrane heated at 170°C for 64 h. (•) 25 °C, (○) 60°C, (△) 100°C, (■) 120°C, (□) 145°C

Figure 4.31 shows the comparison of water vapour isotherms of S-PPSU membranes thermally treated and untreated. It is evident that the heated membranes have a distinctly lower water uptake, which is consistent with the data obtained with liquid water.

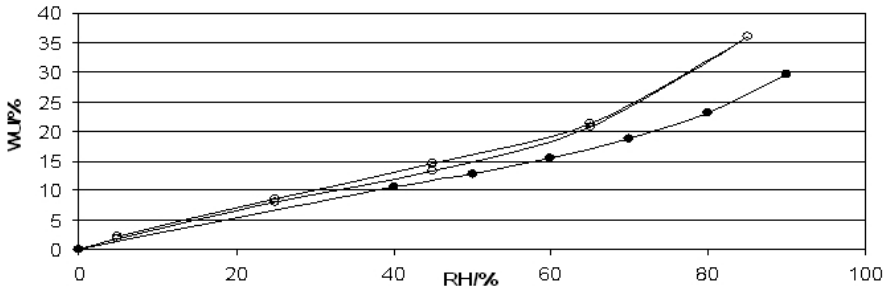

Figure 4.31 Water sorption/desorption isotherms at 50°C of SPPSU membranes (○) untreated, (●) heated 170 °C for 64 h.

4.3.4. Mechanical Properties

4.3.4.1. Stress-Strain Tests

Figure 4.32 shows typical stress strain curves obtained for thermally treated S-PPSU membrane (170(48) red line and 170(64) green line) and untreated membrane. The related mechanical parameters are resumed in **Table 4.6**.

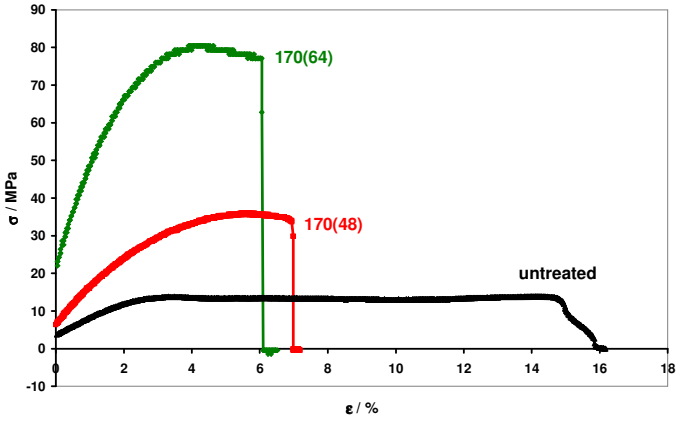

Figure 4.32 Typical Stress-Strain curves of S-PPSU membranes thermally treated

Comparing the results obtained for the untreated membrane with those achieved from the annealed samples, it can be observed that in general the ductility (ε_r) is reduced and the strength (σ) and Young's modulus (E) are increased.

As shown in **Figure 4.32** and as already observed for S-PEEK membranes, mechanical properties are strongly influenced by thermal treatments. In order to obtain the cross-link reaction the temperature is of fundamental importance, but as shown in stress-strain results, annealing time is important too. Comparing the results obtained for the two thermally treated samples, it can be noted that Young's Modulus and the strength of membranes are increased when the annealing time is extended.

Thermal Treatment Temperature (time)[(a)]	***E [MPa]***	***σ [MPa]***	***ε [%]***
Untreated	540±130	13±4	17±6
170(48)	840±200	24±10	6±1
170(64)	2950±300	81±3	7±3

[a] Thermal treatment temperature in °C and time in hours

Table 4.6 Young's Modulus (E), Ultimate Strength (σ) and Elongation at the Rupture (ε) of S-PPSU membranes thermally treated.

4.3.4.2. Dynamic Mechanical Analysis

Figure 4.33 shows storage modulus (**Figure 4.33 (a)**) and tan δ (**Figure 4.33 (b)**) curves for S-PPSU samples, untreated and annealed at 170°C. One observes the slight increase of storage modulus due to loss of plasticizers and the very high glass transition temperature above 210°C. Some very interesting features can be observed, which are characteristic of an in situ curing of the membranes and formation of cross-links between macromolecules [12]. The first heating (curve 1 – first run) shows a glass transition temperature above 160°C. Following this transition, storage modulus increases again and a second peak above 210°C is observed (**Figure 4.33 (b)**). This behaviour can be explained by "in situ" cross-linking, which leads to an increase of storage modulus (**Figure 4.33 (a)**) and a shift of the glass transition to much higher temperature. Consistent with this explanation, the tan δ peak and lowering of storage modulus above 210°C are also observed at following DMA scans (curve 2 – second run) of the same membrane, but the peak above 160°C has disappeared. Previous experiments on S-PPSU membranes showed that cross-linking is observed at 170°C during isothermal annealing; this temperature range is compatible with that observed in DMA.

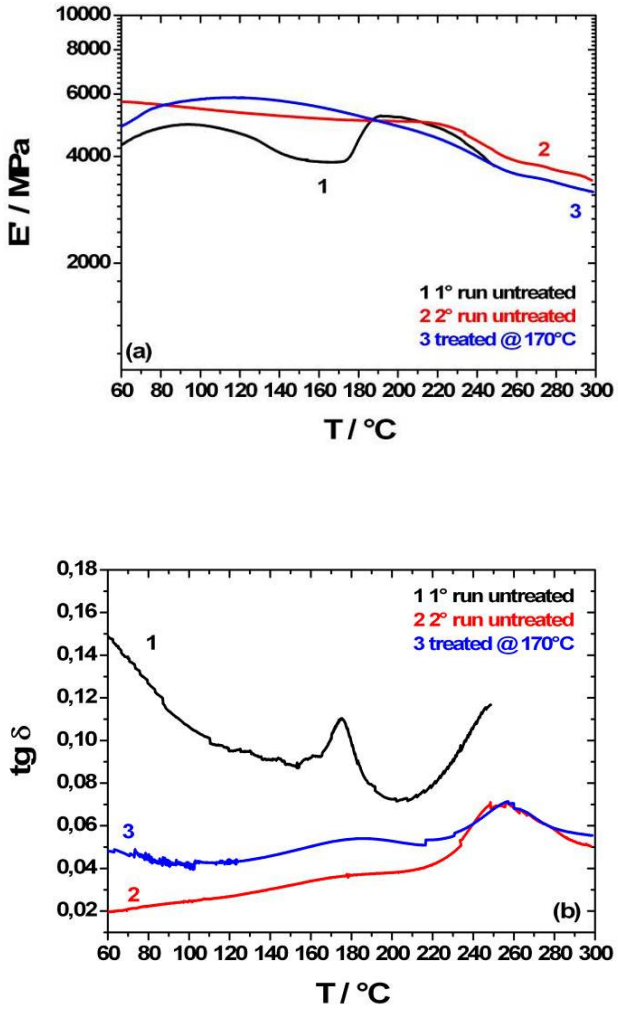

Figure 4.33 (a) Storage Modulus and (b) tan δ of S-PPSU membranes as function of temperature

4.3.5. Dielectric Analysis

Figure 4.34 shows the AC conductivity of S-PPSU membrane annealed at 170°C for 64 hours. During heating, an increase of ionic conductivity was observed until to reach a maximum at around 110°C - 130°C. Above 130°C a decrease of ionic conductivity, probably due to the water loss, was observed. During cooling, the ionic conductivity decreases monotonically with the temperature.

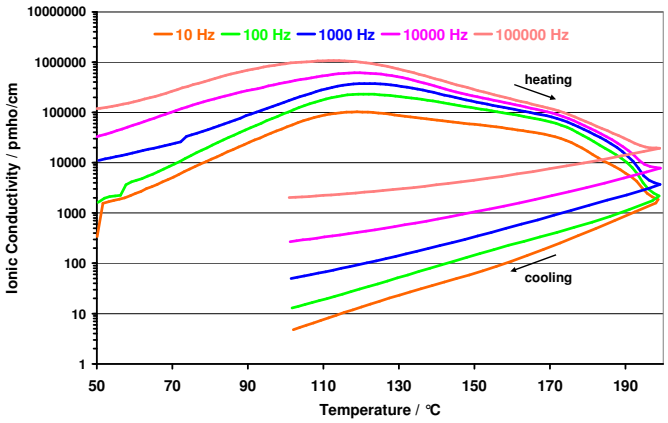

Figure 4.34 AC Conductivity of S-PPSU membrane annealed at 170°C for 64 hours

4.4. Fuel Cell Tests

Membranes that gave the best results were tested in a fuel cell. In this section preliminary results are presented for S-PEEK(0.9) and S-PPSU samples annealed at 160°C and 170°C respectively for 48 hours.

Fuel cells tests were performed at Institute of Physical Chemistry, University of Saarland, Germany.

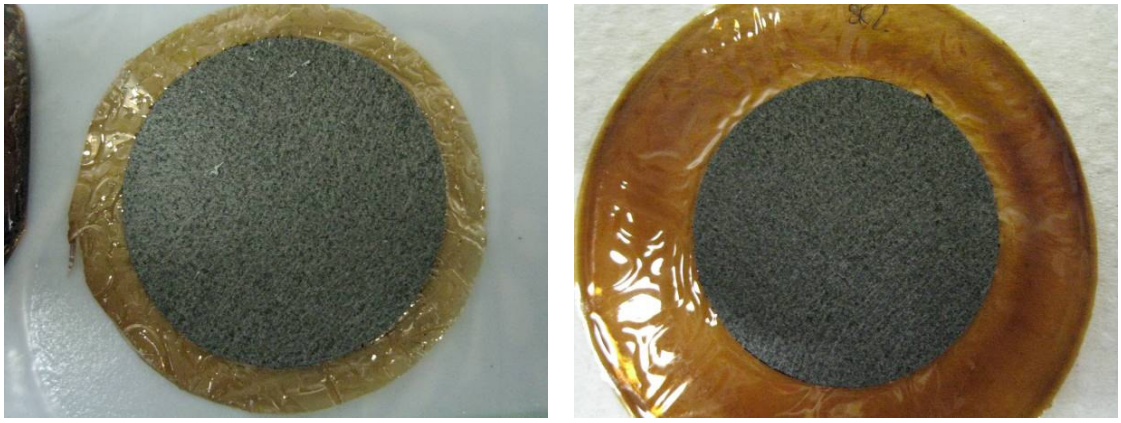

(a) **(b)**

Figure 4.35 MEA of (a) S-PEEK(0,9) and (b) S-PPSU membrane.

S-PEEK (0.9) and S-PPSU (2.0) MEA were prepared by hot pressing technique using commercial electrodes (Anode: Ø 31.4 mm; **ELE 0.163: 0.2 mg-Pt/cm^2**; Catode: **ELE 0.162: 0.4 mg-Pt/cm^2**) and using the following parameters:

- T_{press} *: 125°C*
- P_{press} *: ~0,6 kN/cm²*
- t_{press} *: 6 min*

In both cases any delamination was observed, as shown in **Figure 4.35**.

Before to test the electrolyte in a fuel cell, it is common practice to evaluate the current density in the Ohmic polarization region, which is typically at 0.5 V, and at the OCV. S-PEEK(0.9) (**Figure 4.36**) and S-PPSU (**Figure 4.37**) membrane were tested at room temperature using a 7.7 cm^2 laboratory fuel cell. The gases were humidified by bubbling through liquid water.

The open circuit voltage is slightly below 1 V in both cases, which confirms that the membranes show no open pores and there is no hydrogen permeation through the membrane. The current density is about one of magnitude higher for S-PPSU than for S-PEEK with comparable thickness. Considering that we are in the Ohmic polarization region these results can be related to the higher conductivity of S-PPSU membrane which presents a distinctly higher DS.

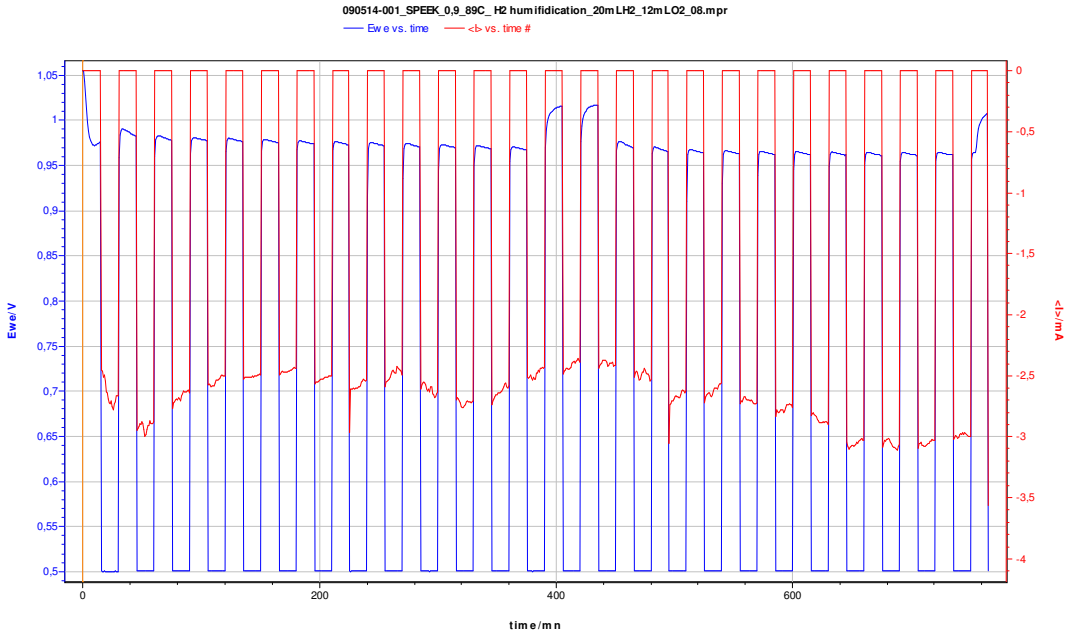

Figure 4.36 Fuel cell test at 25°C (OCV and current at 500 mV) for S-PEEK(0.9) membrane annealed at 160°C for 48 hours. with gas humidification (H_2 20 mL/min, O_2 12 mL/min).

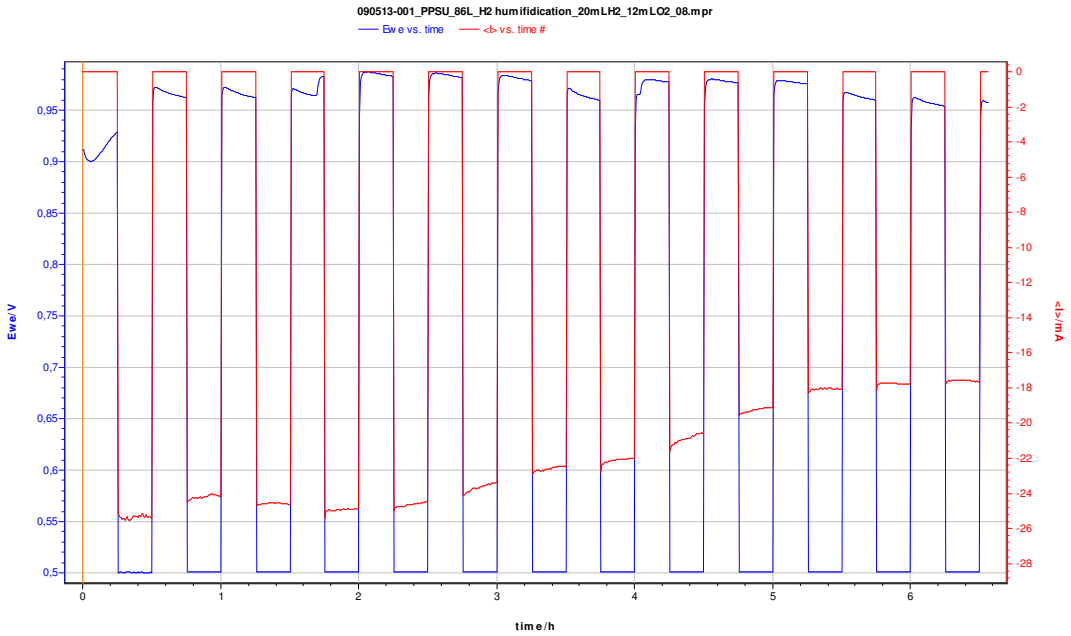

Figure 4.37 Fuel cell test at 25°C (current at 500 mV and OCV) for S-PPSU(2.0) membrane annealed at 170°C for 48 hours. with gas humidification (H_2 20 mL/min, O_2 12 mL/min).

4.5 Discussion

Due to the current mechanical weakness and low durability of non-cross-linked SAP ionomers, many attempts to prepare more stable and mechanical stronger cross-linked SAP (CSAP) membranes were recently performed. Initially, SAP ionomers were cross-linked through bridging bonds between -SO_3H groups and diamines or polyatomic alcohols [26, 27].

In 1998 it was reported for the first time that cross-linked of S-PEEK can be also obtained through inter chain condensation of sulfonic acid groups by thermal treatments at 120°C [28]. However, in 2004, it was clearly demonstrated by Yen et al. [29] that "thermal treatment alone of S-PEEK does not induce any significant cross-linking, at least below 150°C". The contradiction of their results with those claimed in Ref. [30] was evident. A plausible explanation for the observed cross-linking at 120°C was therefore ascribed to fortuitous reactions with glycerine (add as plasticizer) occurred during curing of S-PEEK reported in Ref. [30].

More recently, we found [12] that the conclusions of Yen et al. are true only for S-PEEK membranes obtained from acetone or dimethylacetamide but not for membranes obtained using DMSO. In this latter case, intra/inter chains condensation of acid sulfonic groups can take place if pre-treatments in the temperature range 100°C - 120°C are performed before (in order to

obtain samples in which a certain amount of solvent is still present), followed by a thermal treatment at temperatures ≥ 160°C.

The discovery that true CSAP membranes can now be prepared by simple thermal treatments is of great importance and it must be expected to have a deep impact in the development of PEMFCs membranes, included those for stationary application at temperatures ≥100°C.

Annealing is a well-known concept in metallurgy and ceramics and a thousands of years old technique. However, it is rarely systematically applied on polymers, especially on polymer electrolyte membranes. Recently, it was shown that the loss of performance of Nafion, the most used perfluorinated membrane, is related to morphology changes of the polymer and the magnitude of these changes is in turn related to the treatments previously performed on the membrane [25]. A kinetic investigation of the water-uptake of Nafion after different hydrothermal and thermal treatments suggested that the kinetics of water-uptake is the result of two distinct processes: a very fast one attributed to the time of osmotic equilibration within the thin membrane, and the other, very slow, associated with a slow modification of the Nafion conformation with temperature. The irreversibility of the hydration process with temperature was related to the irreversibility of these conformational changes. The memory of the thermal treatment is due to the fact that ionomers are essentially constituted of an amorphous matrix in which some nanocrystalline phases are embedded [25]. It has been clarified that significant discrepancies between membrane properties observed in the literature can be traced back to the out-of-equilibrium state of the largely amorphous polymers and that they depend on the membrane history, e.g. in terms of thermal treatments. It has also been suggested that there is an elementary correlation between the water uptake of membranes (and thus their electrochemical properties during fuel cell operation) and their mechanical properties, especially the elastic modulus, higher water uptake being related to lower tensile strength of the polymer matrix [12, 25].

The effects of the annealing on PEEK behaviour are well known in literature [31-36]. After thermal treatments the increase of glass transition temperature and mechanical strength are observed in both amorphous and crystalline PEEK polymers [31-33]. All these characteristics were observed in S-PEEK membranes cast using DMAc as solvent even if the temperatures of thermal treatments were well below those used for PEEK annealing. The enhancement of some membrane features cannot be related to the cross-link phenomena, because their immersion in liquid water leads to the dissolution of membranes.

A different behaviour was observed for S-PEEK membranes made using DMSO as solvent. This solvent allows a better control of water uptake as shown in **Figure 4.38**.

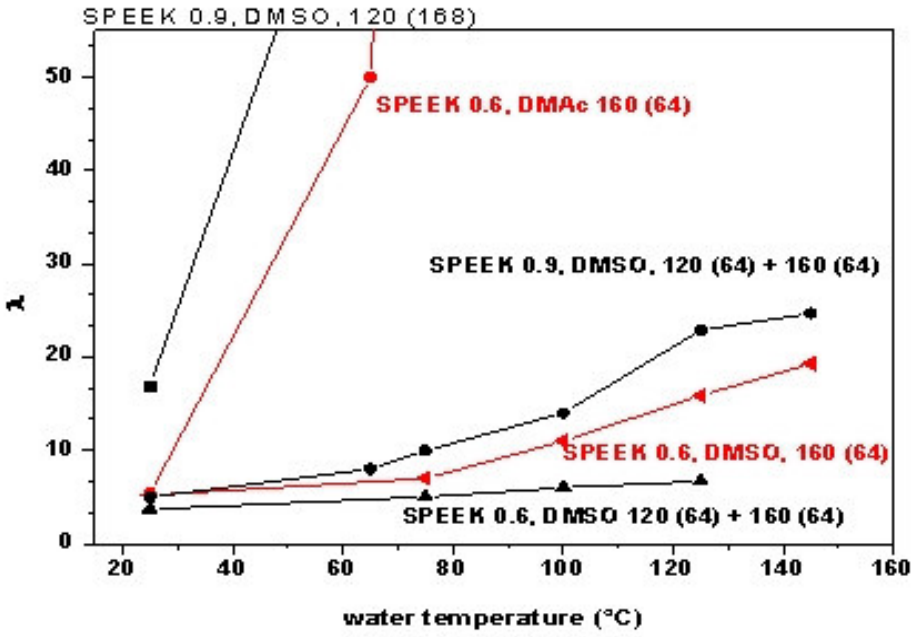

Figure 4.38 Water uptake coefficients obtained for immersion as a function of water temperature for S-PEEK membranes after different thermal treatments and for the two casting solvents DMAc and DMSO.

In principle, changes in the water uptake of ionomer membranes can be related to different reasons such as changes of their conformation and/or degree of crystallinity, and/or elimination of previous permanent deformations (memory) provoked by the water uptake at high temperature [25]. XRD patterns rule out significant changes of polymer crystallinity. The drastic reduction of the water uptake obtained in this investigation, which stabilizes ionomers at high degree of sulfonation even at temperatures as high as 145°C, cannot be due to the mentioned reasons and the only reasonable explanation is the formation of covalent bonds between adjacent polymeric chains, in agreement with FTIR spectra.

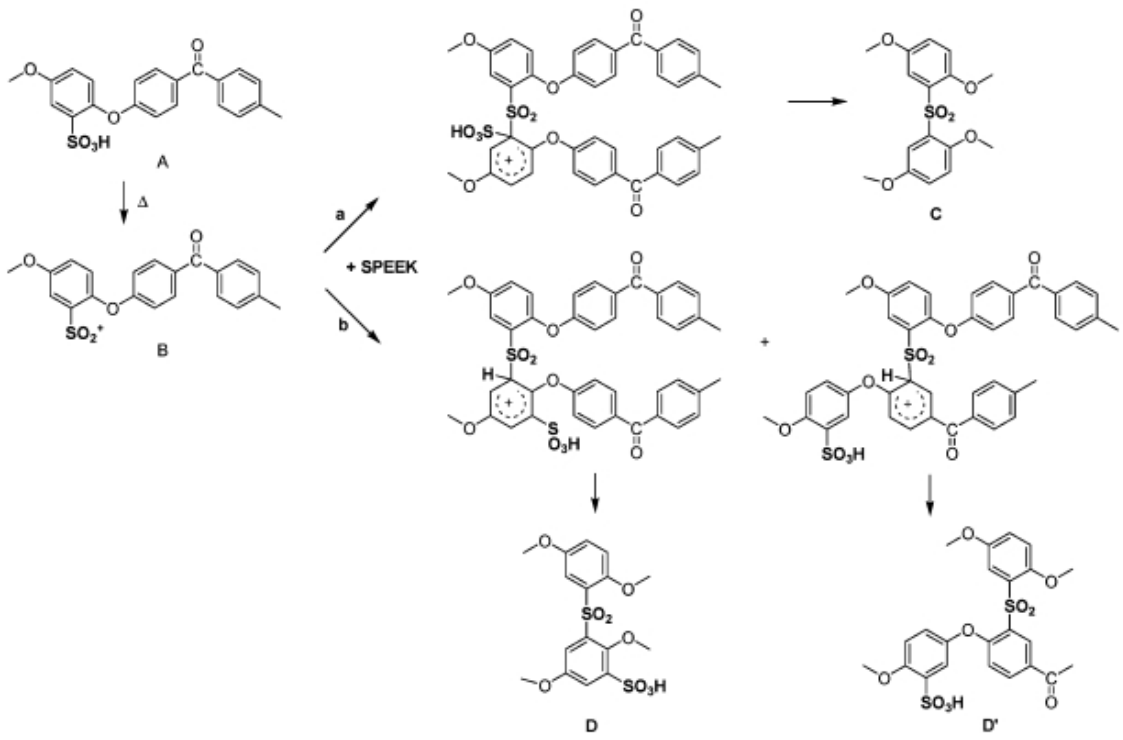

Figure 4.39 Possible pathways for S-PEEK cross-link reaction

NMR spectra of S-PEEK samples show that thermal treatments at 120°C do not induce any structural changes. Thermogravimetry, FTIR and water uptake data indicate that cross-linking occurs when the temperature of the thermal treatment is higher than 120°C for membranes cast in DMSO. **Figure 4.39** shows the possible pathways for the formation of sulfone linkage. The formation of the bridges occurs by an electrophilic aromatic substitution (S_EAr) with a Friedel-Crafts type acylation mechanism *via* a Wheland intermediate [37]. In principle, two routes can be followed: route *a*, the ipso-substitution [28] or route *b*, the H-substitution. In route *b*, the two rings, where the electrophilic attack occurs, are deactivated and consequently two products are expected to be formed: D and D'. Observing **Figure 4.39,** it is clear that route *a* consumes more sulfonic groups, because it involves the loss of SO_2 moieties. A clear NMR analysis of the products obtained by curing DMSO-S-PEEK above 120 °C is not possible, because the thermally treated membranes are insoluble in any usual solvent. The results of elemental analysis are also not unequivocal given the very similar molecular weight of the different compounds.

Role of the Casting Solvent. The presence of residual solvent, 0.4 molecule of DMSO per macromolecule of S-PEEK, plays an important role in the cross-linking reaction. In contrast to membranes cast in DMSO, DMAc-cast samples treated above 120°C were found to be very soluble in many solvents, such as d_6-DMSO. NMR spectra recorded on double-treated DMAc

cast membranes showed a constant DS after the thermal treatment, indicating the absence of a cross-linking reaction. The IEC obtained by titration confirmed this result.

In a recent article, Kaliaguine et al. [29] reported that the thermal cross-linking of S-PEEK does not occur if no cross-linkers, such as polyatomic alcohols, have been added. In these experiments, the membranes were prepared using different casting solvents, but not DMSO. The results of our experiments confirm that no crosslinking occurs in membranes cast from DMAc and NMP. The samples prepared in aqueous solvents (acetone/water) had an intermediate behavior. Excluding a direct participation of DMSO in the reaction (cf. FTIR spectroscopy and the pTSA reaction), the role of the casting solvent can be understood considering its acidity constant. In basic solvents (such as DMAc and NMP), the formation of an acid-base complex between the basic center of the solvent and the sulfonic acid groups prevents the cross-linking reaction. In aqueous media, such as aqueous acetone, the presence of water causes the dissociation of the sulfonic groups, thereby limiting the formation of the electrophilic species (leveling effect of the solvent). Finally, the presence of a polar aprotic solvent, such as DMSO, facilitates the charge separation in the transition state, with a positive effect on the reaction. This effect would be in agreement with the hypothesis that the rate-determining step of the cross-linking reaction is the formation of the electrophilic species. Given the similarity in the DS and the number of residual solvent molecules, one can assume that DMSO is preferentially located near the sulfonic acid groups, where it can assist the formation process of the electrophile during the crosslinking reaction.

The possibility of cross-link reaction was conjectured for other two members of SAP family: S-PES and S-PPSU. The best results were obtained for the latter polymer. S-PPSU membranes have shown all the good features observed for S-PEEK. Moreover the high degree of sulfonation (DS = 2.00) was able to guarantee both a high degree of cross-link and a good proton conductivity (higher content of sulfonic acid groups).

Thermal treatments performed on S-PEEK and S-PPSU membranes above 120°C can importantly modify water uptake behaviour of the membranes. The performed annealing treatments are of important practical relevance, because the water budget is central for the technological viability of membranes either at higher temperature or low relative humidity.

Thermogravimetry, elemental and titration analysis, and FTIR spectra consistently indicate that SAP microstructure stabilization is related to cross-linking of polymer chains by SO_2 bridges promoted by temperature.

S-PEEK and S-PPSU membranes treated at 160°C and 170°C respectively, can resist in liquid water at high temperature (100°C - 145°C). At the same time glass transition temperature

and mechanical properties are strongly enhanced. The presence of cross-linking should also decrease the fuel crossover. The whole of these characteristics make thermally treated SAP membranes most interesting for application in DMFCs.

4.6. References

[1] D. I. Bower, *An Introduction to Polymer Physics*, Cambridge University Press, **2002**, p. 117-161.

[2] G. P. Robertson, S. D. Mikhailenko, K. P. Wang, P. X. Xing, M. D. Guiver and S. Kaliaguine, *Journal of Membrane Science* **2003**, *219*, 113-121.

[3] M. L. Di Vona, D. Marani, C. D'Ottavi, M. Trombetta, E. Traversa, I. Beurroies, P. Knauth and S. Licoccia, *Chemistry of Materials* **2006**, *18*, 69-75.

[4] M. L. Di Vona, E. Sgreccia, S. Licoccia, M. Khadhraoui, R. Denoyel and P. Knauth, *Chemistry of Materials* **2008**, *20*, 4327-4334.

[5] K. D. Kreuer, S. J. Paddison, E. Spohr and M. Schuster, *Chemical Reviews* **2004**, *104*, 4637-4678.

[6] A. Kumar and R. K. Gupta, *Fundamentals of Polymer Engineering*, Marcel Dekker Inc., **2003**, p. 45-47.

[7] C. A. Daniels, *Polymers: Structure and Properties*, CRC Press, **1989**, p. 17-19.

[8] K. P. Menard, *Dynamic Mechanical Analysis: a Practical Introduction*, CRC Press, **1999**, p. 88-120.

[9] H. X. Nguyen and H. Ishida, *Journal of Polymer Science Part B-Polymer Physics* **1986**, *24*, 1079-1091.

[10] H. X. Nguyen and H. Ishida, *Polymer* **1986**, *27*, 1400-1405.

[11] M. L. Di Vona, D. Marani, A. D'Epifanio, E. Traversa, M. Trombetta and S. Licoccia, *Polymer* **2005**, *46*, 1754-1758.

[12] M. L. Di Vona, E. Sgreccia, S. Licoccia, G. Alberti, L. Tortet and P. Knauth, *Journal of Physical Chemistry B* **2009**, *113*, 7505-7512.

[13] F. Wang, M. Hickner, Y. S. Kim, T. A. Zawodzinski and J. E. McGrath, *Journal of Membrane Science* **2002**, *197*, 231-242.

[14] H. L. Wu, C. C. M. Ma, C. H. Li and C. Y. Chen, *Journal of Polymer Science Part B-Polymer Physics* **2006**, *44*, 3128-3134.

[15] D. Marani, M. L. Di Vona, E. Traversa, S. Licoccia, I. Beurroies, P. L. Llewellyn and P. Knauth, *Journal of Physical Chemistry B* **2006**, *110*, 15817-15823.

[16] S. M. J. Zaidi, S. D. Mikhailenko, G. P. Robertson, M. D. Guiver and S. Kaliaguine, *Journal of Membrane Science* **2000**, *173*, 17-34.

[17] R. Guan, H. Zou, D. P. Lu, C. L. Gong and Y. F. Liu, *European Polymer Journal* **2005**, *41*, 1554-1560.

[18] E. Sgreccia, J. F. Chailan, M. Khadhraoui, M. L. Di Vona and P. Knauth, *Journal of Power Sources* **2009**, *in Press*.

[19] G. Alberti, M. Casciola, L. Massinelli and B. Bauer, *Journal of Membrane Science* **2001**, *185*, 73-81.

[20] M. Casciola, G. Alberti, M. Sganappa and R. Narducci, *Desalination* **2006**, *200*, 639-641.

[21] M. Casciola, G. Alberti, M. Sganappa and R. Narducci, *Journal of Power Sources* **2006**, *162*, 141-145.

[22] J. F. Blanco, Q. T. Nguyen and P. Schaetzel, *Journal of Applied Polymer Science* **2002**, *84*, 2461-2473.

[23] D. P. Lu, H. Zou, R. Guan, H. Dai and L. Lu, *Polymer Bulletin* **2005**, *54*, 21-28.

[24] R. Nolte, K. Ledjeff, M. Bauer and R. Mulhaupt, *Journal of Membrane Science* **1993**, *83*, 211-220.

[25] G. Alberti, R. Narducci and M. Sganappa, *Journal of Power Sources* **2008**, *178*, 575-583.

[26] F. Helmer-Metzam, F. Osan, A. Schneller and K. Ledjef in *Polymer Electrolyte Membrane, and Process for the Production Thereof*, *US. Patent 5,438,082* **1995**.

[27] S. S. Mao, S. J. Hamrock and A. Ylitalo in *Crosslinked Ion Conductive Membranes*, *U.S. Patent 6,090,895* **2000**.

[28] S. P. S. Yen, S. R. Narayanan, G. Halpert, E. Graham and A. Yavrounian in *Polymer Material for Electrolytic Membranes in Fuel Cells*, *U.S. Patent 5795496* **1998**.

[29] S. U. D. Mikhailenko, K. P. Wang, S. Kaliaguine, P. X. Xing, G. P. Robertson and M. D. Guiver, *Journal of Membrane Science* **2004**, *233*, 93-99.

[30] J. L. Zhang, Z. Xie, J. J. Zhang, Y. H. Tanga, C. J. Song, T. Navessin, Z. Q. Shi, D. T. Song, H. J. Wang, D. P. Wilkinson, Z. S. Liu and S. Holdcroft, *Journal of Power Sources* **2006**, *160*, 872-891.

[31] C. Carfagna, E. Amendola, A. D'Amore and L. Nicolais, *Polymer Engineering and Science* **1988**, *28*, 1203-1206.

[32] P. Cebe, *Journal of Materials Science* **1988**, *23*, 3721-3731.

[33] P. Y. Jar and H. H. Kausch, *Journal of Polymer Science Part B-Polymer Physics* **1992**, *30*, 775-778.

[34] P. Y. Jar, H. H. Kausch, W. J. Cantwell, P. Davies and H. Richard, *Polymer Bulletin* **1990**, *24*, 657-664.

[35] Y. P. Handa, J. Roovers and F. Wang, *Macromolecules* **1994**, *27*, 5511-5516.

[36] C. Fougnies, P. Damman, D. Villers, M. Dosiere and M. H. J. Koch, *Macromolecules* **1997**, *30*, 1385-1391.

[37] G. A. Olah, T. Mathew and G. K. S. Prakash, *Chemical Communications* **2001**, 2034-2034.

Chapter 5: Conclusions and Future Prospects

The main goal of this thesis was the development of new proton conducting membranes with the definition of suitable synthesis procedures, which allow enhancing the performance of polymeric structures in terms of thermal and mechanical stability with sufficient proton conductivity.

This study confirms the correlation between mechanical strength, water uptake coefficient, and swelling of proton-conducting polymer membranes. In order to reduce swelling during fuel cell operation, a membrane with sufficiently high elastic modulus must be chosen.

Two different approaches have been proposed: the preparation of hybrid composite membranes and the stabilization of sulfonated aromatic polymers by cross-link reactions.

In the quest for improved membranes, composite materials offer a supplementary degree of freedom for conception. Mechanically reinforced composite S-PEEK membranes were prepared by addition of a silylated PPSU minority phase with phenyl-silanol groups. The secondary phase maintains the mechanical stability of the membrane, whereas the main component is responsible for proton conduction. Water uptake coefficients are spectacularly lower than those of pure S-PEEK. A clear correlation exists between the water uptake coefficient and the elastic modulus of the membranes. At 100°C, proton conductivity decreases above 85% RH for pure S-PEEK, but continues to increase for the polymer blend. The mechanical properties, hydration and conductivity are very promising; however, the membrane preparation must be simplified in order to be industrially applicable.

The concept of mechanically reinforced composite S-PEEK membranes by addition of a silylated PPSU minority phase is a promising step to master membrane swelling and develop proton exchange membranes suitable for intermediate temperature PEM fuel cell operation.

A second strategy relies on the simultaneous presence of the polymer matrix and inorganic, organically surface-modified titania particles. In principle, this method allows modulating the desired properties by changing surface functionalization and concentration of oxide particles with the goal of synergistic effects between the two components. With hydrophilic titania, the proton conductivity is high, but the membranes are inhomogeneous due to titania agglomeration. Membranes with hydrophobic titania are instead very homogeneous, but lack high conductivity. To improve properties further, the surface functionalization of titania particles must be further optimized.

All these features identify the prepared blend membranes as promising electrolytes for DMFC operating at intermediate temperature.

In this thesis, we have also shown that thermal treatments of SAP membranes performed above 120°C in presence of residual DMSO can significantly modify the mechanical and water-uptake behavior of the membranes.

Thermogravimetry, elemental analysis, acid-base titration, and FTIR spectra consistently indicate that the SAP microstructure stabilization is related to cross-linking of the polymer chains by SO_2 bridges, which is promoted by temperature and the residual high dielectric constant DMSO facilitating the formation of electrophilic SO_2^+ in the activated complex. The cross-linking leads to loss of sulfonic acid groups; it is therefore important to perform cross-linking on ionomers with high initial degree of sulfonation. In fact, S-PPSU presenting a particularly high DS appears as a very promising candidate ionomer for the future.

The performed annealing treatments are of important practical relevance, because the water budget is central for the technological viability of membranes either at higher temperature or at low relative humidity. S-PEEK membranes treated at 160°C can resist liquid water at high temperature (100°C - 145°C).

The analysis of mechanical properties of proton-conducting SAP membranes by stress–strain tests and DMA show a very important effect of thermal treatments performed on the membranes after solvent casting, with a large increase of glass transition temperature and mechanical strength. DMA gives important complementary insight: removal of residual casting solvent, which acts as plasticizer, leads in all cases to an increase of storage modulus. In the case of S-PPSU, the cross-linking reaction can be observed in situ. Considering the importance of glass transition temperature and mechanical properties for operation of fuel cell membranes, it is clear that thermal treatments appear as a very powerful promising tool for membrane optimization. The presence of cross-linking should also decrease the fuel crossover. The whole of these characteristics make thermally treated SAP membranes most interesting for application in DMFCs.

Based on these conclusions, SAP polymer membranes deemed of low importance for PEM fuel cell application should be re-considered carefully. A future priority will be S-PPSU, which combines high mechanical and hydration stability and good proton conductivity, given the high degree of sulfonation attained in this ionomer.

To summarize this thesis: composite hybrid SAP ionomers show improved properties from the point of view of mechanics and hydration. Composites between two hybrid polymers, a

majority ionomer and a minority "anchor phase" are useful, but the synthesis must be simplified. Composites with surface-functionalized titania must be optimized by designing optimal surface molecules. Cross-linked SAP ionomers by thermal treatment in presence of DMSO are a very appealing possibility, because they have excellent mechanical and hydration properties and the process is easy and inexpensive. However, a sufficient initial IEC is decisive, in order to keep high proton conductivity after cross-linking.

Glossary

CHP	Combined Heat and Power
CSAP	Cross-linked Sulfonated Aromatic Polymers
δ	Mechanical Damping Factor
ΔG	Gibbs Free Energy
D	Diffusion Coefficient
$\tilde{D}$	Self Diffusion Coefficient
DEA	Dielectric Analysis
DMA	Dynamic Mechanical Analysis
DMAc	N,N-Dimethylacetamide
DMSO	Dimethylsulfoxide
DS	Degree of Sulfonation
DSC	Differential Scanning Calorimetry
ε	Strain
ε'	Dielectric Permittivity
ε''	Dielectric Loss Factor
E	Young's Modulus (or Elastic Modulus)
E*	Complex Modulus
E'	Storage Modulus
E''	Loss Modulus
F-TiO_2	Functionalized TiO_2
IEC	Ion Exchange Capacity
λ	Water Uptake Coefficient
MEA	Membrane Electrode Assembly
η_{act}	Activation Overpotential
η_{diff}	Overpotential due to the Mass Diffusion Limitations
η_{iR}	Overpotential due to the Ohimc Resistances
NMR	Nuclear Magnetic Resonance
PEEK	Poly-Ether-Ether-Ketone
PES	Poly-Ether-Sulfone
PPSU	Poly-Phenyl-SUlfone
RH	Relative Humidity

RT	Room Temperature
σ	stress
SAP	Sulfonated Aromatic Polymer
S-PEEK	Sulfonated Poly-Ether-Ether-Ketone
S-PES	Sulfonated Poly-Ether-Sulfone
S-PPSU	Sulfonated Poly-Phenyl-SUlfone
Si-PPSU	Silylated Poly-Phenyl-SUlfone
SiS-PPSU	Silylated and Sulfonated Poly-Phenyl-SUlfone
THF	Tetrahydrofuran
T_g	Glass Transition Temperature
TGA	Thermogravimetric Analysis
TMEDA	N,N,N',N'-tetramethylethylenediamine
U^0	Standard Potential
U_{eq}	Equilibrium Potential
W_e	Electrical Work
W.U.	Water Uptake

List of Tables

List of Figures

List of Papers

1) E. Sgreccia, M. Khadhraoui, C. de Bonis, S. Licoccia, M.L. Di Vona, P. Knauth
Mechanical Properties of Hybrid Proton Conducting Polymer Blends Based on Sulfonated PolyEtherEtherKetones
J. of Power Sources 178 (2008) 667-670.

2) M. L. Di Vona, E. Sgreccia, S. Licoccia, M. Khadhraoui, R. Denoyel, P. Knauth
Composite proton-conducting hybrid polymers: water sorption isotherms and mechanical properties of sulfonated PEEK and substituted PPSU blends.
Chem. Mater. 20 (2008) 4327-4334.

3) M. L. Di Vona, L. Luchetti, G. Spera, E. Sgreccia, P. Knauth
Synthetic Strategies for the Preparation of Proton-Conducting Hybrid Polymers Based on PEEK and PPSU for PEM Fuel Cells.
Comptes Rendus Chimie, 11 (2008) 1074-1081.

4) M. L. Di Vona, E. Sgreccia, S. Licoccia, G. Alberti, L. Torter, P. Knauth
Optimization of S-PEEK Proton Exchange Membranes by Solvent Assisted Thermal Treatments. Analysis of Cross-Linking between Macromolecular Chains
J. of Physical Chemistry B, 113 (2009) 7505-7512.

5) E. Sgreccia, M. L. Di Vona, S. Licoccia, M. Sganappa, M. Casciola, J. F. Chailan, P. Knauth
Self-assembled nanocomposite Organic-Inorganic Proton Conducting SPEEK-based Membranes: Optimized Mechanical, Thermal and Electrical Properties
J. Power Sources, 192 (2009) 353-359.

6) E. Sgreccia, J. F. Chailan, M. Khadhraoui, M.L. Di Vona, P. Knauth
Mechanical properties of proton-conducting sulfonated aromatic polymer membranes: stress-strain tests and dynamic analysis
J. Power Sources, in press (doi:10.1016/j.jpowsour.2009.09.061)

7) M. L. Di Vona, E. Sgreccia, T. Muthusamy, M. Khadhraoui, C. Chassigneux, P. Knauth

High Ionic Exchange Capacity Polyphenylsulfone (SPPSU) and PolyEtherSulfone (SPES) Crosslinked by Annealing Treatment: Thermal Stability, Hydration Level and Mechanical Properties.

J. of Membrane Science. Accepted.

8) E. Sgreccia, M. L. Di Vona, P. Knauth

Composite Membranes Based on SPEEK and (Si,S)-PPSU for PEM Fuel Cells

International J. of Hydrogen Energy. In Preparation**.**

List of Communications

1) E. Sgreccia, M. L. Di Vona, C. de Bonis, S. Licoccia, P. Knauth
New Proton Conducting Hybrid Aromatic Polymers
Solid State Ionics 16 (SSI-16) July 1-6, **2007**, Shanghai, China

2) P. Knauth, E. Sgreccia, S. Licoccia, M. L. Di Vona
Physico-Chemical Properties of Hybrid PEEK-based Proton Conductor Membranes
International Conference on "Polymer Batteries-Fuel Cells, PBFC-2007" June 11-14, **2007**. Rome, Italy.

3) E. Sgreccia, M. Khadhraoui, M. L. Di Vona, P. Knauth
Mechanical Properties of Hybrid Proton Conducting Polymer Blends Based on Sulfonated PolyEtherEtherKetones
2° Ecole d'été Franco-Allemande sur l'Electrochimie et les Nanotecnologies September 2-7. **2007** Lozari, Corsica, France.

4) E. Sgreccia, M. Khadraoui, M. L. Di Vona, P. Knauth
Synthesis, Water Uptake and Mechanical Properties of Hybrid Polymer Membranes
4° Journées Franco-Italiennes de Chimie April 17-18 **2008** Nice, France.

5) M. L. Di Vona, E. Sgreccia, P. Knauth
Composite Membrane Based On Speek For Polymer Electrolyte Membrane Fuel Cell
2nd EuCheMS Chemistry Congress September 16-20 **2008** Turin, Italy.

6) E. Sgreccia, M. L. Di Vona, P. Knauth
Composite Hybrid Polymer Electrolytes
Journées Scientifique du C'Nano Paca, 2ème édition, May 25-27, **2009**, Ile de Porquerolles, France

7) E. Sgreccia, M. L. Di Vona, P. Knauth, Gerhard Auer
Functionalized Titania as Filler for Polymer Electrolyte Membranes

E-MRS 2009 Spring Meeting, Symposium C: Materials for Polymer Electrolyte Membrane Fuel Cells, June 8-12, **2009**, Strasbourg, France.

8) E. Sgreccia, M. L. Di Vona, P. Knauth, Gerhard Auer
Composite Membranes Based on SPEEK And (Si,S)-PPSU for PEM Fuel Cells
E-MRS 2009 Spring Meeting, Symposium C: Materials for Polymer Electrolyte Membrane Fuel Cells, June 8-12, **2009**, Strasbourg, France.

9) M. L. Di Vona, E. Sgreccia, P. Knauth, G. Alberti
Thermally Activated Solvent Mediated Cross-Linking of SPEEK Membranes
E-MRS 2009 Spring Meeting, Symposium C: Materials for Polymer Electrolyte Membrane Fuel Cells, June 8-12, **2009**, Strasbourg, France.

10) P. Knauth, E. Sgreccia, M. L. Di Vona
Proton and Water Diffusion Coefficients in Nanocomposite Polymer Electrolytes
5th International Conference on Diffusion in Solids and Liquids – Mass Transfer, Heat Transfer and Microstructure and Properties (DSL-2009), , June 24-26, **2009**, Rome, Italy.

11) E. Sgreccia; M. L. Di Vona; P. Knauth
Composite Hybrid Polymer Electrolytes
Solid State Ionics 17 (SSI-17) June 28 - July 3, **2009**, Toronto, Canada.

12) E. Sgreccia; M. L. Di Vona; P. Knauth
Composite Membranes Based on SPEEK and (Si,S)-PPSU for PEM Fuel Cells
Hysydays 2009, 3rd World Congress of Young Scientists on Hydrogen Energy Systems, October 7-9, **2009**, Turin, Italy.

13) P. Knauth; E. Sgreccia; M. L. Di Vona
Sulfonated Aromatic Polymers for PEM Fuel Cells: Recent Results
European Fuel Cell Technology & Applications Conference, 3rd - Piero Lunghi Conference (EFC09), December 15-18, **2009**, Rome, Italy

Riassunto

Le membrane a scambio protonico, componenti essenziali delle celle a combustibile ad elettrolita polimerico (PEMFCs), per poter essere utilizzate efficacemente devono esibire differenti proprietà come stabilità morfologica, idrolitica, meccanica ed adeguate proprietà di conducibilità a temperature superiori a 100 °C per bassi valori d'umidità relativa.

Nella presente tesi sono state esplorate due diverse strategie, basate su polimeri solfonati aromatici, per la sintesi di polimeri conduttori protonici: la formazione di ibridi organici-inorganici nanocompositi e la formazione di legami reticolati inter-catena a seguito di trattamenti termici.

L'impiego di materiali ibridi permette di sfruttare l'effetto sinergico dovuto alla contemporanea presenza di una componente organica, polimerica, e di una inorganica. In particolare si è utilizzata una miscela costituita dallo S-PEEK ad alto grado di solfonazione come composto base e da un polimero sililato a base di PPSU come componente minoritario. Lo S-PEEK viene utilizzato per garantire un'elevata conducibilità, mentre l'Si-PPSU garantisce una buona stabilità meccanica (fase "ancora"). Sono stati anche studiati composti nanocompositi ibridi a base di SPEEK in cui è stata dispersa TiO_2 funzionalizzata.

Anche la seconda strategia seguita, la sintesi di composti reticolati, ha dato risultati molto positivi. In particolare si è osservato, per la prima volta, che potevano essere ottenuti legami solfone inter-catena tramite l'utilizzo di opportuni trattamenti termici in presenza di DMSO come solvente di casting. Si è dimostrato che le membrane così ottenute sono in grado di resistere in acqua fino a 145 °C senza dare importanti fenomeni di swelling, mantenendo la stabilità meccanica e buone proprietà di conducibilità.
Le membrane sono state caratterizzate mediante l'utilizzo di molte tecniche, tra cui: l'analisi termo-gravimetrica, le misure meccaniche statiche e dinamiche, le misure di assorbimento d'acqua, sia per immersione, che in fase vapore, la spettroscopie IR ed NMR, la spettroscopia di impedenza e l'analisa dielettrica.

Parole chiavi: Polimeri Aromatici Solfonati - Termoplastici – Materiali Ibridi – Reticolazioni intercatena - Conduttori Protonici – Compositi - Fuel Cells.

Résumé:

Les membranes à échange protonique, composants essentiels des piles à combustibles à membrane polymère (PEMFC) doivent présenter différentes propriétés comme stabilité morphologique, hydrolytique, mécanique et une conductivité adéquate à une température supérieure à 100°C et pour une humidité relative basse.

Dans cette thèse, nous explorons deux stratégies différentes pour la synthèse de polymères conducteurs protoniques, basées sur des polymères aromatiques sulfonatés: la formation de matériaux

hybrides organiques-inorganiques nanocomposites et la formation de liaisons réticulées inter-chaines suite à des traitements thermiques.

L'utilisation de matériaux hybrides permet d'utiliser l'effet synergique due à la présence d'un polymère organique et d'une part inorganique. Nous avons en particulier utilisé un mélange constitué de SPEEK à haut degré de sulfonation comme constituant principal et d'un polymère à base de PPSU contenant des groupements silanols comme constituant minoritaire.

Le SPEEK est utilisé pour garantir une haute conductivité, tandis que le Si-PPSU maintient une bonne stabilité mécanique (phase d'"ancrage"). Nous avons également étudié des composites hybrides à base de SPEEK, dans lequel est dispersé du TiO_2 fonctionnalisé.

La seconde stratégie poursuivie, la synthèse de polymères réticulés, a également donné des résultats très positifs. En particulier, on observe, pour la première fois, que l'on peut obtenir des liaisons sulfones inter-chaines en utilisant des traitements thermiques adaptés en présence de DMSO comme solvant. On a démontré que les membranes ainsi obtenues sont en mesure de résister dans l'eau jusqu'à 145°C sans phénomènes importants de gonflement, maintenant la stabilité mécanique et une bonne conductivité.

Les membranes sont caractérisées par de nombreuses techniques, dont l'analyse thermogravimétrique, les mesures mécaniques statiques et dynamiques, les mesures de sorption d'eau, par immersion et en phase vapeur, la spectroscopie IR et NMR, la spectroscopie d'impédance et l'analyse diélectrique

Mots clés: Polymères Aromatiques Sulfonatés, Thermoplastiques, Matériaux Hybrides, Réticulation, Composites, Conducteurs protoniques, Piles à Combustibles